Micro- and Nano-Topographies to Enhance Non-viral Transfection and Non-viral Neuronal Transdifferentiation of hMSCs

by

Laura Anne Marie Ariel Cameron Edmonds

A thesis
presented to the University of Waterloo
in the fulfillment of the
thesis requirement for the degree of
Master of Applied Science
in
Chemical Engineering (Nanotechnology)
Waterloo, Ontario, Canada, 2018

AUTHOR'S DECLARATION

I hereby declare that I am the sole author of this thesis. This is a true copy of the thesis, including any required final revisions, as accepted by my examiners.

I understand that my thesis may be made electronically available to the public.

ABSTRACT

Transfection and direct conversion, which is referred to as “transdifferentiation” in this thesis, play significant roles in regenerative medicine research including gene therapy, vaccines, modeling of diseases and disorders, drug testing, cell replacement therapy, and tissue engineering. Most of this research has depended on the use of viral vectors, which can be associated with adverse conditions such as genotoxic integration of viral payloads and immunogenicity. Non-viral vectors have the potential to eliminate these problems and have added benefits such as ease of production and targetability, however, they come at the cost of efficiency. Substrates topographies are known to be able to modulate cell behaviors including efficiency of non-viral transfection and non-viral transdifferentiation. However, current research is limited to only a few combinations of cell type, substrate material, and topographical geometry. In this thesis, we specifically investigated the hypotheses that nano- or micro-topographical PDMS substrates would be able to increase non-viral transfection efficiency and/or enhance non-viral neuronal transdifferentiation of human mesenchymal stem cells (hMSCs). We screened the effects of 16 different nano- and micro-scale topographies, with different geometries, on both processes. Results from our transfection study showed that five of the topographical patterns, which included nano- and micro-gratings, concave micro-lenses, micro-holes, and nano-pillars, increased the efficiency of Lipofectamine-mediated transfection. However, these results were not statistically significant, so further rigorous study of these selected topographies is needed. Convex and concave micro-lenses interestingly showed opposite effects on transfection efficiency, and are suggested for further study to investigate the significance of the relationship between direction of lens curvature and transfection efficiency. Our studies on transdifferentiation were neither able to confirm or disprove our hypothesis. No neuronal morphology was seen in samples that went through the transdifferentiation procedure. Immunofluorescent staining for the neuronal lineage marker, microtubule-associated protein 2 (MAP2), showed weak fluorescence in all samples including negative controls. This could have been due to non-specific staining or weak MAP2

expression previously shown to exist in hMSCs without any induction. We found that the hMSCs became over 95% confluent during the transdifferentiation procedure which may have interfered with the transfections or topography-cell interactions during the transdifferentiation procedure. We also found that the poly(amido amine) transfection reagent used during the transdifferentiation procedure was more toxic to hMSCs than, as reported elsewhere, to mouse embryonic fibroblasts or COS-7 cells. Together these observations indicate that parameters affecting cell confluence (such as seeding density or length of transfection phase) and the specific non-viral transfection reagent used should be reconsidered for future work on neuronal transdifferentiation of hMSCs. Alternatively, since the neuronal transdifferentiation procedure has previously been shown to work on fibroblasts, investigations of topographical influence on neuronal transdifferentiation with fibroblasts may lead to more informative results.

ACKNOWLEDGEMENTS

I would like to thank my supervisor, Dr. Evelyn Yim, for the opportunities she has given me, her advice and support, and for all that I have learned from her and from working in her lab.

I thank Dr. Valerie Ward and Dr. Marc Aucoin for their time and effort put towards being committee members for this thesis.

I thank Dr. Kam W. Leong, professor at Columbia University, for the polyplex reagent and transcription factor plasmids. I thank Dr. Marek Kukumberg, researcher at National University of Singapore, for fabricating the MARC chip master mold and some of the MARC chip substrates. I thank Dr. Ting Tsui for use of his SEM. I thank Dr. Marc Aucoin for the code used for principal component analysis and his help with principal component analysis. I also thank him for the competent *E. coli*, LB broth, agar plates, and kanamycin. I thank Paul Brogee for teaching me plasmid amplification.

I have enjoyed working with my lab-mates, and appreciate their help, friendship, and all I have learned from them. Thanks to John Tse, Grace Pohan, Sarah Wen-Hui Chan, Sabrina Mattiassi, Yuan Yao, Yiran Zhou, Muhammad Rizwan, Aung Moe Zaw, Rebecca Mac, Miyeon Noh, and Erica Sharp. I especially thank Moe for reading my thesis and giving me helpful suggestions on it, Sabrina for culturing NPCs which I used to test neuronal antibody concentrations, Sarah for assistance in mold fabrication, and Rizwan for his general guidance.

I would also like to thank my mother Kathie Cameron, my father Jack Edmonds, and my brothers Alex Edmonds, Jeff Edmonds, and Martin Edmonds for all of their constant love and support upon which I depend and am endlessly grateful for. Their encouragement, love, guidance, and companionship has carried me through life and brought me to where I am.

I would also like to thank Marytal Briskin and Athena Malamas for their caring friendships and moral support.

I am grateful to the University of Waterloo Startup Fund and the NSERC Discovery Grant Program for financial support of this project. I thank the Province of Ontario and the University of Waterloo for an Ontario Graduate Scholarship, a President's Graduate Scholarship, and the Murray Moo-Young Biotechnology Scholarship.

DEDICATION

To my Mom.

TABLE OF CONTENTS

LIST OF FIGURES

LIST OF TABLES

LIST OF ABBREVIATIONS

ABOL	4-amino-1-butanol
AFM	atomic force microscopy
AGM	4-aminobutylguanidine
ANOVA	analysis of variance
BAM	Brn2, Ascl1, and Myt1l
BAMN	BAM and NeuroD1
BSA	bovine serum albumin
CBA	cystamine bisacrylamide
DAPI	4′,6-diamidino-2-phenylindole
DHM	digital holographic microscopy
DMEM	Dulbecco's modified Eagle's medium
DNA	deoxyribonucleic acid
DOPC	dioleoylphosphatidylcholine
DOPE	dioleoylphosphatidylethanolamine
ECM	extracellular matrix
EGFP	enhanced green fluorescent protein
ESC	embryonic stem cell
GFP	green fluorescent protein
HFF	human fetal fibroblast
hESC	human embryonic stem cell
hMSC	human mesenchymal stem cell
hiNRP	human induced neuronal restricted progenitor
HPF	human postnatal fibroblast
IF	immunofluorescence
iN	induced neuron
iPSC	induced pluripotent stem cell
LB	lysogeny broth
MAP2	microtubule-associated protein 2
MARC	MultiARChitecture
MEF	mouse embryonic fibroblast
mNPC	mouse neuronal progenitor cell
mRNA	messenger ribonucleic acid
NPC	neuronal progenitor cell
NRP	neuronal restricted progenitor
NSC	neuronal stem cell
PAA	poly(amido amine)
pABOL	poly(N,N-cystaminebisacrylamide-4-amino-1-butanol)
PBAE	poly(β-amino ester)
PBS	phosphate buffered saline
PC	polycarbonate
PCA	principal component analysis
PDMS	polydimethylsiloxane
PEI	polyethylenimine
PFA	paraformaldehyde
PLGA	poly(lactide-coglycolide)

PMMA	poly(methyl methacrylate)
PMEF	primary mouse embryonic fibroblast
PPSU	polyphenylene sulfone
PS	polystyrene
RNA	ribonucleic acid
SEM	scanning electron microscopy
SiOH	silanol
siRNA	small interfering RNA
SM	small molecules
SS-PAA	poly(amido amine)s with repeating disulfide linkages
TBS	tris-buffered saline
TCPS	tissue culture polystyrene
TF	transcription factor
TTF	tail tip fibroblast
TES	triboelectric simulator
Tuj1	neuron-specific class III β-tubulin
WT	wild type

Chapter 1: Introduction and Literature Review

1.1. Introduction

This thesis project was developed as a result of the interest in generating relevant cell types that can be used in regenerative medicine, modeling of diseases and disorders, and drug testing. In regenerative medicine, specific cell types are important for use in cell therapies where they are delivered into a site of injury to integrate and replace damaged tissue or to release signaling factors that can promote self-healing of the damaged tissue. Regenerative medicine also makes use of specific cell types in tissue engineering to create tissue mimics that can be used to replace or repair diseased tissue and sometimes full organs[1]. In disease and disorder modeling, specific cell types can be used to demonstrate specific processes that occur in affected tissues to further understand how the conditions develop and for testing potential treatments[2].

While some specific cell types can be harmlessly taken from the body and expanded for further use, some clinically relevant cell types such as cardiomyocytes, neurons, pancreatic cells, and hepatocytes cannot[3]. This is due to their low regenerative capacity *in vivo* or inability to proliferate *in vitro*. These cell types must therefore be generated starting from a different cell type. Furthermore, it can be beneficial to produce cells from a specific patient creating an ideal genetic match. For these reasons, it is beneficial to begin with an accessible source of starting material, like cells from skin or bone marrow, and convert these cells into the desired cell type.

This project focuses on the development of induced neurons (iNs), which are cells artificially derived from somatic cells that exhibit neuronal morphology, neuron-specific gene products, and functional properties of neurons[4, 5]. According to the World Health Organization, neurological disorders

affect up to one billion people worldwide[6]. This includes neurodegenerative diseases, such as Alzheimer's disease and Parkinson's disease, as well as other disorders including stroke[6]. For these neurodegenerative diseases and for many neurological disorders including autism spectrum disorders, there are currently no long-term cures and there is a lack of means to understand their physiopathology. As a result, there is a demand for an appropriate neuronal cell source for cell-replacement therapy and cellular modeling. Due to low regenerative capacity in the body, neurons cannot be transplanted or explanted from donors or from the living tissue of a patient; they must be created from other cells types. Current methods for generating neurons from other cell types include differentiation of embryonic stem cells or differentiation of induced pluripotent stem cells, however these methods are tedious[7 8], have ethical issues[9], and can be tumorigenic[10]. Therefore, an appealing solution is to use transdifferentiation, which is the direct conversion of one somatic cell type to another[8]. This approach eliminates ethical issues, reduces the time needed to generate the final cell type, and eliminates the use of tumorigenic stem cells.

Researchers have developed ways to generate mouse and human induced neuronal cells from accessible and expendable cell types by transdifferentiation[11, 12]. However, they have typically been carried out using viral vectors to deliver nucleic acids to the cells[8]. The use of viral vectors is associated with adverse conditions such as genotoxic integration of viral payloads and immunogenicity, limiting the acceptance of these methods into clinical practice[13 14]. Non-viral transdifferentiation has also been used to convert mouse cells into induced neuronal cells, however the efficiency of this conversion was very low (7.6%) [15]. Human cells are even more difficult to convert[8, 12]. Therefore, increasing efficiency of non-viral methods is necessary.

Micro- and nano-topographical surfaces have been shown to be able to increase non-viral transfection efficiency[16, 17] and to influence cells towards the neuronal lineage[18-20]. Our objective is to investigate the influence of micro- and nano-topography on enhancing non-viral transfection and neuronal transdifferentiation of human mesenchymal stem cells (hMSCs) from bone marrow.

1.2. Differentiation, Reprograming, and Transdifferentiation

Differentiation, reprogramming, and transdifferentiation are all possible routes that may be taken to switch one cell type into a different cell type. The route selected for cell switching is dependent on the desired cell type and application.

Cells used in clinical applications that are intended to be placed into a patient or induced *in vivo*, have the most requirements to meet. Ideally these cells would originate from the patient's own body to reduce the risk of immune rejection and would avoid pluripotency to avoid the risk of being tumorigenic [8]. Also, ideally their induction would be fast, safe, and efficient. While methods have been developed which meet some of these requirements, it has been challenging to find a single method that meets all of these ideal characteristics. In this pursuit, there has been a wealth of research conducted on methods of cell switching.

Differentiation is the process by which a less specialized cell develops or matures to become more distinct in form and function[21]. The use of differentiation became highly relevant to regenerative medicine in 1981 when mouse embryonic stem cell (ESC) lines were established and in 1998 when the first human ESC lines were created [22-24]. ESCs can be used to derive any cell type of the three germ layers through differentiation. However, a major limitation of using ESCs is that to create ESCs, human embryos have to be destroyed. Other major concerns are that cells derived from ESCs have a risk of being tumorigenic due to ESC pluripotency and have a risk of immunogenic rejection after implantation due to genetic dissimilarity to patients[25, 26].

The second type of cell switching involves reprograming, which is the conversion of a somatic cell type to an induced pluripotent stem cell (iPSC). Motivated by the discovery of human ESCs, and to avoid the ethical issues associated with ESCs, researchers discovered in 2006 that mouse fibroblasts could be reprogrammed into iPSCs and in 2007 human iPSCs were successfully produced [27 28].

Similar to ESCs, iPSCs can be used to derive any cell type of the three germ layers through differentiation. iPSCs can also be made out of a patient's own cells, thus genetically matching the patient and reducing the risk of rejection after implantation. However, the serious concern of tumorigenicity remains, limiting clinical applicability of cells derived from iPSCs[29].

Finally, transdifferentiation is defined as the conversion of one cell type to another[30]. One type of transdifferentiation is the conversion of somatic cells into another lineage without going through an intermediate proliferative pluripotent stem cell stage[8], which has been referred to as "direct conversion" in the literature. The conversion of somatic cells into another cell type can be induced by two different approaches[8]. One of them is by overexpression of lineage-specific factors[11, 31-37]. This approach generates terminal cells without going through pluripotency or multipotency[38]. The other approach is by transient expression of the Yamanaka factors to propel the cells toward an epigenetically unstable state (no pluripotency), before directing them toward the target cell lineage[39-41]. This approach generates multipotent precursor cells without going through pluripotency, however it does involve the transient opening of multipotent pathways[38]. In this thesis project we investigated direct conversion, which is referred to as "transdifferentiation" throughout the thesis.

The first instance of induced transdifferentiation was reported in 1987, when mouse fibroblasts were transfected with a single transcription factor (TF), MyoD, which converted them into myoblasts[31]. This discovery occurred well before the discovery of iPSCs, however, recently interest in studying transdifferentiation as a means to acquire valuable cell types has grown due to the challenges caused by using iPSCs. This method avoids passing cells through a pluripotent teratoma-forming state, and reduces the number of steps needed to arrive at the final cell type. Without the need to reprogram cells and differentiate them again, direct conversion can decrease the time required for the full process to take place, which could be of high importance in clinical applications where a patient must wait for the cells. Additionally, with fewer steps in the process, there is less opportunity for compounding loss of efficiency

in the conversion. Transdifferentiation has great promise as a tool for producing cell types needed in regenerative medicine, disease modeling, and drug testing.

1.3. Methods of Inducing Neuronal Transdifferentiation

Within the past 10 years, transdifferentiation has emerged as one of the preferred strategies to develop specific cells types for medical applications[42]. Method development has gotten quite a bit of attention but is still an active area of research as researchers strive to improve safety and efficiency of the conversion processes and safety of the final induced cells for use in clinical applications. The methods that have been researched include use of TFs, microRNA, and small molecules which can be delivered to cells to induce conversion.

Transdifferentiation induced by TFs or microRNA is often classified further into viral and non-viral methods which refer to the methods used to deliver the nucleic acids (TFs or microRNA) into the cells. Both viral and non-viral methods have benefits and limitations. Viral methods have been most widely used, are better understood, and have high transfection efficiency. Non-viral methods may be more clinically relevant by addressing the safety concerns tied to viral methods including genotoxic integration of viral payloads and immunogenicity. Transdifferentiation by small molecules doesn't require a carrier since small molecules can freely diffuse into cells, but small molecules have mostly been studied in the context of being used in combination with TFs or microRNA. This thesis focuses on the use of TFs, therefore, methods using microRNAs and small molecules won't be reviewed in detail.

1.3.1. Transdifferentiation by Delivery of Transcription Factors

The most popular way to achieve transdifferentiation is by delivery of genes encoding TFs[43]. TFs are proteins that regulate the gene expression in a cell by controlling the rate of transcription of DNA into messenger RNA (mRNA) by binding to specific DNA sequences[44]. Abnormal overexpression of certain TFs or combinations of TFs can cause one cell type to transition into a different cell type[43]. There are two types of TFs that can be used to induce transdifferentiation. The first is lineage-specific TFs which, during natural development, regulate cell-type-specific gene expression patterns. The first example of induction of transdifferentiated cells used a lineage-specific TF[31]. It is thought that when inducing transdifferentiation, lineage-specific TFs activate salient features of the target cell type and auto-regulatory activation of downstream TFs reinforce expression of cell-fate-determining genes, leading to an induced stable transcriptional program[35]. However, this mechanism is hypothetical and has not been proven. The second type of TFs are pluripotency TFs. Transient expression of pluripotency TFs can create an epigenetically unstable state which can then be more easily influenced towards the desired cell type by supplying exogenous inductive signals[45].

Investigations into inducing neuronal transdifferentiation by TFs started by studying the conversion of mouse fibroblasts to neuronal cells. The first research paper documenting neuronal transdifferentiation was published in 2010 and achieved direct conversion of mouse fibroblasts to functional induced neurons (iNs) by use of lineage-specific TFs[35]. In this study, 19 genes that were known to be specifically expressed in neural tissue, known to play important roles in neuronal development, or previously used in epigenetic reprograming were screened to find the most successful combination for inducing cell conversion. It was found that the combination of Brn2, Ascl1, and Myt1l (BAM) could produce mature iNs with the highest efficiency. Mouse embryonic fibroblasts (MEFs) and tail tip fibroblasts (TTFs) were harvested from TauEGFP knock-in mice, which are genetically modified so that enhanced green fluorescent protein (EGFP) is selectively expressed in neuronal cells, which allowed them

to carefully ensure exclusion of neuronal cells from their initial MEF and TTF populations and identify cells converted to the neuronal linage. The TF genes were cloned into doxycycline-inducible lentiviral vectors. Cells were infected overnight, then cultured in MEF media with doxycycline for 48 hours, and then transferred into N3 neuronal induction media with doxycycline. After viral BAM transfection, iNs from MEFs expressed microtubule-associated protein 2 (MAP2) and synapsin neuronal markers, and those induced from TTFs expressed TauEGFP, Tuj1, NeuN, and MAP2 neuronal markers. This study estimated the conversion efficiency by dividing the number of Tuj1-positive cells per area by the number of cells initially plated per area. This calculation was validated by the observation that iNs become postmitotic, and therefore stop dividing, 24 hours after transgene activation. They reported conversion efficiencies of up to 19.5% using BAM factors and lentiviral delivery. The iNs showed functional neuronal properties such as action potentials and functional synapses. This discovery inspired researchers to investigate whether other combinations of TFs could generate specific neuronal phenotypes for disease modeling and whether this method could be used on human cells to generate patient-specific neurons for cell therapy. A following study validated the principle of using iNs for modeling autism-spectrum disorder[46]. Their primary objective was to determine whether iNs produced from a mutated organism would have the same phenotype as the endogenous neurons of that organism. They directly converted MEFs from mice with autism-spectrum disorder-associated point mutation R704C and MEFs from littermate wild type (WT) mice into iNs. These mice were also designed to express EGFP at the endogenous tau gene locus. The transdifferentiation was carried out by transduction of BAM factors with doxycycline-inducible lentiviral vectors as previously described. MEFs transdifferentiated into iNs reproduced the phenotype caused by the autism-associated mutation. The conversion efficiencies from R704C and WT MEFs were 18.2% and 20.4% respectively, as measured by the fraction of cells that activated the TauEGFP reporter. These findings gave evidence that iNs transdifferentiated from non-neuronal cells can be used to examine neuropsychiatric diseases.

To advance this research, neuronal transdifferentiation by delivery of TFs was investigated on human cells. There are many differences in the gene regulatory networks of mouse and human neural development, therefore the induction of human neuronal transdifferentiation was unlikely to use the same method as mouse cells. It was shown that when three independent primary human fetal fibroblast (HFF) lines were transduced with BAM factors, in the same manner as the mouse studies[35], they did induce cells with immature neuronal morphologies and expressing Tuj1, however these cells were functionally immature[12]. Twenty additional factors were screened for one that could improve the generation of human iNs using the BAM factors. NeuroD1 was found to improve the efficiency two to three fold after three weeks. Conversion efficiencies of HFFs and human postnatal fibroblasts (HPFs) to iNs by BAM factors and NeuroD1 (BAMN factors) were similar, ranging from 2-4% of cells seeded. Human iNs were able to generate action potentials and many could mature to form synaptic contacts when co-cultured with primary mouse cortical neurons. These methods could hopefully lead to generation of patient-specific neurons for *in vitro* disease modeling or regenerative medicine.

When transplanted into a host, iN cells have poor survival and function because of their limited ability to proliferate. Therefore, neuronal restricted progenitors (NRPs) may be a more beneficial cell type for neuron replacement therapy to treat neurodegenerative diseases, because they have the ability to proliferate, migrate, and develop into neurons. A more recent study made use of TFs to induce direct conversion of human fibroblasts into NRPs[47]. They investigated a group of eight TFs, known to either convert fibroblasts into stem cells with proliferative features, promote fibroblasts to acquire neural progenitor characteristics, or give induced cells the capacity to become neurons. It was found that Sox2, c-Myc, and either Brn1 or Brn4 (which were interchangeable), delivered by lentivirus, could directly convert HFFs into human induced NRPs (hiNRPs). These hiNRPs had neuronal morphology, showed expression of multiple neuronal markers, and had self-renewal capacity. Additionally, they could be differentiated into various terminal neurons with functional membrane properties. These hiNRPs could

have potential to be used for neuronal developmental studies as well as therapeutic strategies for neurodegenerative diseases.

Various specific neuronal subtypes and other cell types of the nervous system have also been induced by viral delivery of TFs. For example, there have been efforts in producing dopaminergic neurons, the cell type lost in Parkinson's disease. Transduction, using doxycycline-inducible lentiviral vectors, was used to deliver lineage-specific transcription factors that act during brain development, Ascl1, Nurr1, and Lmx1a, in order to induce transdifferentiation of mouse and human fibroblasts into dopaminergic neurons[11]. MEFs were converted to induced dopaminergic neurons with a conversion efficiency of around 18%. Induced dopaminergic neurons were obtained from human fetal fibroblasts and adult fibroblasts with conversion efficiencies of around 6% and 3%, respectively. It was also reported that the cells did not pass through any detectable intermediate neuronal stages. In another study, dopaminergic neurons were induced by lentiviral delivery of Lmx1a and FoxA2, two genes involved in dopamine neuron generation, along with the BAM factors [36]. Motor neurons could be induced from MEFs with between 5% and 10% efficiency, by forced expression of seven TFs including BAM factors, Lhx3, Isl1, Hb9, and Ngn2, delivered by retroviral transfection[48]. They also found that these fibroblasts did not go through a neural progenitor state on their way to becomig motor neurons. When NEUROD1 was added as an eighth TF, retroviral transfection of human embryonic fibroblasts could generate human motor neurons, but with conversion efficiency under 1%. Finally, myelinogenic oligodendrocyte progenitor cells were induced by delivery of eight TFs, Myrf, Myt1, Nkx2.2, Olig1, ST18, Nkx6.2, Olig2, and Sox10, to MEFs by lentiviral transfection[49]. However the conversion efficiency was around 1%. The same phenotype could be achieved with a subset of three TFs, Sox10, Olig2, and Nkx6.2, however the conversion efficiency was even lower.

Because of safety concerns restricting the clinical use of viral delivery systems, the development of non-viral methods is actively under investigation[13]. The first non-viral neuronal transdifferentiation study was published in 2012. It was shown that primary mouse embryonic fibroblasts (PMEFs) could be

transdifferentiated into neuronal cells by non-viral delivery of the BAM factors using a bioreducible linear poly(amido amine)[15]. Repeated dosing was used to sustain a high level of the transgenes which was essential for successful transfection. An efficiency of 7.6% conversion to Tuj1+ cells relative to the number of PMEFs seeded was reported. Further increase in efficiency may be necessary to apply this method to more resistant adult human cells. In a recent study, a triboelectric simulator (TES) was used in conjunction with poly(β-amino ester) (PBAE) transfection of genes encoding BAM TFs to enhance the non-viral conversion efficiency of PMEFs to iN cells[50]. The *in vitro* conversion induction began with BAM transfection by electroporation followed by cell seeding. Two days after, the cells were transfected a second time using C32-122 poly(β-amino ester) nanoparticles. Starting on day 3, the PMEF medium was replaced with neuronal induction medium and cells were exposed to the TES for 60 min/day each day. Conversion efficiency was calculated as the percentage ratio of Tuj1-positive cells to total number of cells seeded. On days 12-14, conversion efficiency was 6.41% without TES, and 14.17% when TES was used following transfection. Their *in vivo* study using mice involved injections of BAM TF/poly(β-amino ester) polyplex into mouse dermal fibroblasts followed by use of electrocardiogram patches to expose the injection sites to TES for 30 min/day for 14 days. Conversion efficiencies were measured to be 0.04% and 5.86%, with and without exposure to TES respectively.

1.3.2. Transdifferentiation by Delivery of MicroRNA or Small Molecules

MicroRNAs are short non-coding RNAs that bind to complementary pieces of mRNA after transcription and inhibit their translation. In this way, they can inhibit expression of specific genes which have influence over cell type. They have potential benefits in comparison to the use of TFs[43]. For example, they can be obtained by chemical synthesis reducing the risk of mutation and their small size allows multiple microRNAs to be delivered in the same vector. MicroRNAs have been shown to enhance transdifferentiation by TFs and to induce transdifferentiation alone. Direct conversion of human postnatal

fibroblasts to iNs has been achieved by delivery of a combinations microRNAs and TFs with conversion efficiency of up to ~10 % [51, 52]. Human fibroblasts have also been converted to striatal spiny neurons, the primary cell type affected in Huntington's disease, with a combination of microRNAs and TFs[53]. Finally, microRNAs alone have induced neuronal conversion of human fibroblasts but transfection efficiencies were very low (around 1%)[52]. All of these studies used viral vectors.

Small molecules (SMs) are defined as being chemical compounds with a low molecular weight[54]. Small molecules that target signaling pathways, epigenetic modifications, or metabolic processes can regulate cell development, fate, and function[54]. Major benefits in using small molecules, instead of TFs or microRNAs, are that there is no need to use a delivery vector and no involvement of transgenes. This reduces the complexity of the transdifferentiation process and eliminates safety and efficiency concerns caused by the use of delivery vectors and transgenes. Additional benefits include cost-effectiveness and easy synthesis[54]. Some studies have shown successful neuronal induction of human and mouse fibroblasts by small molecules alone[55-57] , however, most often small molecules have been used as additional components to enhance transdifferentiation driven by viral delivery of transgenes[58, 59].

1.3.3. Comparison of Conversion Efficiencies across Methods for Neuronal Transdifferentiation

In Table 1 we compare the conversion efficiencies achieved with various methods of transdifferentiation. The approximation commonly used for reporting conversion efficiency of neuronal transdifferentiation was established in the first study showing induced neuronal transdifferentiation, and has been widely accepted since then[35]. Typically this is the number of Tuj1+ cells over the number of cells initially seeded, however, in some studies one or more different neuronal marker(s) may be considered along with or instead of Tuj1. Sometimes, the neuronal purity of the final cell culture is

reported in addition to or instead of the actual conversion efficiency (these values were not included in Table 1).

Another critical factor that should be considered when comparing methods of inducing transdifferentiation is their safety for clinical applications. This includes considering whether final induced cells are safe to be implanted after *in vitro* conversion, or whether the conversion can safely take place inside a patient when using *in vivo* conversion.

Table 1 Comparison of Methods and their Conversion Efficiencies in Neuronal Transdifferentiation. Values are from in vitro studies.

Method	Conversion Efficiency (%)		Clinical Applicability	Ref.
	Average	Highest		
Viral Delivery of TFs (Mouse)	19.4	20.4	Limited by safety of transgene delivery strategies	35 46
Viral Delivery of TFs (Human)	~3	~3	Limited by safety of transgene delivery strategies	12
Non-viral Poly(amido amine) Delivery of TFs (Mouse)	7.6	7.6	Promising, but limited by conversion efficiency	15
Non-viral Electroporation & Poly(β-amino ester) Delivery of TFs, followed by TES (Mouse)	14.17	14.17	Promising, but limited by conversion efficiency	50
Viral Delivery of MicroRNAs and TFs (Human)	9	10	Limited by safety of transgene delivery strategies	51 52
Small Molecules and Viral Delivery of TFs (Human)	~355.45	~ 500	Limited by safety of transgene delivery strategies	58 59
Small Molecules Only (Human)	21	21	Promising. Further investigation of safety is required.	57

In Table 1, it is clear that human cells are more difficult to convert at high efficiencies than mouse cells. This can be seen by comparison of the studies done on conversion by viral delivery of TFs to mouse and human cells. This is important because for clinical applications, it is necessary to induce human cells. Although non-viral methods have higher potential to be safe in clinical applications, their efficiencies are already low in studies using mouse cells. It is likely that non-viral TF methods would be even less effective in human cell conversion, limiting their clinical applicability. Non-viral TF transdifferentiation efficiency was increased by the additional use of electroporation and TES. The group who did this study also showed that PBAE nanoparticles complexed with BAM TF expressing plasmids could be transfected into mouse dermal fibroblasts through intradermal injection followed by applying

TES-generated electrical stimulation through electrocardiogram patches. This produced skin tissue with 5.86% Tuj1+ cells [50]. This showed some potential for development of a strategy for non-viral *in vivo* neuronal transdifferentiation for therapeutic applications, however the strategy seems fairly complex which could limit its potential. Therefore, a point of future study should be in continuing to develop strategies for making non-viral TF methods more efficient.

MicroRNA provides an additional way to influence gene regulation, and when used along with TFs can achieve improved conversion efficiency of human cells. However, it will still be advantageous to develop efficient non-viral methods for safe *in vitro* and *in vivo* delivery of microRNAs and TFs.

Finally, small molecules appear to provide extreme enhancement in conversion efficiency. Although knowing that neurons are postmitoctic, it is surprising to see that conversion efficiencies could be far over 100%. These values were reported as the percentage of Tuj1+ cells in relation to the initial number of plated cells, as is common[58]. These values indicate that their methods must accommodate a large increase in cell number during conversion, presumably before neuronal conversion is complete. It is worth noting that these high conversion efficiencies were achieved when small molecules were used along with virally delivered TFs, which limits clinical applicability due to the safety concerns associated with the use of viruses. Small molecules have also been used alone to induce neuronal cells with a conversion efficiency surpassing those achieved by viral delivery of TFs[58]. This is very promising because such a method eliminates the need to design efficient transgene delivery systems and eliminates the safety concern of integrating transgenes. This method could potentially be used for clinical applications such as cell replacement therapy of neurological disorders. However, it still needs to be explored whether functional neurons can be induced by small molecules *in vivo* against disease or injury.

1.4. Non-viral Gene Delivery for Transdifferentiation

Some of the methods for inducing transdifferentiation, described previously, require the delivery of nucleic acids to the start cells in order to initiate their conversion. For example, TF mediated transdifferentiation requires the delivery of plasmid DNA containing TF-encoding genes. Because nucleic acids are highly charged, they cannot penetrate the hydrophobic core of a cell membrane. There has been plenty of research done on gene delivery systems for medical applications including gene therapy, vaccines, and controlling cell fate[60-62 63]. Most research uses viral gene carriers because their intrinsic ability to transfect cells is very efficient. However, there are safety concerns limiting the use of viral vectors in clinical practice, such as genotoxic integration of viral payloads and immunogenicity, making non-viral gene delivery systems preferable. However, non-viral vectors often have lower transfection efficiency and cause lower transdifferentiation efficiency, and therefore methodologies need to be improved.

Retroviral and lentiviral vectors have been used extensively in research using TF induced transdifferentiation. They each have characteristics that can be useful depending on how one wishes the delivered genes to be incorporated and expressed in the cell. Both retrovirus and lentivirus are capable of transducing dividing cells and integrating transgenes into the host cell's genome which provides a permanent genetic modification and the possibility of perpetual transgene expression[63]. However, this integration also has the potential to cause complications such as oncogene activation or tumor-suppressor gene inactivation, causing cancer. Lentiviral vectors can also transduce non-dividing cells, which makes them applicable to more cell types than standard retroviral vectors and most non-viral vectors, and they can be used to enable transient gene expression. In addition to the risk of tumorigenicity, viral vectors also have greater risk of causing immunogenic problems. Due to these concerns, there has been a focus on finding non-viral alternatives for gene delivery systems that could be lower risk for clinical applications.

1.4.1. Methods of Non-viral Delivery

Nonviral transfection has been approached in many different ways including both physical methods (e.g. electroporation), biochemical methods (e.g. calcium phosphate co-precipitate, lipoplex and polyplex mediated gene delivery), and physical-biochemical hybrid methods (e.g. nucleofection and magnetofection). Although only a few non-viral gene delivery methods have been used in research on transdifferentiation, there are lot of new developing non-viral systems used in studies for other types of cell conversion (differentiation and reprogramming) and for other medical applications including gene therapy and vaccines. These methods could also potentially be used for inducing transdifferentiation. The examples of non-viral gene delivery systems described here are ones that have already been used in studies on cell conversion.

1.4.1.1. Electroporation and Nucleofection

A very common physical method, which has even been used in neuronal transdifferentiation, is electroporation[50]. Electroporation allows DNA to enter cells by disrupting the cell membrane and making it more penetrable to the highly charged nucleic acids. This is achieved by applying an electrostatic field across a cell and DNA suspension. As a result, pores are formed in the cell's membrane through which the DNA can travel to the inside of the cell. Electroporation can be used *in vitro* and *in vivo* and can transfect cells efficiently compared to other non-viral methods. However, it can also cause cell death making it less desirable in clinical applications. Nucleofection is a technique that uses electroporation along with cell-type specific reagents that enable nucleic acids to travel directly into the nucleus during electroporation. This non-viral technology is special for its ability to transfect non-dividing cells at high efficiencies in comparison to other methods which rely on cell division for DNA to enter the nucleus.

1.4.1.2. Nanoparticles

Many other systems of non-viral gene delivery make use of nanoparticles. These are often classified as biochemical methods. Nanoparticles can be loaded with DNA in various ways and are an ideal size to enter cells by endocytosis[64, 65]. For example, mesoporous silica nanoparticles have high loading capacity due to their highly porous structure, tunable charge, and low cytotoxicity which make them useful for gene delivery[66]. DNA can be electrostatically adsorbed to the interior walls of positively charged mesoporous silica nanoparticles and then delivered to cells. This technology has been used to differentiate iPSCs to definitive-lineage cells[67]. Another nanoparticle gene delivery system is calcium phosphate co-precipitation. In this system, DNA is mixed with calcium chloride in a saline/phosphate solution to generate calcium-phosphate-DNA co-precipitate in the form of small particles. These particles bind to the cell wall due to the calcium phosphate and enter cells through endocytosis. This was used in the first artificially induced transdifferentiation when embryonic mouse fibroblasts were converted to myoblasts with delivery of MyoD[31]. Calcium-phosphate co-precipitate particles can also help improve viral transfection by increasing the density of viral carriers that coat the cell surface followed by their entry into cells by endocytosis[68].

A nanoparticle method that combines both biochemical and physical influence to achieve gene delivery is magnetofection. DNA is first adsorbed onto magnetic nanoparticles made of biodegradable iron oxide, which are then added to cell culture medium and forced to approach cells using a magnetic field. The magnetic particles can form complexes with bare nucleic acids or form complexes with nucleic acids which are prepackaged in protective viral or non-viral carriers. Magnetofection promotes cellular uptake of DNA by forcing the entire dose towards the cells so that all cells come in contact with a large number of DNA complexes. Magnetofection has been used to non-virally reprogram mouse fibroblasts into iPSCs[69]. It has also been shown to have potential in aiding control *of in vivo* transfection by confining gene delivery to an area defined by the applied magnetic field[70].

Recently, nanoparticle systems have been used to mediate gene delivery using peptide-modified dendrimer-entrapped gold nanoparticles[71]. Nanoparticle systems have also been applied to deliver TFs as proteins rather than genes. For example, this has been done using cationic bolaamphiphile particles and chitosan nanoparticles[72, 73]. Functionalized nanoparticles are not only being used as delivery vehicles, but also tools which themselves can promote cell differentiation[74, 75].

These nanoparticle systems have all been applied to some extent to induce either differentiation, reprogramming or transdifferentiation, although they have been primarily studied in the context of other clinical applications.

1.4.1.3. Lipoplexes and Polyplexes

More common methods of non-viral gene delivery are the use of lipoplexes and polyplexes. These are complexes formed through the electrostatic interaction between DNA and cationic lipids or polymers, respectively. These synthetic vectors have been widely considered as promising alternatives to viral vectors for their improved safety, greater flexibility and easier manufacturability[76]. Many efforts have gone into the optimization of these systems to advance the clinical applicability of non-viral gene delivery. This is especially true for polyplex systems which have characteristics important for *in vivo* gene delivery, such as extracellular stability and targeted release [76, 77].

Lipofection, the use of lipoplexes to transfect cells, was first reported in 1987[78]. Lipopelxes form into heterogeneous populations of structures. These include more dense structures with DNA being surrounded by lipid as well as large structures with DNA outside of lipid structures or holding multiple lipid structures together[79]. These complexes enter cells through endocytosis and can be designed to promote endosomal escape to release DNA into cytoplasm. The cationic lipids can be categorized based on their structure into (1) monovalent aliphatic lipids with single amine functionality in their head group,

(2) multivalent aliphatic lipids with several amine functionalities in their head group, or (3) cationic cholesterol derivatives[80]. The addition of neutral lipids, such as dioleoylphosphatidylethanolamine (DOPE), dioleoylphosphatidylcholine (DOPC) and cholesterol, to the complexes can improve transfection efficiency. This is thought to be because they help destabilize lipid bilayers which promotes endosomal escape[79]. There are many commercially available cationic lipid transfection reagents including Cellfectin, Lipofectamine, and Lipofectin. Choosing which reagent to use will depend on the cell type and culture conditions used. Lipoplex systems often show cytotoxicity due to accumulation of positive charge inside cells [81].

Polyplexes have received lots of attention due to their promising tunable properties[76, 77]. Linear, branched, or dendritic polymers can be used. DNA-binding groups can be incorporated into the polymer backbone, pendant groups or grafted molecules. They can also be designed with tunable biodegradability which helps with DNA release and reduces cytotoxicity[76, 82]. Polyethylenimine (PEI) was one of the first polymers used for effective gene delivery in 1995 [83]. PEI can be targeted to specific cell types by the conjunction of specific ligands and can aid endosomal escape through the proton-sponge effect [76, 84]. Poly(amido amine) (PAA) dendrimers have also been used for polyplex gene delivery. These dendrimers are highly soluble and their size and surface charge can be precisely controlled. They have surface amine groups that can be highly functionalized to control surface charge. These polymers are also thought to elicit the proton sponge effect. Poly(lactide-co-glycolide) (PLGA) has also been used for gene delivery and has unique characteristics for controlled release, however its transfection efficiency suffers from its slow release of DNA. Finally, chitosan has been popular due to its excellent biocompatibility and biodegradability[85]. Chitosan has low toxicity and low immunogenicity, however it is insoluble at physiological pH. The polymers described have certain beneficial characteristics and show great potential for optimization and modification due to their tunability and functionalizability.

There are still significant challenges to face in designing the ideal polymer gene delivery system. The primary obstacle is their low transfection efficiency, which is much lower than that of viral gene

delivery. Current polyplex systems tend to lack the necessary functionality to cross at least one of the many barriers encountered during gene delivery. These barriers can include gene packaging, serum stability, cell-specific targeting, endolysosomal escape, transport through cytoplasm, nuclear localization, and unpackaging[76]. Specifically, it can be a challenge to design polymers that can balance complex stability and protection of DNA during the delivery stage with efficient release of DNA inside the cell [82]. Another challenge is to decrease their cytotoxicity. Cytotoxicity can occur due to accumulation of positive charge inside cells. As a result, there has been a focus on developing polyplexes that are hydrolytically degradable such as poly(β-amino ester)s (PBAEs). Their degradation both decreases cytotoxicity and is thought to improve the unpacking of DNA[82]. PBAEs have been used in non-viral neuronal transdifferentiation [50]. However, they are not hydrolytically stable in the extracellular environment making them worse at protecting the DNA during transportation. PAAs are much more hydrolytically stable allowing them to successfully transport DNA to cells, however their hydrolytic degradation is very slow and does not contribute to the unpacking of DNA inside cells. One research group had the idea to use poly(amido amine)s with repeating disulfide linkages (SS-PAAs) which allowed the polymer to be hydrolytically stable, but also quickly degradable by reduction of the disulfide linkages[82]. By allowing degradation of the polymer to depend on reduction, the idea was to have the vectors selectively degrade inside cells where there are high concentrations of reductases, such as glutathione and thioredoxin reductase, capable of breaking the disulfide linkages. These polymers did show increased transfection efficiency and lower cytotoxicity compared to PEI controls[82].

Several SS-PAAs were designed with different primary amine monomers, which had previously appeared to be favorable in gene delivery research (Figure 1). The 4-amino-1-butanol (ABOL) side groups showed good transfection efficiency and cell viability compared to the other SS-PAAs. This polymer has been used in the non-viral neuronal transdifferentiation of primary mouse embryonic fibroblasts[15].

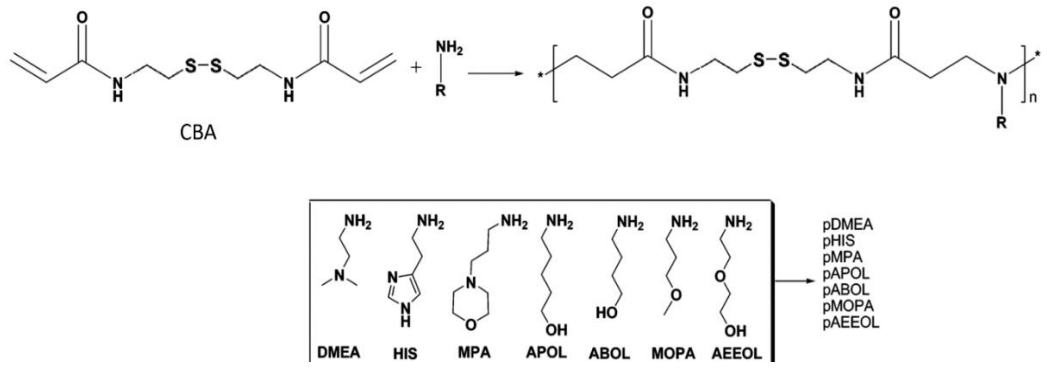

Figure 1 Bioreducible poly(amido amine)s with repetitive disulfide linkages[82].

Reprinted with permission from Lin, C.; Zhong, Z.; Lok, M. C.; Jiang, X.; Hennink, W. E.; Feijen, J.; Engbersen, J. F., Novel bioreducible poly(amido amine)s for highly efficient gene delivery. *Bioconjug Chem* **2007,** *18* (1), 138-45. Copyright 2007 American Chemical Society.

1.5. Topography-enhanced Transfection Efficiency

For successful transfection, genes must reach the nucleus of a cell where they can be expressed, and translated into proteins. Many barriers are encountered as the DNA complexes travel to a cell's surface, pass into a cell, travel through the cytoplasm, and enter the nucleus[86]. Each barrier reduces the overall efficiency of transfection. Since viruses have evolved to cross these barriers efficiently, viral vectors are much more efficient at transfecting cells than non-viral vectors. Low efficiency is the main limitation of the use of non-viral vectors compared to their viral counterparts due to imperfect performance at overcoming these barriers, which is not always well understood, and the compounding effect this can have on overall transfection efficiency. Development of ideal non-viral DNA carriers has been the focus of research efforts in improving efficient non-viral transfection systems, however substrate influences can also have significant effects on cells and their transfection efficiency[86].

Non-viral vectors enter cells by endocytosis. Macropinocytosis and clathrin- and caveolae-mediated endocytosis are the most studied in the context of non-viral carriers and can occur to varying

degrees depending on cell type and DNA complex characteristics[86]. Substrate characteristics can influence endocytosis through various mechanisms. The nano- and micro- topography of a substrate is known to affect a cell's rate of cell proliferation, cell differentiation, protein expression, cell spreading, and focal adhesion turnover. These cell functions can then affect the process of endocytosis. Investigating the influence of nano- and micro-topographies on the internalization of non-viral vectors may be a promising route for improving transfection efficiency.

Previous research studying the effects of substrate nano- and micro-topography on cellular endocytosis has shown that grating topographies of micron-width on fused silica substrates could cause an increase in phagocytosis by murine macrophages with increasing grating depth (ranging from 44 to 282nm)[87]. It has also been observed that human fibroblasts cultured on poly(methyl methacrylate) (PMMA) substrates with nano-pillars (160nm height, 100nm diameter, and 230nm pitch) would attempt to internalize the pillars through clathrin-mediated endocytosis[88]. Human osteoblasts have also been seen to attempt internalization of fixed titanium micro-pillars (5μm height, 5μm diameter, and 5μm pitch) through caveolae-mediated phagocytosis[89]. Electrospun PMMA fibrous scaffolds can modulate the mechanical properties and morphologies of human osteosarcoma cells which in turn modulate uptake of polystyrene nanoparticles[90].

Substrate topography has also been used to influence endocytosis to enhance the efficiency of non-viral transfection. One study screened a library of 160 different micro-scale pit geometries on polydimethylsiloxane (PDMS) substrates and found that the efficiency of Lipofectamine-mediated green fluorescent protein (GFP) transfection of human dermal fibroblasts could be improved 25% with pits of 4μm width and 1μm spacing compared to unpatterned substrates[16]. Another study compared nano- and micro-topographical effects as well as the effects of isolated pillar topographies and continuous grating topographies on endocytosis and transfection efficiency[17]. One of the findings was that a PMMA surface patterned with 200nm pillars could increase the efficiency of GFP delivered to hMSCs by Lipofectamine-mediated transfection in comparison to unpatterned controls.

1.6. Topography-enhanced/induced Differentiation and Transdifferentiation

Substrate topography has also been shown to have significant direct influence on cell conversions including differentiation and transdifferentiation[91]. Topography can enhance the differentiation of neuronal stem cells (NSCs), neuronal progenitor cells (NPCs), ESCs, and iPSCs to neurons as well as the neuronal transdifferentiation of fibroblasts and MSCs [18, 19, 92-98]. One study screened various topographies with different isotropic and anisotropic geometries and both nano- and micro-dimensions on PDMS substrates for their influence on mNCP differentiation [92]. Anisotropic nano- and micro-gratings as well as isotropic micro-pillars promoted neuronal differentiation while isotropic micro-pillars and holes promoted glial differentiation. Differentiation of mNPCs on PDMS substrates with gratings of 2μm width, 2μm spacing, and varying depth has shown that neurite elongation, alignment, and neuronal differentiation all increase with grating depth[93]. Electrospun polyphenylene sulfone (PPSU) nanofibers have been shown to be able to enhance neuronal differentiation of NSCs compared to 2D substrates as well as increase the activity of the neurons and control the direction of neural signals[99]. Screening of various micro- and nano-scale gratings, pillars, wells and hierarchical topographies on PMMA substrates showed that anisotropic patterns like gratings promoted neuronal differentiation of hESCs, and isotropic patterns such as pillars and wells promoted glial differentiation of hESCs[95]. Another study looked at differentiation of iPSCs into neuronal cells on electrospun fibrous substrates made from tyrosine-derived polycarbonate compared to 2D substrates of the same material made by spin coating[96]. The cells were infected with lentivirus to deliver the single transcription factor NeuroD1 before being seeded onto fibrous substrates. It was reported that the 3D fibrous substrates could guide maturation, electrical activity, and cell type purity *in vitro*. iN cells on 3D fibrous scaffolds around 100μm in size (with fibers around 3μm thick) were injected into *ex vivo* brain tissue and showed improved neurite outgrowth, cell survival, and electrical activity compared to cells injected without microscale substrates. Finally, when injected *in vivo* to mouse striatum, the fibrous scaffolds improved cell survival and engraftment.

Neuronal transdifferentiation of both hMSCs and MEFs has been enhanced by topographical influence. Additionally, hMSCs have been converted to neuronal-like cells by topography influence alone[18, 19, 97, 98]. hMSCs cultured on PDMS substrates with 350nm gratings acquired aligned and elongated cytoskeletons and nuclei, and showed up-regulation of neuronal markers[18]. When biochemical cues were additionally used to influence hMSCs towards neuronal lineage, the up-regulation of neuronal markers was further enhanced, however the nano-gratings were shown to have the largest impact on the transdifferentiation. Another study reported findings suggesting that nano-gratings induce this differential gene expression in hMSCs because hMSCs sense and transduce topographical signals through focal adhesions and actomyosin cytoskeleton contractility[19]. The influence of nano-topography on transdifferentiation of mouse embryonic fibroblasts to induced neurons by lentiviral delivery of BAM transcriptions factors has also been investigated [97]. The topographies studied included micro-posts (1µm diameter with 4µm spacing and 5µm depth, and 4µm diameter with 1µm spacing and 5µm depth) and micro-gratings (5µm width, spacing and depth) on polystyrene (PS) substrates. Final iN purity, conversion efficiency, and gene expression were improved with the micro-gratings, and neurite branching was increased on the micro-posts, but decreased with micro-gratings while neurite length was increased with both gratings and posts. Substrate topographies have also been shown to be beneficial in producing dopaminergic neurons by transdifferentiation[98].

1.7. PDMS Used for Patternable Substrates

Polydimethylsiloxane (PDMS) is a very commonly used polymeric organosilicon compound. It has been used extensively in microfluidics and soft lithography as well as biomedical applications such as drug delivery vehicles, blood-contacting biomaterials and microfluidics involving mammalian cell culture[100, 101]. This material is also often used to fabricate substrates for studying topographical or other

mechanical influence on cells. PDMS has ideal characteristics for cell culture including nontoxicity, biocompatibility, transparency, thermal stability and durability[100, 102]. Also the material can be patterned with micro- or nano-topographies by soft lithography and these topographies can be fabricated with good repeatability [92, 103, 104].

The structure of PDMS is shown in Figure 2. PDMS is made using a base (which is predominantly dimethylvinyl-terminated dimethylsiloxane), a curing agent (mostly comprised of dimethylhydrogen siloxane), and a metal-centred catalyst to promote crosslinking[105]. After curing, the surface of PDMS is hydrophobic which does not facilitate cell adhesion. Plasma oxidation can be used to make the PDMS surface more hydrophilic by adding silanol (SiOH) groups to the surface[106, 107]. The hydrophilicity achieved by plasma oxidation may decrease over time due to surface reorganization which can make PDMS poor at supporting cell cultures for long periods of time[100]. Longer cell culture on PDMS can be promoted by coating with extracellular matrix (ECM) proteins such as fibronectin, laminin, and collagen to support prolonged cell adhesion.

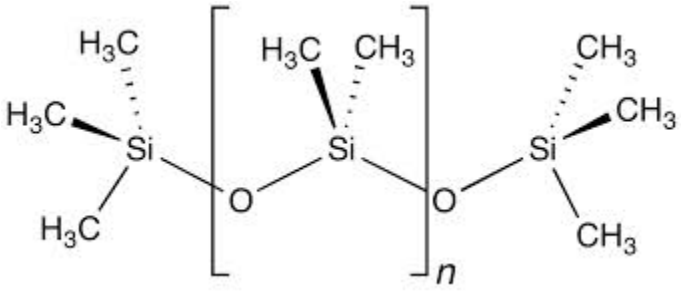

Figure 2 Molecular structure of PDMS. n indicates the repeating monomer.

Due to its tunable stiffness, elasticity, patternability, and compatibility with cell culture, PDMS has been used extensively to investigate the influences of substrate physical properties on cell behavior. For example, stiff and soft PDMS substrates were made to have a 10-fold difference in Young's modulus by using a 10:1 and 50:1 ratio of base to curing agent[108]. With these substrates, it was shown that mouse

hippocampal neurons cultured on stiff substrates had enhanced neuronal network activity. Another study used PDMS as a flexible cell culture substrate in a stretching device and showed cyclic stretching of soft substrates induces spreading and growth of PMEFs[109]. Finally, the patternability of PDMS has allowed investigation of the influence of micro- and nano-topographical substrates on cell behaviors including studies mentioned earlier looking at topographical influence on non-viral transfectability of cells and cell conversion[16, 18, 19, 110 17].

1.8. Project Motivation, Hypotheses, and Thesis Outline

Having a source of neuronal cells suitable for medical applications would be of great value. Cells fabricated by differentiation of ESCs or reprogramming followed by differentiation of iPSCs have their limitations, but have provided insight and inspired further study of other possible cell conversion processes. Transdifferentiation is a promising solution to many of the limitations associated with the use of ESCs and iPSCs, however most successes in the study of transdifferentiation have depended on the efficiency of viral transfection which is a hindrance to its clinical translatability. Non-viral neuronal transdifferentiation of mouse embryonic fibroblasts has been achieved with delivery of BAM neuronal lineage-specific transcription factors, but with low conversion efficiencies[15, 50]. In order to apply neuronal transdifferentiation to human cells and to make the process of neuronal induction relevant for use, neuronal transdifferentiation efficiency must be improved.

Interestingly, influence from nano- and micro-topography of cell substrates has been shown to enhance non-viral transfection and non-viral neuronal transdifferentiation in certain scenarios. The studies that relate to topographical effects on non-viral transfection which were most impactful in motivation of this thesis project showed that (1) PMMA substrates patterned with nano-pillars could increase the efficiency of non-viral Lipofectamine-mediated transfection of hMSCs compared to unpatterned

substrates[17] and (2) PDMS substrates patterned with micro-pits could increase the efficiency of non-viral Lipofectamine-mediated transfection of human dermal fibroblasts compared to unpatterned substrates[16]. Furthermore, the studies demonstrating topographical effects on non-viral transdifferentiation which were most impactful in the motivation of this project showed that (1) hMSCs cultured on PDMS substrates with nano-gratings showed up-regulation of neuronal markers[18, 19] and (2) transdifferentiation of mouse embryonic fibroblasts could be enhanced by topographies on PDMS substrates including micro-pillars, micro-holes, and micro-gratings[20]. In this study, we screened an array of nano- and micro-scale patterns with a wide variety of geometries on PDMS substrates for the effect that they have on non-viral transfection and non-viral neuronal transdifferentiation of hMSCs.

Our hypotheses are:

1. Nano- or micro-topographical PDMS substrates would be able to increase non-viral transfection efficiency of hMSCs.
2. Nano- or micro-topographical PDMS substrates would be able to enhance non-viral neuronal transdifferentiation of hMSCs.

In the next chapters of this thesis, the methods, results, and discussion of the two main components of this project will be presented, followed by a conclusion and recommendations for future work. Chapter 2 presents our work on topographical influence on non-viral transfection of hMSCs. Chapter 3 studies the topographical effects on non-viral neuronal transdifferentiation of hMSCs. Finally, Chapter 4 presents our conclusions and recommendations for future work.

Chapter 2: Non-viral Transfection of hMSCs on Topographically-patterned Substrates

2.1. Introduction

This chapter covers the methods and results of experiments aiming to address the hypothesis that nano- or micro-topographies can influence the efficiency of non-viral transfection of hMSCs. For these investigations, Lipofectamine 2000 was used to transfect hMSCs with an EGFP-expressing plasmid on topographically-patterned PDMS substrates. Lipofectamine was chosen as the non-viral transfection reagent for these studies since it is commonly used and commercially available. The EGFP-encoding plasmid was used so that transfection efficiency could be easily quantified using fluorescence imaging. PDMS MultiARChitecture (MARC) chip substrates were used to screen an array of micro- and nano-topographies (including gratings, lenses, pillars, wells, and hierarchical structures). MARC chip substrates increased screening throughput and decreased variability by enabling screening of all topographies with a single sample.

2.2. Methodology

2.2.1. PDMS MARC Chip and Unpatterned Chamber Substrate Fabrication

The original MARC chip master mold was prepared previously [92, 95, 103]. This master mold was composed of polycarbonate (PC) patterned areas arranged onto a silicon substrate and fused together into

a single layer with PDMS which formed unpatterned areas which framed the patterned PC areas (Figure 3). This was used to make a PDMS mold (Figure 4A), which had mirror image replicas of the topographies. The PDMS mold was then used to make the PDMS MARC chip substrates by soft lithography (Figure 4A). To do this, the PDMS mold was silanized by placing the mold into a vacuum chamber with 25µl of Trichloro(1*H*,1*H*,2*H*,2*H*-perfluorooctyl)silane (silane, Millipore Sigma) which was vacuum pumped for 30 minutes to create a low pressure environment that would cause the silane to vaporize. The vacuum was then turned off and the mold was left exposed to the silane vapor overnight. PDMS (Sylgard 184, Corning) was mixed at a 10:1 mass ratio of base to curing agent and poured onto the mold. The liquid PDMS was degassed for 15 minutes to remove large air bubbles and for an additional 30 minutes with a coverslip placed on top to encourage the complete filling of mold features. Afterwards, the filled mold was placed in an oven at 60°C overnight (around 12 hours) for PDMS curing. The newly formed PDMS MARC chip substrate was then peeled off the mold and placed back into the oven at 60°C for up to seven days in order to reduce the risk of having un-crosslinked oligomers in the PDMS substrates which could be toxic to cells during longer-term cultures. Soft lithography was repeated to make multiple MARC chip substrates. As an additional precaution, the first five MARC chips made from the mold after silanization were not used for cell culture experiments to reduce the risk of having residual silane transfer from the mold onto the cell substrate surfaces.

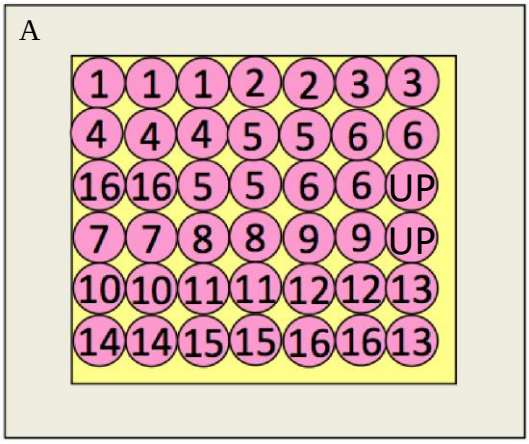

B

1. 250 nm lines, 250 nm space, 250 nm height
2. 250 nm lines, 250 nm space, 110 nm height
3. 460 nm lines, 70 nm space, 40 nm height
4. 2 µm lines, 2 µm space, 2 µm height
5. 1 µm lines, 2 µzam space, 120 nm height
6. 2 µm lines, 1µm space, 80 nm height
7. 250 nm lines on 2 µm lines (perpendicular)
8. 250 nm lines on 2 µm lines (parallel)
9. 250 nm pillars on 2 µm lines
10. 1 µm diameter & pitch, 0.3 µm sag concave microlens
11. 1 µm diameter & pitch, 0.3 µm sag convex microlens
12. 1.8 µm diameter, 2 µm pitch, 0.7 µm sag concave microlens
13. 1.8 µm diameter, 2 µm pitch, 0.7 µm sag convex microlens
14. 2 µm pillars, 12 µm pitch, 2 µm height
15. 1 µm holes, 6.5 µm pitch, 1 µm depth
16. 250 nm pillars, 400 nm pitch, 250 nm height

Figure 3. Topographical patterns and layout of MARC chip substrates. (A) Schematic diagram showing the arrangement of topographical patterns on MARC chip master molds made of PC (pink), PDMS (yellow), and Si backing covered by a PC sheet (brown). The PC areas labeled UP are unpatterned control areas. (B) List of patterns on MARC chip master mold and replicated onto PDMS MARC chip substrates.

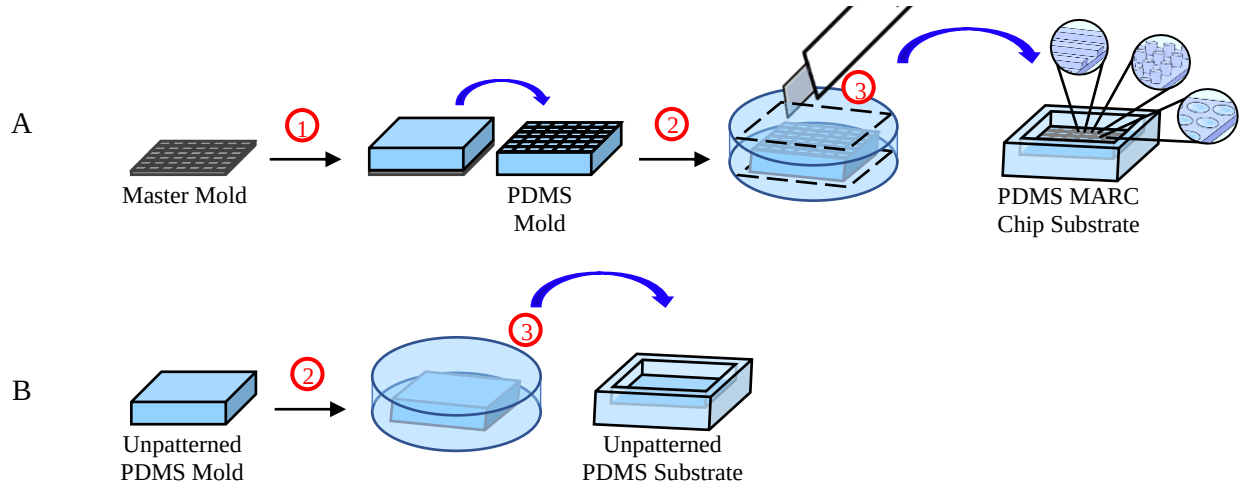

Figure 4. PDMS MARC chip and unpatterned chamber substrates fabrication. (A) Fabrication of MARC chip substrates by soft lithography. (B) Fabrication of unpatterned chamber substrates. (1) PDMS (10:1 ratio of base to curing agent) is poured onto the master mold, degassed, and cured overnight. (2) PDMS Mold is silanized, PDMS (10:1 ratio of base to curing agent) is poured onto the PDMS mold, degassed, and cured overnight. (3) PDMS is cut with extra space around mold to create chamber walls.

The MARC chips fit into the wells of a 6-well tissue culture plate, however, during fabrication these substrates were also made to have their own chamber walls (Figure 4A and Figure 5A). These helped to keep cells from falling off the MARC chip during cell seeding, and helped to reduce the consumption of reagents by limiting excess space around the cell culture surface area of interest.

Unpatterned PDMS control substrates with chamber walls (Figure 5B) were made similarly by pouring PDMS onto unpatterned PDMS molds followed by the same procedure (Figure 4B).

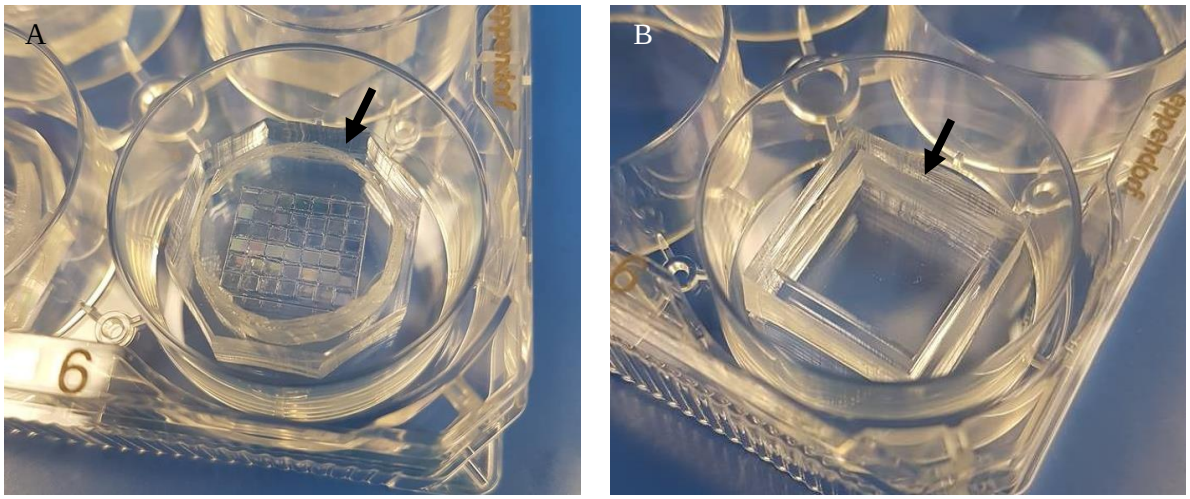

Figure 5. PDMS MARC chip and unpatterned chamber substrates in 6-well tissue culture plates. (A) MARC chip chamber substrate. (B) Unpatterned chamber substrate. Arrows point out PDMS chamber walls.

2.2.2. Sample Preparation for Scanning Electron Microscopy for Verification of Substrate Topographies

In preparation for scanning electron microscopy (SEM) imaging, PDMS substrates were cut into sections to fit onto 0.5" aluminum stubs (Agar Scientific). PDMS samples were adhered to the stubs with double sided carbon tape (Electron Microscopy Sciences) and the edges were coated with silver conductive paste (Sigma Millipore) to make a conductive bridge to the top surface of the sample (Figure 6). After at least 24 hours of letting the silver paste dry, the samples were gold coated with a Denton Vacuum Desk II sputter coater. Samples were put in a degasser, vacuum pumped for 30 minutes to create a low pressure environment, and left overnight to help remove moisture from the samples the night before imaging. Samples were then imaged using a LEO 1550 SEM (Ziess Germany).

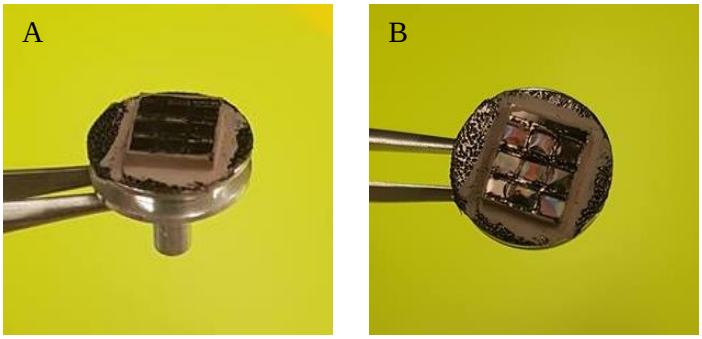

Figure 6. Mounted section of MARC chip substrate prepared for SEM imaging. (A) Angled view. (B) Top view.

2.2.3. Cell Culture and Substrate Sterilization

Human MSCs (Lonza) were thawed in Dulbecco's modified Eagle's medium (DMEM, Gibco) with 10% MSC qualified fetal bovine serum (Gibco) and expanded in MesenPRO RS medium (Gibco), a reduced serum (2%) medium formulated to support the growth of hMSCs, supplemented with 2 mM L-glutamine (Gibco) following Gibco's protocol. They were seeded for experiments between passages 5 to 7. Prior to seeding, PDMS substrates were plasma treated (Zepto, Diener Electronic), sterilized by sitting submerged in 70% ethanol for 30 minutes followed by UV irradiation for 20 minutes, and briefly rinsed with sterile phosphate buffered saline (PBS, Fisher BioReagents). Glass substrates were flame sterilized before cell seeding.

2.2.4. EGFP Plasmid Amplification

EGFP plasmid was shipped as purified plasmid from the Mechanobiology Institute, National University of Singapore, and tested upon arrival by observing fluorescence in transfected fibroblasts. For plasmid amplifications, 5 µl of plasmid DNA was combined with 50 µl of NEB 5-alpha Competent *E. coli* (New England BioLabs), which were generously provided to us from Dr. Marc Aucoin's lab at the

University of Waterloo, and then incubated on ice for 30 minutes. The cells were then heat shocked in a water bath at 42 °C for 45 seconds to transform the bacterial cells and then put back on ice. Five hundred microliters of SOC media (Sigma) was then added to the cells which were then incubated with shaking at 37 °C and 275 rpm for 1 hour. After incubation, 50 µl of the cell suspension was spread onto an agar plate containing kanamycin (Bio Basic). The plate was incubated at 37 °C overnight. The next day cells from an isolated colony on the agar plate were added to 25 ml of lysogeny broth (LB) with kanamycin and incubated in a flask on a shaker overnight at 37 °C and 275 rpm. The plasmid was purified using a QIAGEN Plasmid Midi Kit. The final purified plasmid concentration was measured with a NanoDrop ND-1000 Spectrophotometer.

2.2.5. Lipofectamine-mediated EGFP Transfection, Sample Staining, Fluorescence Imaging, and Transfection Efficiency Quantification

All Lipofectamine-mediated transfections were carried out with Lipofectamine 2000 (Invitrogen) by following Invitrogen's recommended protocol with a 36 hour transfection incubation time. Unless otherwise specified, samples were then prepared for fluorescence imaging. First, media was removed from the samples. The cells were washed once with PBS, and then fixed with pH adjusted 4% paraformaldehyde (PFA, Millipore Sigma) in PBS for 15 minutes. After fixing, samples were washed again with PBS and then permeabilized with 0.1% Triton X-100 (Sigma Millipore) in PBS for 15 minutes. After permeabilization, samples were washed once more with PBS, after which the cells were stained with either 1:2500 4′,6-diamidino-2-phenylindole (DAPI, Sigma Millipore) in PBS or with both 1:2500 DAPI and 1:750 Alexa Fluor 546 Phalloidin (Invitrogen) in PBS at 4 °C overnight. After staining, samples were washed again with PBS and then mounted onto glass coverslips with Fluoromount

(Invitrogen) for imaging. Imaging was done using epi-fluorescence microscopy (Zeiss Axio Observer.Z1).

To quantify transfection efficiency from the fluorescence images, the total number of cells in the images were counted using ImageJ software (NIH) and the number of EGFP expressing cells were counted by visual inspection. The transfection efficiency was quantified as the percentage of total cells imaged that expressed EGFP (Equation 2.1). A minimum of 100 cells were considered for each sample unless otherwise specified.

$$Transfection\ Efficiency = \frac{Number\ of\ EGFP\ Positive\ Cells}{Total\ Number\ of\ Cells} \times 100\% \qquad (2.1)$$

2.2.6. Determining Optimum Lipofectamine Concentration for hMSC Transfection

Following Invitrogen's recommendation, a few different DNA (µg) to Lipofectamine (µl) ratios were tested for our application before proceeding to our topography experiments. Ratios of 1:0.4, 1:2, and 1:3 were tested. The amount of EGFP-expressing plasmid DNA delivered to cells was held constant at 0.25 µg/cm^2. Negative controls did not receive any plasmid DNA. These tests were conducted on unpatterned glass substrates. Samples transfected with a 1:0.4 ratio were also made on unpatterned PDMS substrates to control for the effect of substrate material on Lipofectamine-mediated transfection. Human MSCs were seeded at a density of 5000 cells/cm^2. Thirty-six hours after seeding, cells were transfected followed by staining with DAPI and transfection efficiency was quantified using the methods described in section 2.2.5.

2.2.7. Determining Appropriate Seeding Density for Transfection studies on PDMS Substrates

To determine the seeding density that could be used to achieve 50-90% confluence of hMSCs on PDMS substrates, as is recommended by Invitrogen for optimal Lipofectamine-mediated transfections, hMSCs were seeded at 2000, 5000, and 8000 cells/cm^2 on PDMS substrates. Thirty-six hours after seeding, cells were fixed and stained with DAPI and Alexa Fluor 546 Phalloidin (as described in section 2.2.5). Cells were imaged with fluorescence microscopy to observe the resulting confluence. Samples seeded at 5000 and 8000 cells/cm^2 were found to give better confluence and so were transfected with EGFP-expressing plasmid (as previously described in section 2.2.5) with a DNA (µg) to Lipofectamine (µl) ratio of 1:0.4, in order to determine if this change in seeding density would affect transfection efficiency. Cells were fixed and stained with DAPI and Alexa Fluor 546 Phalloidin for fluorescence microscopy and transfection efficiency quantification as previously described (section 2.2.5).

2.2.8. Screening Topography Influence on Lipofectamine-mediated Transfection

To screen for influence of topographies on transfection efficiency, hMSCs were seeded at 8000 cells/cm^2 onto PDMS MARC chip substrates, transfected with EGFP-expressing plasmid using a 1:0.4 plasmid (µg) to Lipofectamine (µl) ratio, and stained with DAPI and Alexa Fluor 546 Phalloidin with methods described (section 2.2.5). Two by two tiled 10X magnification fluorescence images were taken of each patterned area of the MARC chip to capture the entirety of each area (Figure 7). Transfection efficiency for each pattern was calculated as the total number of EGFP positive cells combined from each area corresponding to the pattern divided by the total number of cells imaged on those areas. Any image with zero cells was not included in the analysis. Also, if the total number of cells combined from all the areas corresponding to a pattern on one MARC chip sample was less than 50, that pattern on that MARC

chip was not included in the presented results. Results from each MARC chip were normalized to the results from the unpatterned area of the MARC chip to account for possible sample-to-sample variation.

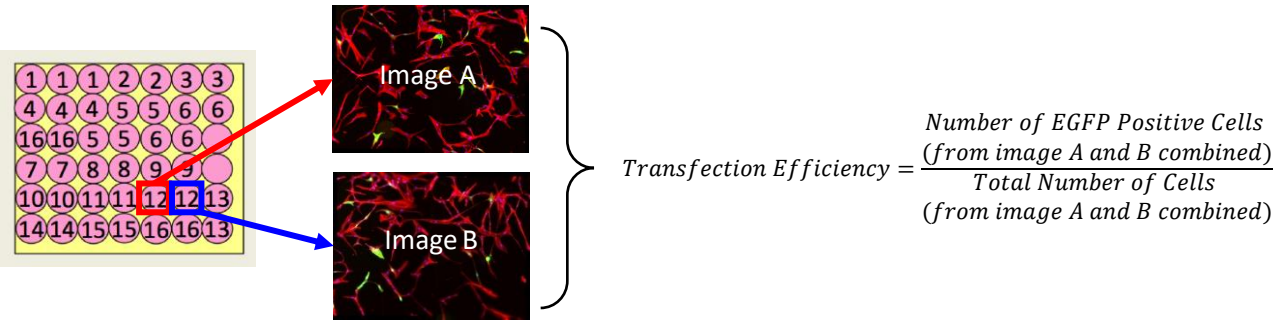

Figure 7. Quantification of transfection efficiency for patterns on MARC chip samples. Transfection efficiency for each topography was measured by taking fluorescence images of each area corresponding to the pattern and counting the percentage of cells expressing EGFP. EGFP-positive and total cell counts from all images corresponding to a pattern were pooled together to calculate transfection efficiency.

2.2.9. Investigating Cell Density and Cell Area on MARC Chip Topographies

Both cell density and average cell area were quantified for each topography of the MARC chip from fluorescent images taken during the transfection study (section 2.2.8). Cell density was quantified by dividing the cell count by the area of the image. These values were normalized by dividing by the average cell density of the unpatterned areas of the same MARC chip. Cell densities and transfection efficiencies were calculated from the same images. Average cell area was quantified by obtaining the fraction of the area containing cells using ImageJ software, multiplying by the total image area, and dividing by the cell count for that image.

2.2.10. Statistical Analysis

Statistical analyses were performed using a one-way analysis of variance (ANOVA) test with Dunnett's or Tukey's multiple comparisons test or using an unpaired t-test using Prism (GraphPad). All values are presented with mean values ± standard deviation. Statistical tests were considered significant when $P \leq 0.05$ (noted by *), $P \leq 0.01$ (noted by **), $P \leq 0.001$ (noted by ***), and $P \leq 0.0001$ (noted by ****).

2.3. Results

2.3.1. Scanning Electron Microscopy Verification of PDMS Substrate Topographies

The presence of topographical patterns on PDMS MARC chip substrates was verified by SEM imaging (Figure 8). The images show that soft lithography was an effective method for patterning the substrates with both micro- and nano- topographies. Line spacing of 250 nm high nano-gratings (pattern 1) were sometimes inconsistent (Figure 5 red arrow). This was likely due to the merging of multiple gratings on the PDMS mold.

Figure 8. SEM images of topographical patterns on PDMS substrates. The red arrow on pattern 1 points out inconsistent spacing of 250 nm high nano-gratings.

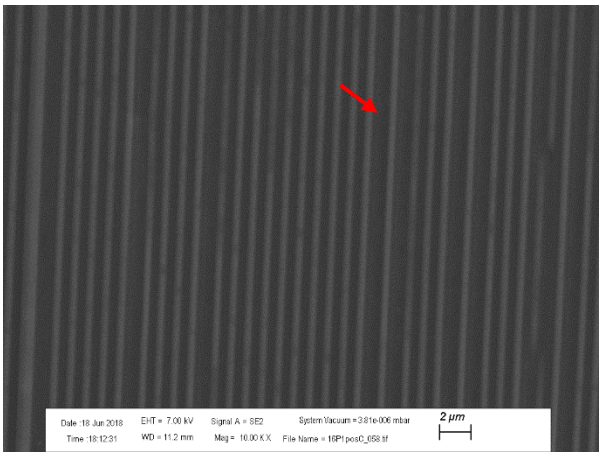

1 - 250 nm lines, 250 nm space, 250 nm height

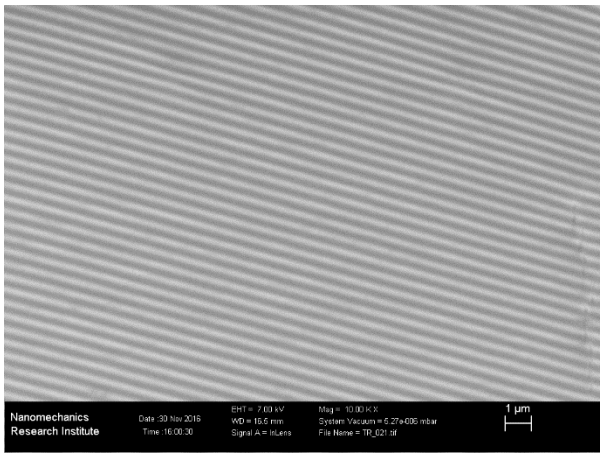

2 - 250 nm lines, 250 nm space, 110 nm height

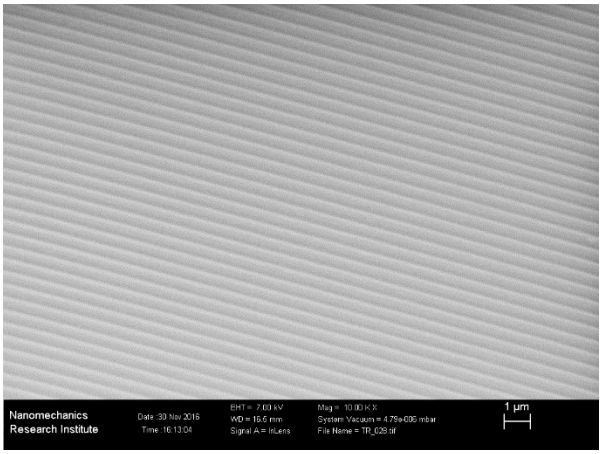

3 - 460 nm lines, 70 nm space, 40 nm height

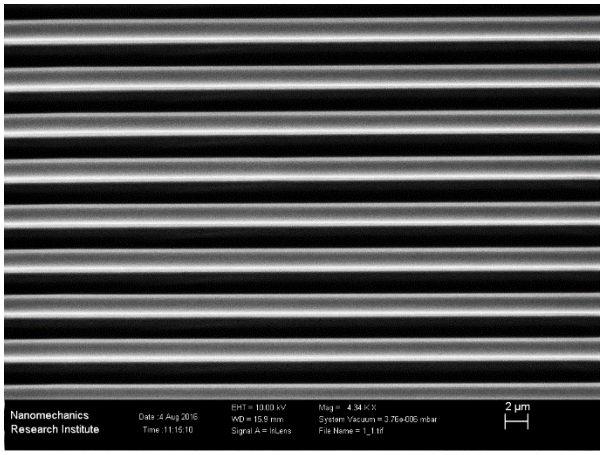

4 - 2 µm lines, 2 µm space, 2 µm height

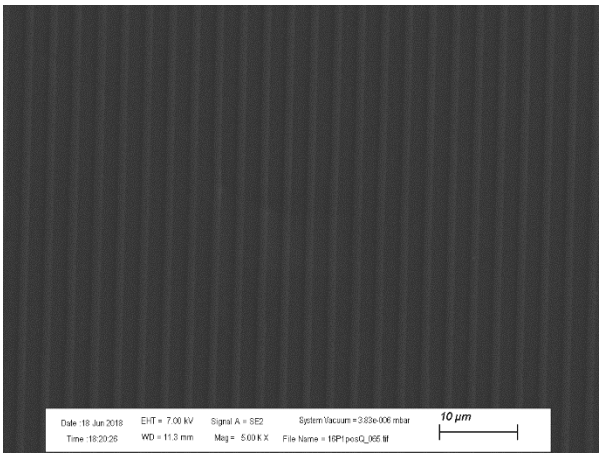

5 - 1 µm lines, 2 µm space, 120 nm height

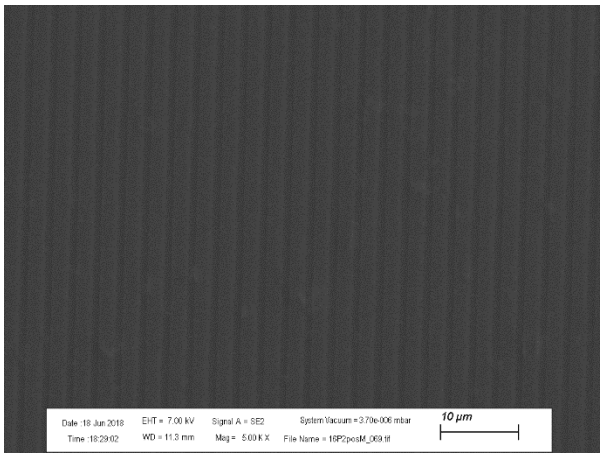

6 - 2 µm lines, 1µm space, 80 nm height

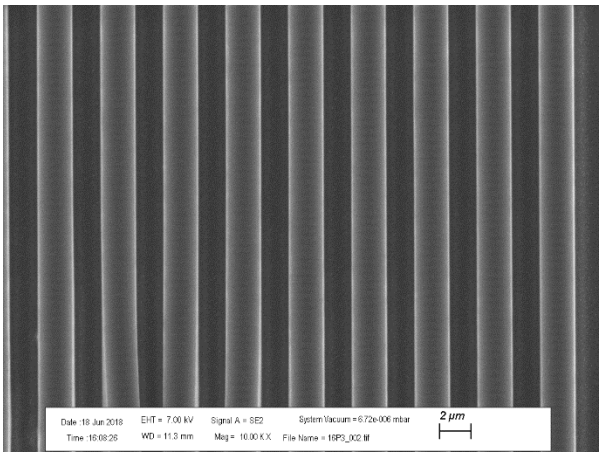

7 - 250 nm lines on 2 µm lines (perpendicular)

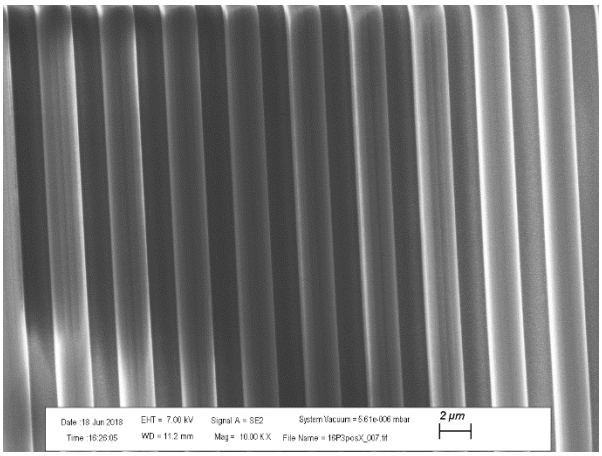

8 - 250 nm lines on 2 µm lines (parallel)

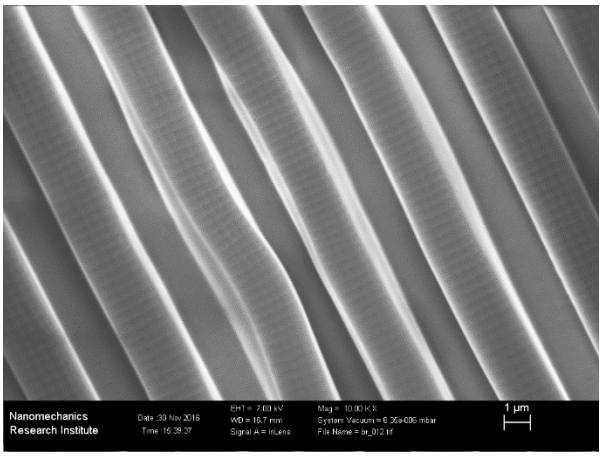

9 - 250 nm pillars on 2 µm lines

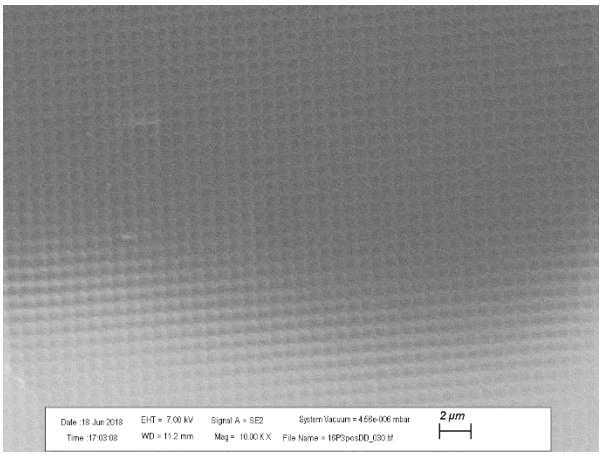

10 - 1 µm diameter & pitch, 0.3 µm sag concave lenses

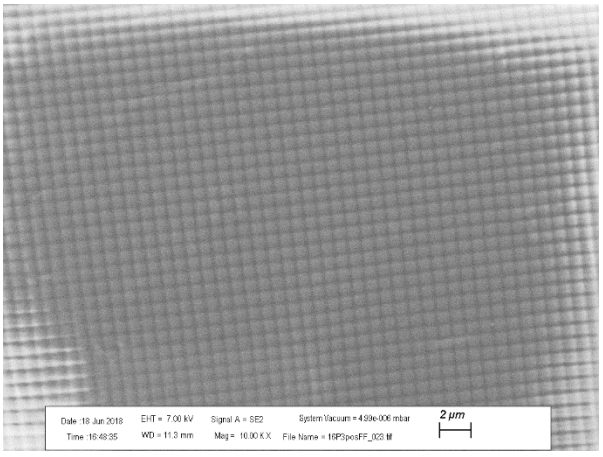

11 - 1 µm diameter & pitch, 0.3 µm sag convex lenses

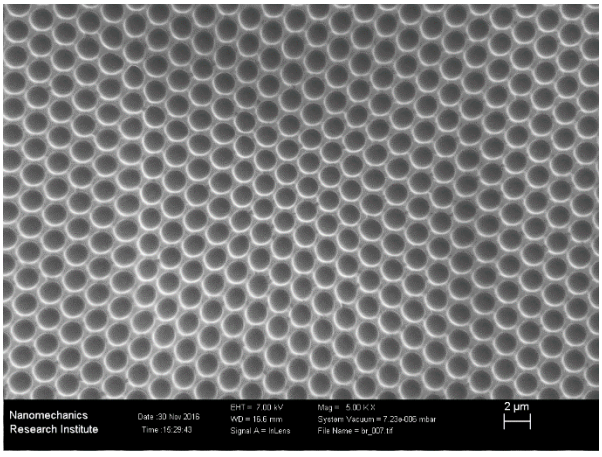

12 - 1.8 µm diameter, 2 µm pitch, 0.7 µm sag concave lenses

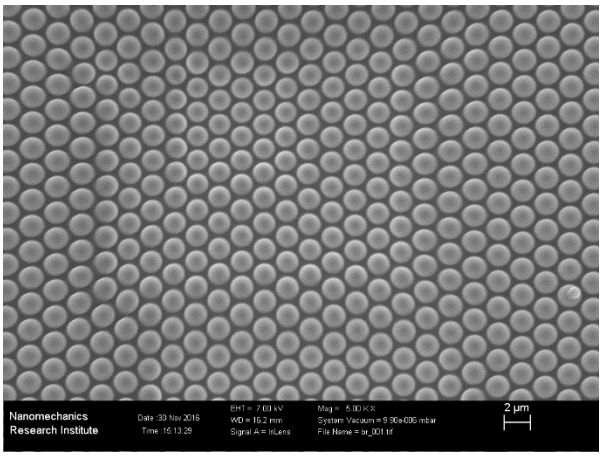

13 - 1.8 µm diameter, 2 µm pitch, 0.7 µm sag convex lenses

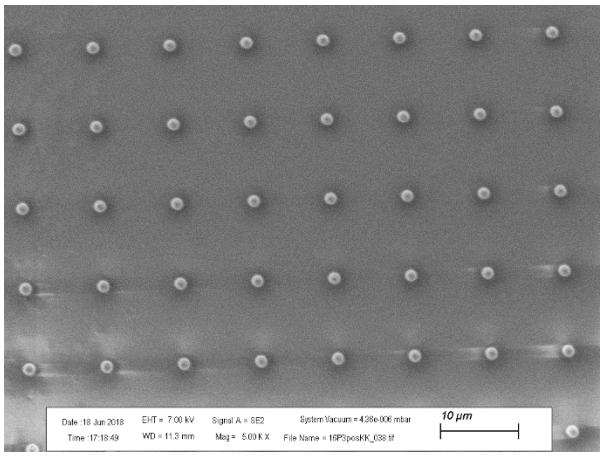

14 - 2 µm pillars, 12 µm pitch, 2 µm height

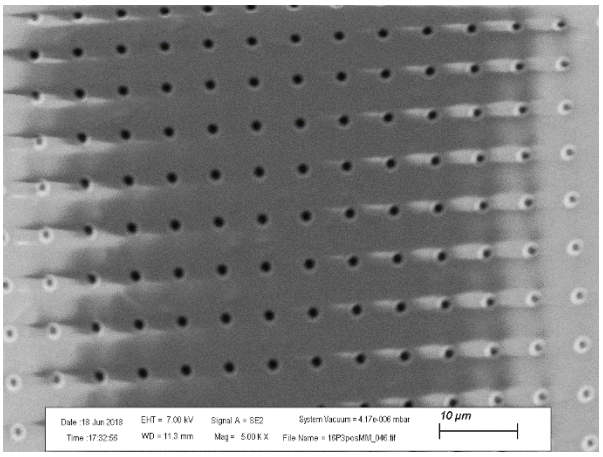

15 - 1 µm holes, 6.5 µm pitch, 1 µm depth

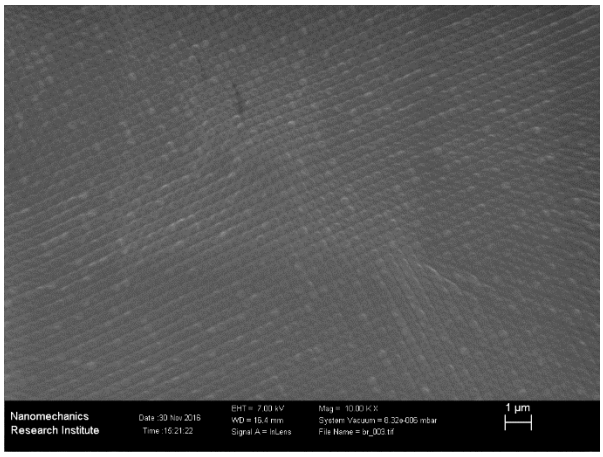

16 - 250 nm pillars, 400 nm pitch, 250 nm height

2.3.2. Effect of Plasmid to Lipofectamine Ratio on hMSC Transfection Efficiency

Fluorescence images of hMSCs on unpatterned glass substrates transfected with three different ratios of DNA (µg) to Lipofectamine (µl) showed that similar transfection efficiencies were achieved by transfections with a ratio of 1:0.4 as were achieved with higher ratios of Lipofectamine (Figure 9). Quantification of transfection efficiency confirmed these observations (Figure 10). Average transfection efficiencies of 6.9 ± 1.74%, 6.0 ± 0.44%, and 7.1 ± 1.33% resulted from using ratios of 1:3, 1:2, and 1:0.4

respectively. hMSCs seeded on unpatterned PDMS substrates transfected with a 1:0.4 ratio had transfection efficiency of 6.1% ± 0.91%, which showed that using a PDMS substrate did not affect performance of Lipofectamine-mediated transfection. Because no significant difference in transfection efficiency was observed between any of the samples, the lowest tested ratio of Lipofectamine (1:0.4) was used for all of the subsequent experiments to reduce risk of toxicity to cells as well as unnecessary consumption of the reagent.

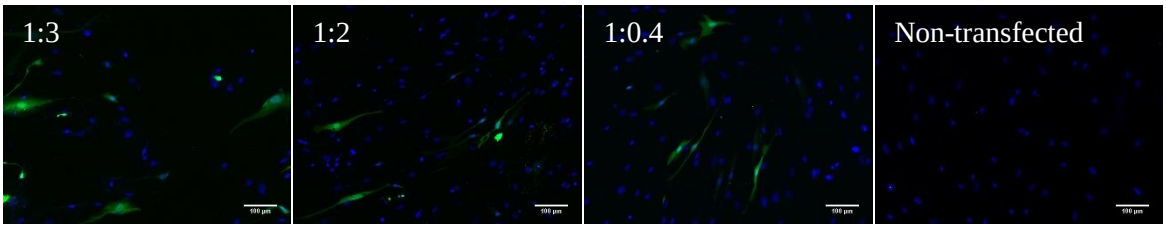

Figure 9. Fluorescence images of hMSCs transfected with varying ratios of DNA to Lipofectamine. The first three images from left to right represent the percentage of cells expressing EGFP (green) after transfection using 1:3, 1:2, and 1:0.4 ratios of DNA (µg) to Lipofectamine (µl). The image on the right shows non-transfected controls. Cells are stained with DAPI (blue). These samples were on unpatterned glass substrates. Scale bars are 100 µm.

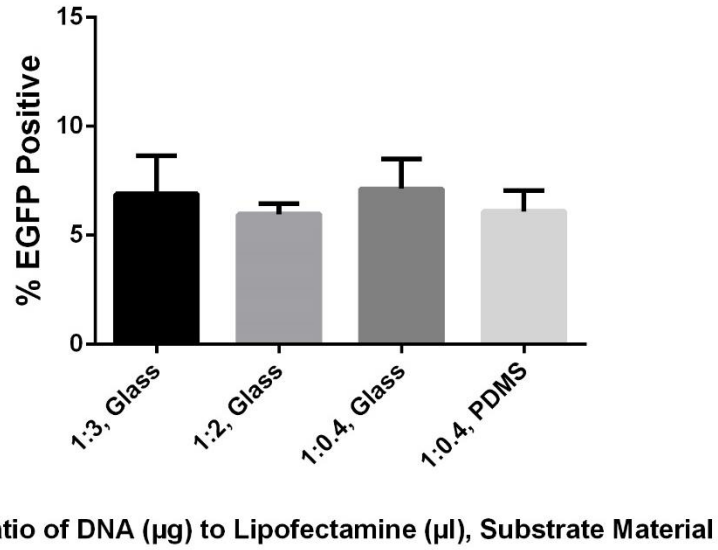

Figure 10. Quantification of transfection efficiency of hMSCs transfected with varying ratios of DNA to Lipofectamine. Transfection efficiency of hMSCs transfected by using 1:3, 1:2, and 1:0.4 ratios of plasmid (µg) to Lipofectamine (µl) on unpatterned glass substrates and using a 1:0.4 ratio on unpatterned PDMS substrates (n=3).

2.3.3. Effect of Seeding Density on Confluence of hMSCs on PDMS Substrates and Evenness of Seeding across PDMS MARC Chip Substrates

In order to determine seeding density on PDMS substrates that would achieve 50-90 % cell confluency, recommended for Lipofectamine transfections, cells were seeded at 2000, 5000, and 8000 cells/cm^2. Based on fluorescence imaging 36 hours after seeding, a seeding density of 8000 cells/cm^2 gave the best results on unpatterned PDMS substrates (Figure 11 A-C). Increasing seeding density from 5000 to 8000 cells/cm^2 did not have any effect on the efficiency of Lipofectamine-mediated transfection (Figure 11 D).

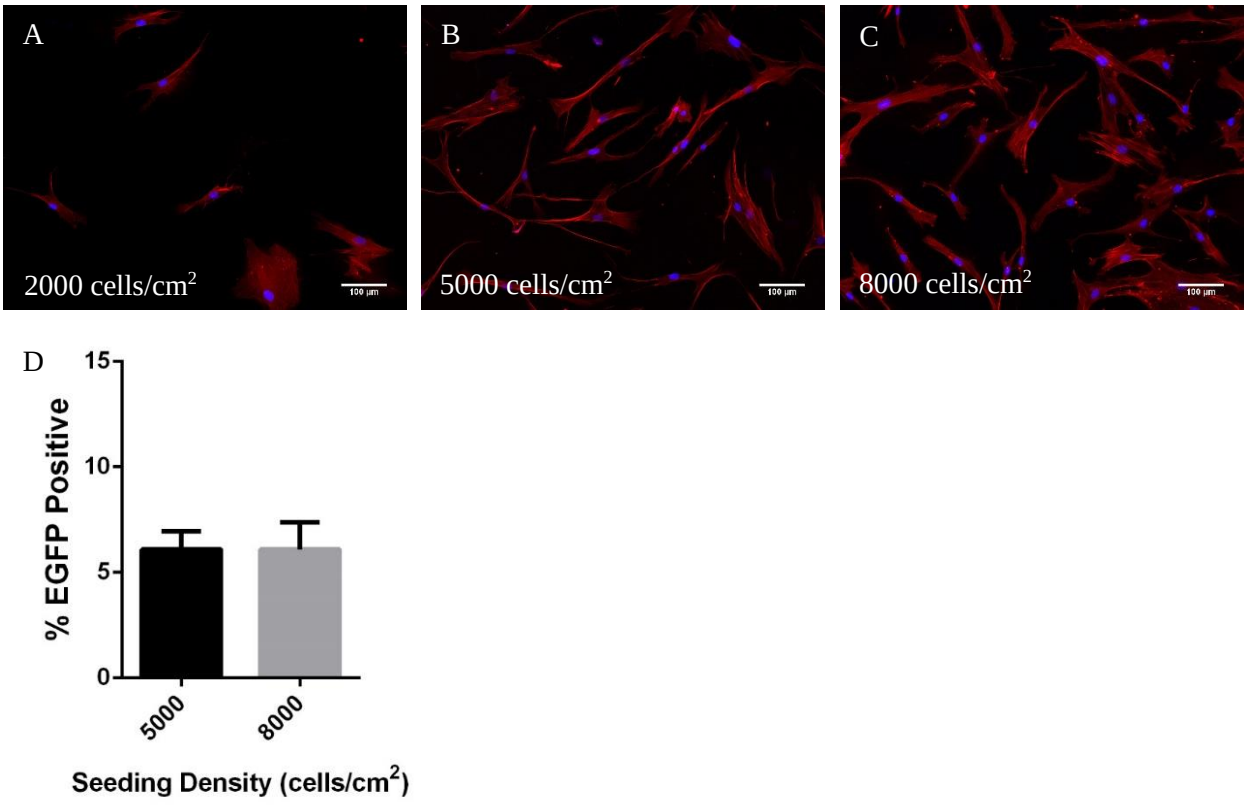

Figure 11. Confluence and transfection efficiency after seeding hMSC at varying densities. Fluorescence microscopy images showing resulting confluence of hMSCs seeded on unpatterned PDMS substrates at (A) 2000, (B) 5000, and (C) 8000 cells/cm^2. Cells are stained with Alexa Fluor 546 Phalloidin (red) and DAPI (blue). Scale bars are 100 µm. (D) Resulting transfection efficiency of cells seeded at 5000 and 8000 cells/cm^2 on unpatterned PDMS substrates (n=2).

When cells were seeded onto a PDMS MARC chip at 5000 cells/cm^2, only about 11% of the patterned areas had over 20% cell confluency. These areas were dispersed across the MARC chip. The other patterned areas only had cells close to their edges. This could have been due to variable effects that the topographies have on cell attachment. With a higher seeding density of 8000 cells/cm^2, cells were more uniformly seeded across all topographical areas of the MARC chip at 36 hours after seeding. For this reason, in all subsequent experiments presented in this chapter, cells were seeded at 8000 cells/cm^2. Figure 12 shows the confluence of cells, seeded at 8000 cells/cm^2, on various patterns of the MARC chip after the cells were transfected (72 hours after seeding).

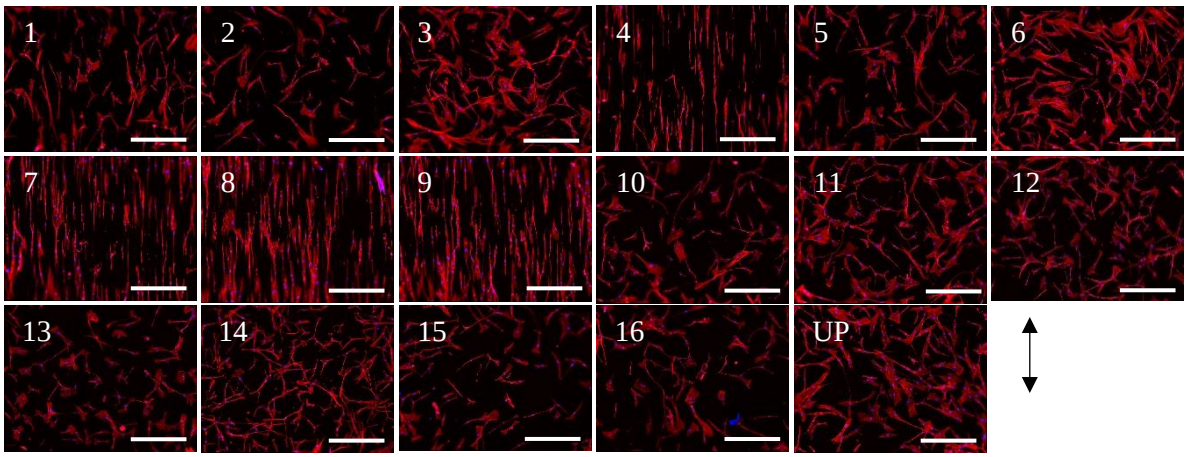

Figure 12. Cell density on MARC chip patterns after seeding at 8000 cells/cm^2. Fluorescence images of hMSCs on areas of PDMS MARC chip patterned with topographies (1 to 16) and on unpatterned area of MARC chip (UP), 72 hours after cells were seeded at 8000 cells/cm^2. Cells are stained with Alexa Fluor 546 Phalloidin (red) and DAPI (blue). The arrow (bottom right) represents the direction of gratings. Scale bars are 500 µm.

2.3.4. Effects of Topographies on Cell Density and Cell Area

Quantification, from fluorescence images taken of hMSCs on MARC chip topographies after transfection, showed that none of the topographies caused statistically significant differences in final cell density compared to the unpatterned areas of the MARC chips (Figure 13 A). Quantification of average

cell area on the MARC chip showed that the hierarchical topography with 250 nm pillars on 2 µm gratings with 2 µm spacing and 2 µm height (pattern 9) caused a statistically significant decrease in average cell area compared to the unpatterned areas of the MARC chips with $P \leq 0.05$ (Figure 13 B). It was notable that all of the topographies involving 2 µm wide gratings with 2 µm spacing and 2 µm height (patterns 4, 7, 8, and 9) caused a decrease in the mean cell area. This is likely related to the fact that cells aligned along the 2 µm grating topographies only extending along the grating axis and not extending in other directions, as can be seen in Figure 12.

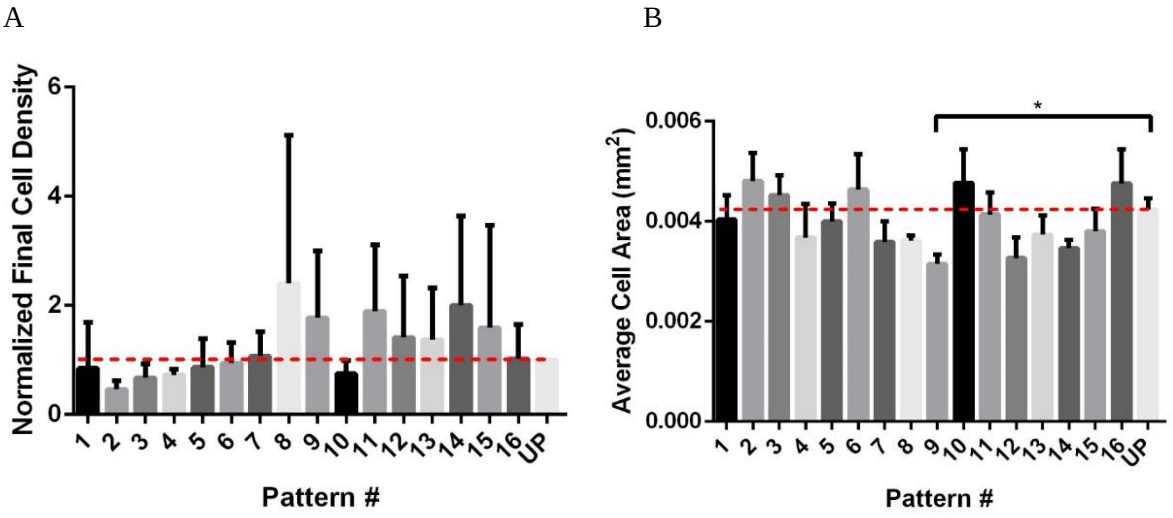

Figure 13 Normalized final cell density and average cell area on patterns of the MARC chip after transfection. (A) Final cell density values from each pattern of a MARC chip were normalized to the results of the unpatterned area of the same MARC chip. $2 \leq n \leq 7$ is the number of MARC chips. (B) $4 \leq n \leq 8$ is the number of patterned areas, on two different MARC chips, from which data was taken. * denotes statistical significance with $p \leq 0.05$. The red lines indicate the levels of normalized final cell density and average cell area on unpatterned areas of MARC chips.

2.3.5. Effects of Topographies on Efficiency of Lipofectamine-mediated Transfection

Screening of Lipofectamine-mediated EGFP transfection of hMSCs on PDMS MARC chip substrates did not show statistically significant changes in transfection efficiency caused by the topographical patterns (Figure 14). However, a subset of topographies which were seen to have the

highest positive or negative effect on transfection were selected for further study based on the trends seen in these results. The topographies selected were gratings with 250 nm width, spacing, and height (pattern # 1), gratings with 1 µm width, 2 µm spacing, and 120 nm height (pattern #5), concave lenses with 1 µm diameter and pitch, and 0.3 µm sag (pattern # 10), convex lenses with 1 µm diameter and pitch, and 0.3 µm sag (pattern # 11), holes with 1 µm diameter, 6.5 µm pitch, and 1 µm depth (pattern #15), and pillars with 250 nm diameter, 400 nm pitch, and 250 nm height (pattern # 16). Figure 15 shows representative fluorescence microscopy images of transfected cells on these selected patterns.

The topography patterns selected due to their increase in transfection efficiency were 1, 5, 10, 15, and 16 (6 was not included because it is similar to pattern 5; pattern 6 was gratings of 2 µm width, 1µm spacing, 80 nm height). Pattern 11 was selected because of particular interest in its contrasting effects compared to pattern 10. Since the two patterns are inverse of each other (concave and convex micro-lenses of the same dimensions), we would be interested to see if the direction of curvature would correlate to an effect on transfection efficiency. Interestingly, patterns 1, 5, and 10 which increased the mean transfection efficiency also showed decreased cell density compared to unpatterned controls (Figure 13 A).

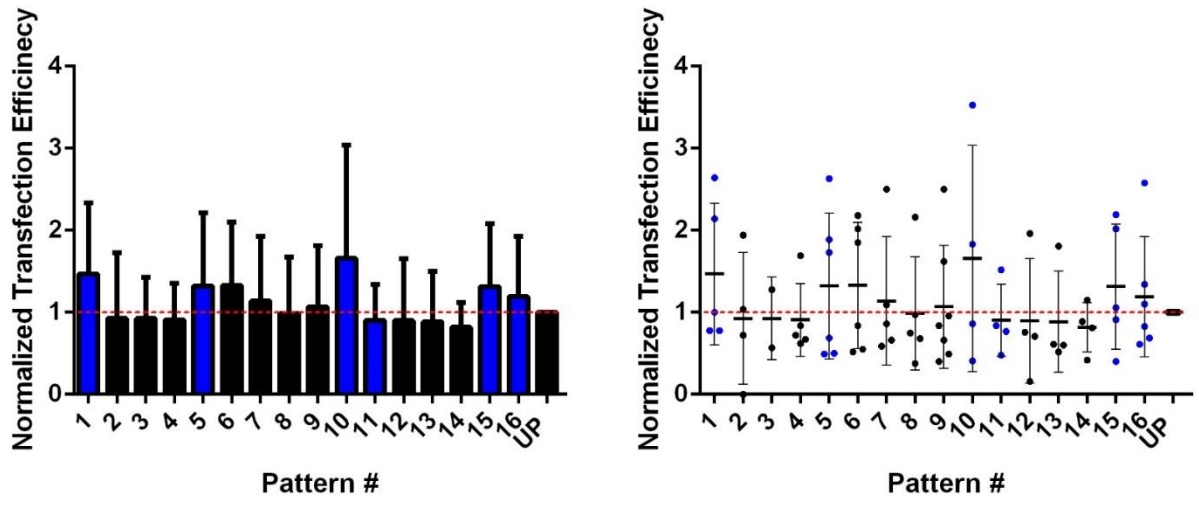

Figure 14. Transfection efficiency achieved on patterned areas of MARC chip. Values are normalized to results from unpatterned areas of the same MARC chip sample ($2 \leq n \leq 7$). Red line indicates the level of transfection on unpatterned areas of MARC chips. The same data is represented in the bar graph (left) and dot plot where each dot represents an experiment replica (right). Blue indicates the patterns that were of interest for further study.

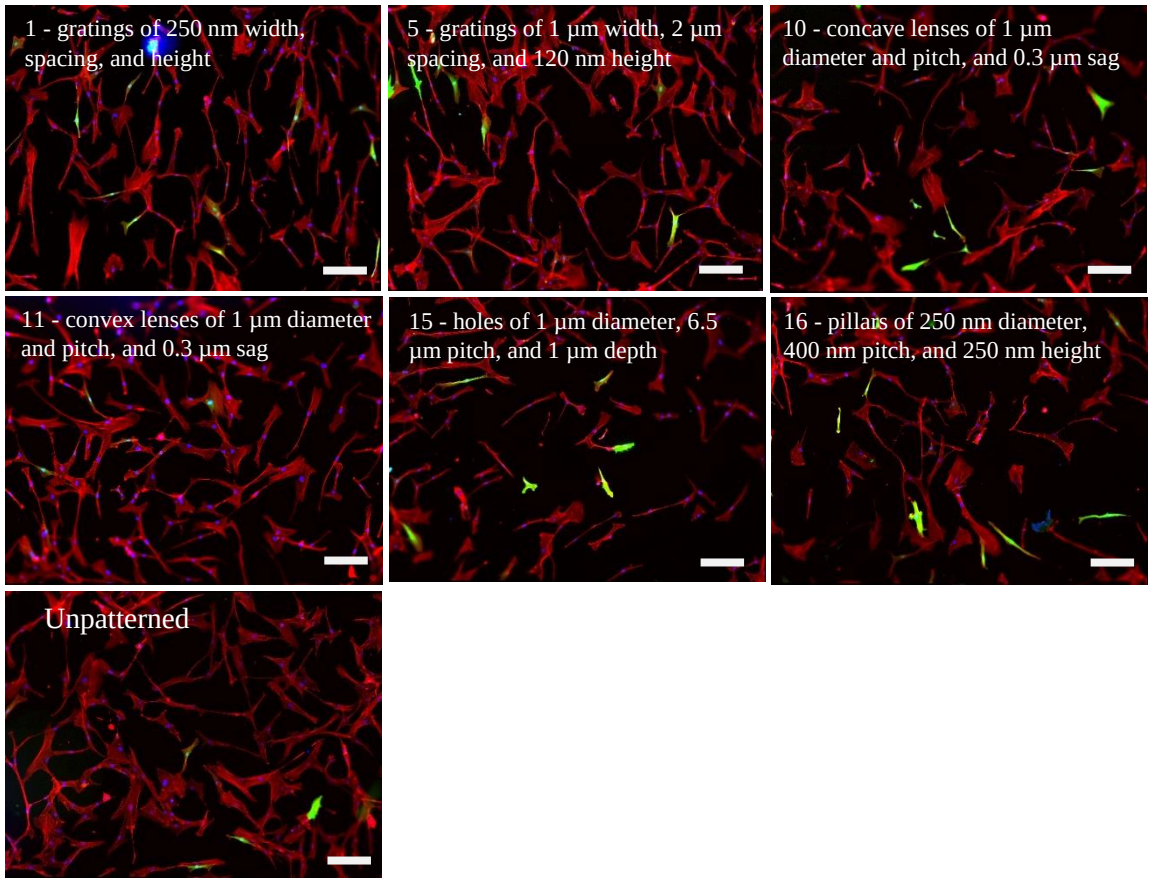

Figure 15. Representative fluorescence microscopy images of EGFP transfected cells on patterned areas of MARC chip for selected patterns. Numbers and labels identify the topographical patterns. Cells are stained with Alexa Fluor 546 Phalloidin (red) and DAPI (blue). Scale bars are 200 µm.

2.3.6. Correlation of Transfection Efficiency with Cell Density and Cell Area

Based on the observation that certain topographies with the strongest positive effect on transfection efficiency also have a negative effect on cell density (patterns 1, 5, 6, and 10) and that certain topographies with a negative effect on transfection efficiency also have a positive effect on cell density (patterns 11, 12, 13, and 14), we were interested to see how these two factors were correlated in our data. The scatter plot presented in Figure 16 shows the mean normalized transfection efficiency observed on each topography of the MARC chip versus the mean normalized final cell density of each topography.

Each dot represents a topography as defined in the figure. The data sets were calculated to have a Pearson product-moment correlation coefficient (R) of -0.34 and a coefficient of determination (R^2) of 0.11. We can see this low negative correlation represented in the scatter plot.

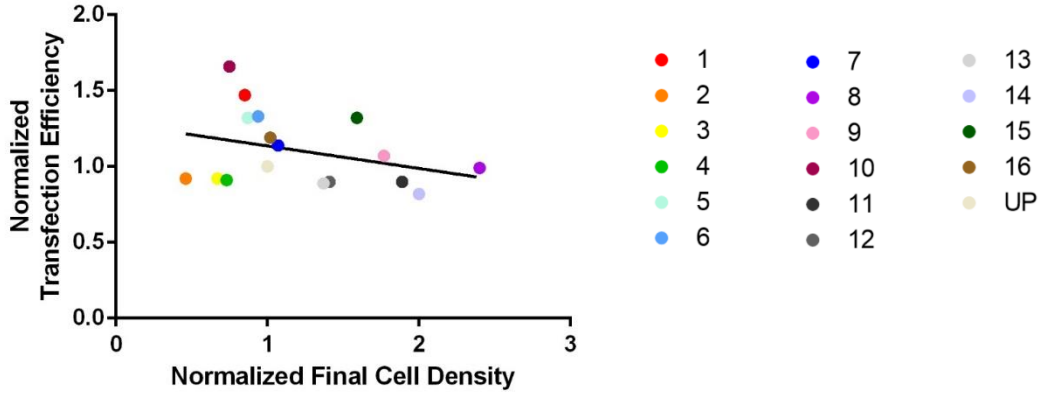

Figure 16 Scatter plot showing low negative correlation between the mean normalized transfection efficiency and mean normalized final cell density. Each dot represents results from one topography of the MARC chip. The line of best fit (black) has R = -0.34 and R^2 = 0.11.

In the scatter plot of mean normalized transfection efficiency versus mean normalized final cell density (Figure 16), there are three clusters that each closely follow different trend lines. These clusters are more clearly shown on separate graphs in Figure 17. We were curious to see if the topographies in each cluster were related in some way. We considered their geometry (lenses, pillars, gratings or holes), height (h, > 300 nm or ≤ 300 nm), height to width aspect ratio (h/w, > 0.3 or ≤ 0.3), size scale (nano or micro), and average cell area (> 0.0042 mm^2 or < 0.0042 mm^2; 0.0042 mm^2 was the average cell area on unpatterned areas of the MARC chip) (Table 2). Different geometries were dispersed among all three clusters. Interestingly, 5 out of the 6 patterns in cluster 1 had height ≤ 300 nm and 3 out of the 4 patterns in cluster 2 have height ≥ 700 nm while cluster 3 had topographies with height ranging between 40 nm and 2 µm. Clusters 1 and 3 had a mix of high and low average cell area as well as micro and nano-scale

topographies. Cluster 2, however, uniquely contained micro-scale topographies that also cause low average cell area.

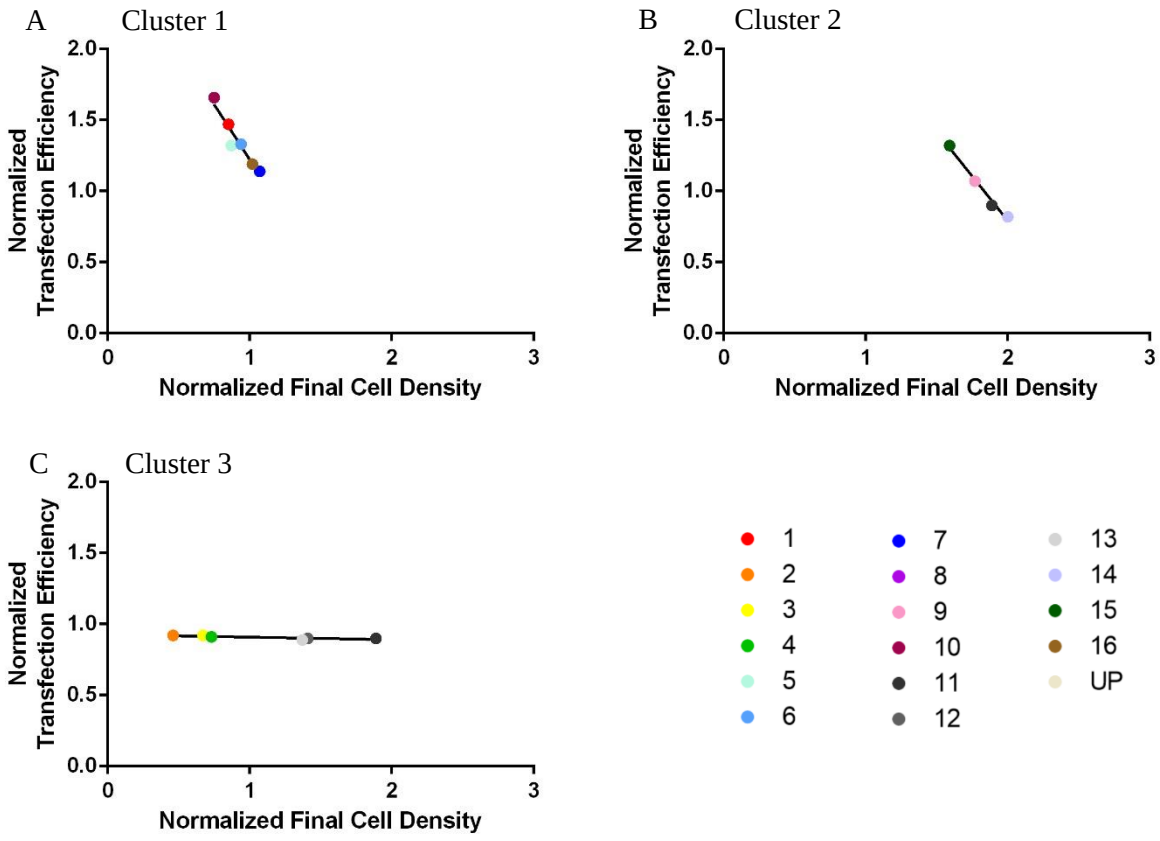

Figure 17. Clusters found within the scatter plot of mean normalized transfection efficiency versus mean normalized final cell density. (A – C) Three different clusters of data on the scatter plot of mean normalized transfection efficiency versus mean normalized final cell density. (A) Cluster 1 follows a trend line with R = -0.96 and R^2 = 0.92. (B) Cluster 2 follows a trend line with R = -0.99 and R^2 = 0.99. (C) Cluster 3 follows a trend line with R = -0.82 and R^2 =0.67. Each dot represents results from one topography of the MARC chip.

Table 2 Comparison of the characteristics of topographies in clusters found within the scatter plot of mean normalized transfection efficiency versus mean normalized final cell density. Topographies were considered Nano if all of their features (width, height, and spacing) were less than 1µm and were considered Micro if at least one of their features was greater than 1µm. High average cell area is defined as > 0.0042 mm^2. Low average cell area is defined as < 0.0042 mm^2. 0.0042 mm^2 was the average cell area on unpatterned areas of the MARC chip. Topographies were considered micro-scale if they had any micro-scale dimension.

Cluster	Normalized Transfection Efficiency	Normalized Cell Density	ID	Topography Description	Lenses / Pillars / Gratings / Holes	h Deep (>0.3µm) or Shallow (≤0.3)	h/w High (>0.3) or Low (≤0.3)	Nano or Micro	Avg. Cell Area (higher or lower than on UP)
1	1.66	0.75	10	1 µm diameter & pitch, 0.3 µm sag concave microlens	Lenses	Shallow	Low	Micro	High
	1.47	0.85	1	250 nm lines, 250 nm space, 250 nm height	Gratings	Shallow	High	Nano	Low
	1.32	0.87	5	1 µm lines, 2 µm space, 120 nm height	Gratings	Shallow	Low	Micro	Low
	1.33	0.94	6	2 µm lines, 1µm space, 80 nm height	Gratings	Shallow	Low	Micro	High
	1.19	1.02	16	250 nm pillars, 400 nm pitch, 250 nm height	Pillars	Shallow	High	Nano	High
	1.14	1.07	7	250 nm lines on 2 µm lines (perpendicular)	Gratings	Deep	High	Micro	Low
2	1.32	1.59	15	1 µm holes, 6.5 µm pitch, 1 µm depth	Holes	Deep	High	Micro	Low
	1.07	1.77	9	250 nm pillars on 2 µm lines	Gratings	Deep	High	Micro	Low
	0.90	1.89	11	1 µm diameter & pitch, 0.3 µm sag convex microlens	Lenses	Shallow	Low	Micro	Low
	0.82	2.00	14	2 µm pillars, 12 µm pitch, 2 µm height	Pillars	Deep	High	Micro	Low
3	0.92	0.46	2	250 nm lines, 250 nm space, 110 nm height	Gratings	Shallow	High	Nano	High
	0.92	0.67	3	460 nm lines, 70 nm space, 40 nm height	Gratings	Shallow	Low	Nano	High
	0.91	0.73	4	2 µm lines, 2 µm space, 2 µm height	Gratings	Deep	High	Micro	Low
	0.89	1.37	13	1.8 µm diameter, 2 µm pitch, 0.7 µm sag convex microlens	Lenses	Deep	High	Micro	Low
	0.90	1.41	12	1.8 µm diameter, 2 µm pitch, 0.7 µm sag concave microlens	Lenses	Deep	High	Micro	Low
	0.90	1.89	11	1 µm diameter & pitch, 0.3 µm sag convex microlens	Lenses	Shallow	Low	Micro	Low

The correlation between cell area and transfection efficiency was also examined. The scatter plot in Figure 18 shows the mean normalized transfection efficiency observed on each topography of the MARC chip versus average cell area observed on each topography. Each dot represents a topography as defined in the figure. The data sets were calculated to have a correlation coefficient of 0.38. We can see this low positive correlation represented in the scatter plot.

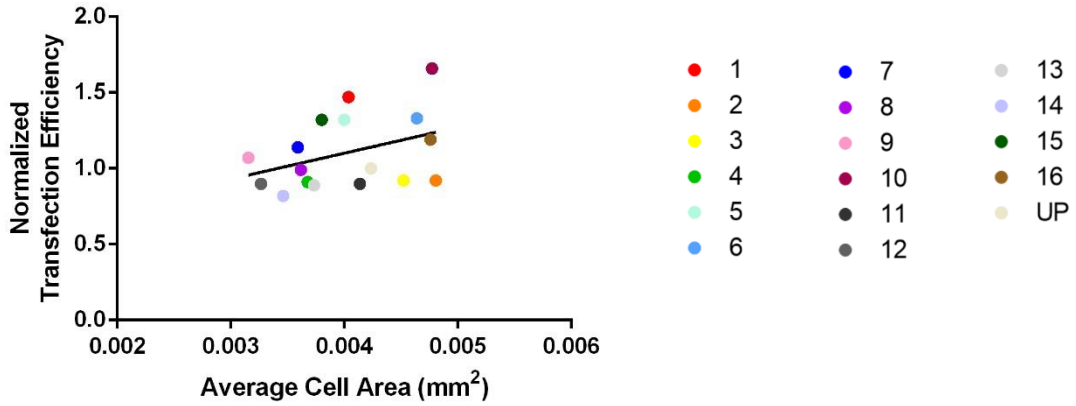

Figure 18. Scatter plot showing low positive correlation between the mean normalized transfection efficiency and average cell area. Each dot represents results from one topography of the MARC chip. The line of best fit (black) has R = 0.38 and R^2 = 0.14.

Principal component analysis was performed on measurements of normalized transfection efficiency, normalized average cell area, and normalized cell density, from five different MARC chips, as well as independent variables describing the features of each topography, and is presented in Appendix A.

2.4. Discussion

The work covered in this chapter first looks at the fabrication and characterization of the patterned PDMS substrates. SEM images showed that all patterns were successfully replicated onto the PDMS substrates. The width and spacing of the topographical pattern # 1, designed to be gratings with

250 nm width, spacing, and height, were inconsistent. This was likely due to the merging of multiple gratings on the PDMS mold before fabrication of substrates. Lateral collapse or pairing is a common problem with PDMS gratings, most commonly seen in high aspect ratio PDMS topographies[111-113]. Using PDMS with a higher ratio of curing agent to base might help mitigate this problem. The width and spacing of other topographical features were as expected. For more precise verification of the fidelity of topographical feature height, other techniques would be required. Techniques that could be used to measure the height of these features are atomic force microscopy (AFM) or digital holographic microscopy (DHM). For our purposes, we were satisfied with seeing the presence of the topographies and that they were predominantly as expected.

Next, we set out to define the experimental parameters we would use for our studies of Lipofectamine-mediated transfection of hMSCs on PDMS substrates. This involved selecting the ratio of DNA to Lipofectamine to use for our transfections and determining the seeding density to achieve appropriate hMSC confluency on PDMS substrates. After testing a few DNA (µg) to Lipofectamine (µl) ratios, 1:0.4 was found to be an effective ratio for Lipofectamine transfections and was therefore used in all subsequent tests. A seeding density of 8000 cells/cm^2 was found to give close to 50 % confluence which was deemed appropriate. It was also verified that the change in confluence between a seeding density of 5000 cells/cm^2 and 8000 cells/cm^2 did not affect the transfection efficiency.

It was repeatedly observed that on a single sample, areas of abnormally high or low cell confluence caused large variations in transfection efficiency (Figure 19 A and B). Areas of 95-100 % confluence had extremely low transfection compared to the average transfection efficiency of the sample, while areas with greater than 0 % and lower than 10 % confluence tended to have inflated transfection efficiency. This is not surprising since confluent cells have a slower growth rate which impedes transfection as cell division is required for Lipofectamine-mediated transfection [86, 114].

The fluctuation in cell density might not affect statistical analysis if we have a sufficiently large population of cells on a large cell culture area. However, it is a concern when working with the MARC

chip as each pattern is confined to a small area of the substrate. If this area happens to have too many or too few cells compared to the rest of the substrate, due to uneven seeding, then the data on transfection efficiency for that pattern could be strongly influenced by cell density causing increased variance. Hence, we made extra effort to ensure seeding on MARC chip substrates was even across each patterned area of the sample. Even seeding was more easily achieved with a seeding density of 8000 cells/cm^2 rather than 5000 cells/cm^2 which confirmed our choice of seeding density.

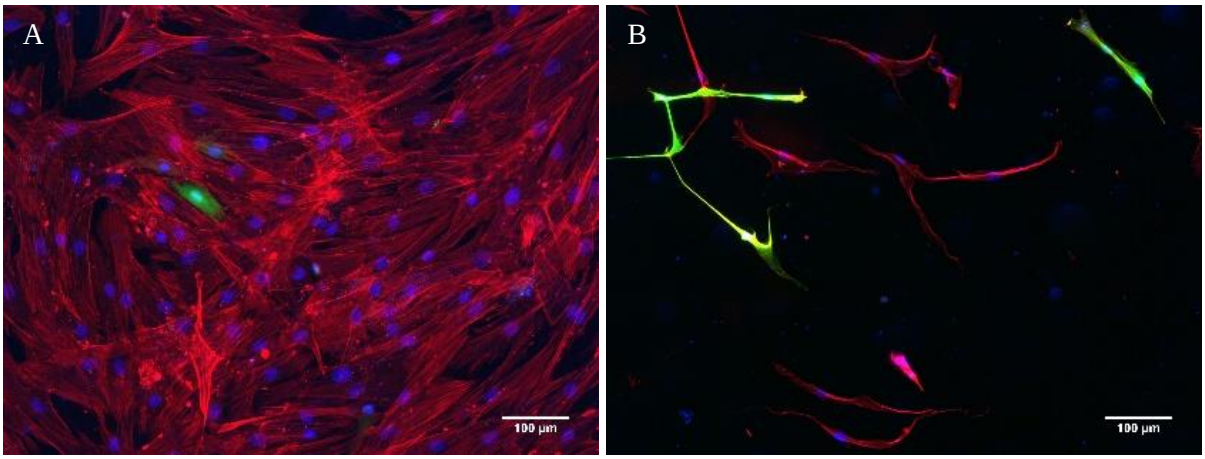

Figure 19. Variation in transfection efficiency seen in areas of a sample with abnormally high or low cell confluence. (A) Low percentages of EGFP (green) transfection resulting from abnormally high cell confluence and (B) high percent transfection resulting from abnormally low cell confluence due to uneven seeding of a sample seeded at 5000 cells/cm^2 on unpatterned PDMS. Cells are stained with Alexa Fluor 546 Phalloidin (red) and DAPI (blue). Scale bars are 100 µm.

Transfection experiments on the MARC chip allowed us to select topographical patterns for further study based on trends that were seen in the transfection efficiency. Five of the selected topographies were selected based on their positive effect on transfection efficiency. These were 250 nm gratings (pattern # 1), 1 µm gratings with 2 µm spacing (pattern #5), 1 µm concave lenses (pattern # 10), 1 µm holes (pattern # 15), and 250 nm pillars (pattern # 16).

We looked at the effect that the topographies had on cell surface density to see if there would be a correlation between this and transfection efficiency. Overall there was a low negative correlation between

transfection efficiency and cell density with a correlation coefficient of -0.34. In particular, it was interesting to see that 1 μm concave lenses (pattern # 10) increased mean transfection efficiency while decreasing cell density, while the inverse pattern (# 11, 1 μm convex lenses) showed a slight decrease in transfection efficiency and a slight increase in cell density. Hence, pattern 11 was also included for further study to compare to pattern 10 to determine the effect of direction of curvature of 1 μm lenses on transfection efficiency and cell density.

Finally, we looked at the effect that the topographies had on average cell area to see if there would be a correlation between this and transfection efficiency. Overall there was a low positive correlation between transfection efficiency and average cell area with a correlation coefficient of 0.38. An equal number of topographies that had decreased cell area, were seen to have increased and decreased transfection efficiency. However, three of the five topographies that showed increased average cell area also showed increased transfection efficiency including gratings of 2 μm diameter, 1μm spacing, 80 nm height (pattern # 6), 1 μm concave lenses (pattern # 10), and 250 nm pillars (pattern # 16). Two of these patterns (pattern # 10 and # 16) were already selected for further study. Although cell area did not strongly correlate with transfection efficiency, it would be interesting to continue to monitor cell area in future studies especially on 1 μm concave and convex lenses (pattern # 10 and # 11) which again showed opposite effects.

It is important to note that no statistically significant differences were seen in the MARC chip data on transfection efficiency or final cell density, and very little statistical significance was seen in the MARC chip data on cell area. This is not surprising, due to the nature of these small sample areas. To determine statistical significance, further study should be done on single-patterned substrates with larger patterned areas.

A subset of topographies showing a linear relationship between transfection efficiency and cell density (with $R = -0.99$) shared characteristics of micro-scale dimension, caused decreased average cell area (compared to unpatterned areas of the MARC chip), and had normalized cell densities ≥ 1.59. Three

out of 4 of these topographies also had height ≥ 700nm. Also, topographies showing a different linear relationship between transfection efficiency and cell density (with R = -0.96) all had normalized cell densities ≤ 1.07. Five out of 6 of these topographies had height ≤ 300 nm. This supports that there may be a relationship between (i) topography size, (ii) cell spreading, (iii) cell density, and (iv) the relationship between cell density and transfection efficiency, which could not be quantified in this work.

Other studies in the literature have also investigated topography influence on non-viral transfection. One study investigated nano- and micro-topographical patterns fabricated on PMMA substrates including pillars with 2 μm diameter and height (similar to pattern 14 in our study), pillars with 200 nm diameter and 400 nm height (most similar to pattern 16 in our study, but with larger spacing between pillars), and gratings with 250 nm width and height (similar to pattern 1 in our study)[17]. They tested topography effects on Lipofectamine-mediated GFP transfection of hMSCs and found that the highest transfection efficiency occurred on nano-pillars and that the enhancement was statistically significant compared to their unpatterned control. Their 2 μm pillars and 250 nm gratings also showed increases in transfection efficiency, however these were not determined to be statistically significant. In our study, we also found that nano-gratings (pattern 1) and nano-pillars (pattern 16) caused an increase in transfection efficiency. This shows that these topographies can increase transfection efficiency whether the substrate material is PMMA or PDMS, and encourages further study of these topographies on large substrates to determine whether our results could show statistical significance. We did not, however, find that 2 μm pillars (pattern 14) caused any increase in transfection efficiency. In their study this topography showed the lowest increase, and differences between our results and theirs could be due to variability since neither our results nor theirs showed statistical difference compared to unpatterned controls.

Studies have also looked into topographical influence on endocytosis. One study showed that human fibroblasts on PMMA nano-columns (160nm height, 100nm diameter, and 230nm pitch) would attempt to internalize the columns through clathrin-mediated endocytosis[88]. Also, the previously mentioned study found that micro- and nano-pillars could increase internalization of dextran by hMSCs

and monkey kidney fibroblasts (COS7), which suggests that these topographies increase the rate of micropinocytosis[17]. Lipoplexes specifically have been found to enter cells by clathrin-mediated endocytosis, however other transfection reagents have been shown to depend on other types of endocytosis, such as polyplexes which depend on both clathrin- and caveolae-mediated endocytosis[115, 116]. Due to the observations in our study and in literature that nano-pillars can increase transfection efficiency as well as the observation in literature that nano-pillars appear to induce clathrin-mediated endocytosis, it is a possibility that the increased transfection is caused by the enhancement of endocytosis. This relationship would need to be further studied to find evidence of causation.

Another study screened a library of 160 different micro-scale pit geometries on PDMS substrates and found that the efficiency of Lipofectamine-mediated GFP transfection of human dermal fibroblasts could be improved 25% with pits of 4μm with and 1μm spacing compared to unpatterned substrates[16]. Our observation that holes of 1 μm diameter, 6.5 μm pitch, and 1 μm depth (pattern 15) increased transfection efficiency may relate to these findings. Their findings showed that pits with 1 μm diameter and 4μm spacing (a topography more similar to our pattern 15) increased the percentage of transfected cells compared to unpatterned controls, however this increase was not found to be statistically significant. This encourages the idea of pursuing further study of the effect that pattern 15 has on non-viral transfection of hMSCs, and possibly comparing the effects of this pattern to the effects of holes with larger diameter and smaller spacing.

Chapter 3: Non-viral Neuronal Transdifferentiation of hMSCs on Topographically-patterned Substrates

3.1. Introduction

This chapter focuses on the methods and results of experiments investigating the effects of nano- and micro-topography on neuronal transdifferentiation of hMSCs induced by non-viral delivery of BAM (Brn2, Ascl1, and Myt1l) transcription factors. In these investigations, poly(N,N-cystaminebisacrylamide-4-amino-1-butanol) (pABOL) was used as the non-viral transfection reagent because of its potential to be translated to clinical applications. The protocol used in these experiments to induce transdifferentiation was adapted from a method described previously to induce neuronal cells from fibroblasts [15, 20]. This protocol uses serial dosing of polyplexes followed by an induction period. First tests were done on unpatterned substrates to optimize the transdifferentiation test conditions and then transdifferentiation was carried out on the MARC chip to investigate topographical influence.

As cells convert to neurons, they are expected to become post-mitotic. Hence, it was important to consider our initial cell seeding density before the transdifferentiation process to ensure a reasonable number of cells would remain by the end of the 2-3 week process. To increase the chances of having a desirable number of cells at the end, we were inclined to increase the seeding density, however, this could have detrimental effects on transfection efficiencies due to contact inhibition if high confluence were reached [86, 117]. Therefore, to determine a reasonable seeding density for our studies, we investigated the effect that an increased seeding density of 12000 cells/cm^2 would have on final cell density and transfection efficiency after serial transfections compared to a standard hMSC seeding density of 5000 cells/cm^2.

The dose of polyplex delivered at each transfection was also evaluated. Dosage can affect cell viability as well as the percentage of transfected cells in the final cell population. An ideal dosage would result in the highest possible number of transfected cells per area by balancing high transfection efficiency with cell health. The alamarBlue toxicity assay and phase contrast imaging were used to determine the impact of different doses on hMSC viability. Flow cytometry was used to measure the impact of different doses on the final percentage of transfected cells. Estimations were then made to determine which dose resulted in the overall largest final population of transfected cells per area.

Transdifferentiation was then carried out with the determined dosage and cell density on MARC chips to screen for topography-effects on the success of conversion. Immunofluorescence (IF) staining was used to analyze the presence of the neuronal marker, MAP2, after transdifferentiation as well as neuronal morphology by inspecting images.

3.2. Methods

3.2.1. Fabrication and Characterization of Substrates

MARC chip and unpatterned PDMS chamber substrates were the same type as the ones used in experiments described in Chapter 2. Their fabrication has been described in section 2.2.1 and their characterization was presented in section 2.2.2 and 2.3.1.

3.2.2. Cell Culture and Substrate Preparation

Cell culture and substrate sterilization were carried out in the same ways as described in section 2.2.3. However, for transdifferentiation, the substrates were additionally coated with fibronectin from bovine plasma (Millipore Sigma) prior to cell seeding. The fibronectin was diluted in PBS and added to substrates at 1µg/cm^2. Coating was carried out for 2 hours at 37 °C in the incubator. The excess fibronectin solution was removed from substrates before cell seeding.

3.2.3. BAM Factor Plasmid Amplification and Purification

Ascl1 and Myt1l-expressing plasmids (Invitrogen) were received from Professor Kam W. Leong's group at Columbia University. Brn2-expressing plasmid were cloned at the National University of Singapore by Dr. Christopher L. Grigsby of Professor Kam W. Leong's group at Columbia University. Plasmids were amplified as described in section 2.2.4, but with GT116 cells (InvivoGen), Blas TB Broth (InvivoGen), and Blas LB Agar (InvivoGen). They were then purified using a QIAGEN Plasmid Midi Kit. Final purified plasmid concentration was measured with a NanoDrop ND-1000 Spectrophotometer.

3.2.4. Transfection Using pABOL Polyplexes

Plasmid DNA was first diluted in pABOL buffer, composed of 20mM HEPES (Gibco) with 5 weight percent glucose (Sigma) in molecular grade water (Sigma), at a concentration of 75 µg/ml. When BAM plasmids were being used, they were combined at an equimolar ratio. pABOL was fabricated and given to us by Professor Kam W. Leong's group at Columbia University as a solid lyophilized product.

This was constructed into a stock solution by dissolving it at 50 µg/µl in molecular grade water. For transfections, pABOL was diluted to 844 µg/ml in pABOL buffer. Both diluted DNA and pABOL solutions were vortexed briefly and then added together at a 45:1 polymer:DNA mass ratio and vortexed for 20 seconds to form polyplexes. The media of samples to be transfected was changed to pre-warmed (37 °C) Opti-MEM (Gibco) in advance and polyplex was added to the media at the specified dose followed by a 4 hour transfection incubation at 37 °C in the incubator. After this incubation, the media was changed back to MesenPRO RS medium.

3.2.5. Cell Fixing and Immunofluorescent Staining

Before fixing, samples were washed once with PBS. They were then fixed in filtered pH-adjusted 4 % (w/v) PFA (Sigma-Aldrich) for 15 minutes and washed once again with PBS. Cells were then permeabilized with 0.1% (v/v) TritonX-100 (Sigma) for 15 minutes and washed once with tris-buffered saline (TBS, Fisher BioReagents). Blocking was done in blocking medium containing 1% (w/v) bovine serum albumin (BSA, Sigma) and 10% (v/v) goat serum (Lifetech) at 4 °C overnight. Primary antibody incubation with anti-MAP2 (abcam), Anti-β-Tubulin III (Millipore Sigma), or Anti-Synapsin I (abcam) were done at 1:500, 1:5000, and 1:500 dilution in TBS with 1% goat serum respectively. Primary antibody incubation was done at 4 °C overnight. Samples were then washed once with washing buffer, composed of 0.05% triton-X and 1% goat serum in TBS, and then incubated with secondary antibodies Alexa-Fluor 546 goat anti-rabbit (Invitrogen) and/or Alexa-Fluor 488 goat anti-mouse (Invitrogen) both at dilution 1:1000 in TBS at 4 °C overnight. The next day, samples were washed once with TBS and stained with DAPI at a dilution of 1:2500 in TBS for at least 1 hour at room temperature. Finally cells were washed once with TBS and mounted onto glass coverslips with Fluoromount (Millipore Sigma).

3.2.6. Determining Appropriate Seeding Density for Transdifferentiation

In order to investigate the effect of increased seeding density on final cell density and transfection efficiency after serial transfections, hMSCs were seeded at 5000 and 12000 cells/cm^2 on PDMS and glass substrates. The cells were transfected with 0.5 µg/cm^2 EGFP-expressing plasmid three times at 48 hour intervals according to the timeline below (Figure 20). Transfections were done with both polyplex (3.2.4) and Lipofectamine (2.2.5 with a 1:0.4 plasmid (µg) to Lipofectamine (µl) ratio). Samples were stained with Alexa Fluor 546 Phalloidin and DAPI and then imaged by fluorescence microscopy (as described in section 2.2.5). Cell density and the percentage of cells expressing EGFP were quantified using ImageJ software.

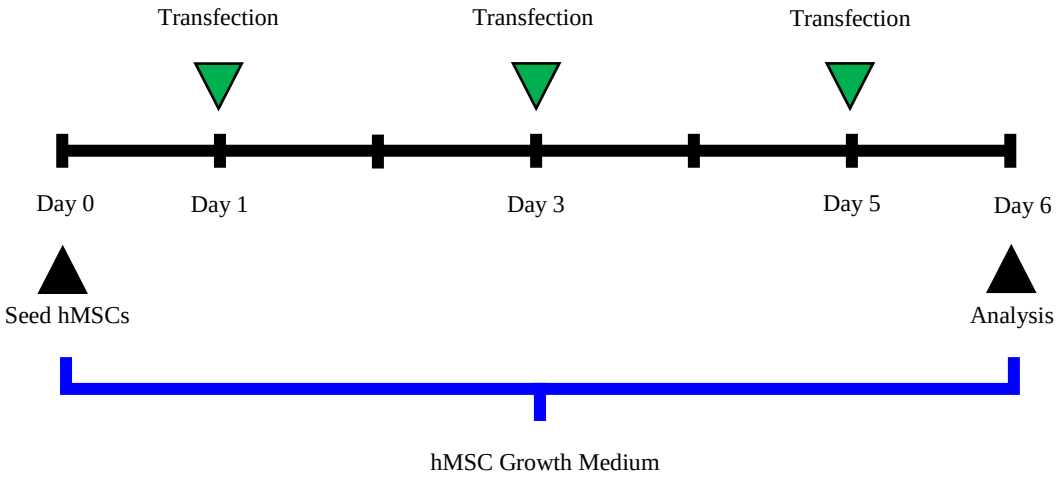

Figure 20 Timeline for serial transfections. Analysis on day 6 involved fluorescence imaging (of DAPI and phalloidin staining as well as EGFP expression) for studies determining appropriate seeding density (section 3.2.6) and involved the alamarBlue assay, fluorescence imaging (of EGFP expression only), and flow cytometry for studies determining polyplex dosage effects on cell viability and transfection efficiency (section 3.2.7 and 3.2.8).

3.2.7. AlamarBlue Assay to Determine Polyplex Dosage Effects on Cell Viability after Serial Transfections

AlamarBlue is a cell viability indicator that uses the reducing power of living cells to convert resazurin to the fluorescent molecule resorufin (Figure 21). The amount of fluorescence produced in cell culture medium after incubation with alamarBlue is proportional to the number of living cells in the culture and the incubation time. AlamarBlue reagent was added as 10% of the sample volume and then incubated for a set amount of time. After incubation, the fluorescence intensity was measured for each sample. Additionally, samples with 100% reduction were made by autoclaving media containing 10% alamarBlue reagent and negative controls (with 0% reduction) were made by incubating a sample of media containing 10% alaramBlue with no cells along with test samples. From fluorescence readings, the percent of alamarBlue that was reduced by living cells in each sample (% reduction) was calculated using the formula below (Equation 3.1).

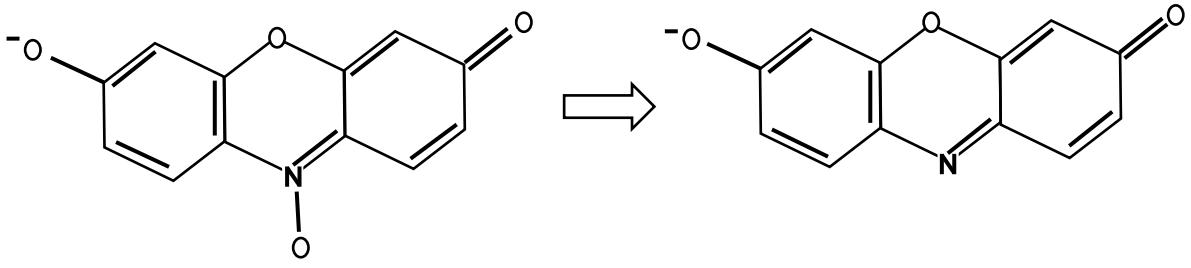

Figure 21. Resazurin conversion to resorufin. Resazurin (left) is the molecule in alamarBlue that becomes the fluorescent molecule, resorufin (right), upon reduction. [118]

$$\%\ \text{Reduction} = \frac{\begin{pmatrix}\text{Fluorecence}\\ \text{Reading of Sample}\end{pmatrix} - \begin{pmatrix}\text{Fluorecence Reading}\\ \text{of 0\% Reduced Sample}\end{pmatrix}}{\begin{pmatrix}\text{Fluorecence Reading}\\ \text{of 100\% Reduced Sample}\end{pmatrix} - \begin{pmatrix}\text{Fluorecence Reading}\\ \text{of 0\% Reduced Sample}\end{pmatrix}} \quad (3.1)$$

The appropriate incubation time for the alamarBlue assay can change depending on the cell line being studied [119].To ensure that we were using an appropriate incubation time for our study, hMSCs were seeded in tissue culture plates at various densities around the expected density of our experiment samples (500, 2000, 5000, 8000, & 12000 cells/cm^2). Twenty-four hours after seeding, alamarBlue was added to the wells. The samples were then returned to the incubator and fluorescence was measured at 2, 4, 6, 8, and 24 hours with 530-560nm excitation and 590nm emission. Plots of percentage of reduction versus seeding density for various incubation times allowed us to find an appropriate incubation time.

To determine the effect of three different polyplex dose sizes on hMSC viability, cells were seeded at 8000 cells/cm^2 and then transfected three times with either a dose of 0.25, 0.5, or 1 µg plasmid/cm^2 according to the timeline shown in Figure 20. This was done on unpatterned PDMS substrates. Lipofectamine transfection with the 0.5 µg/cm^2 dose and non-transfected samples were used as positive and negative controls respectively. Additionally, to control for substrate material effects, polyplex and Lipofectamine transfection with a 0.5 µg/cm^2 dose and non-transfected controls were carried out on tissue culture polystyrene (TCPS). Twenty-four hours after the last transfection, alamarBlue was added to the samples followed by a 7 hour incubation. Finally, fluorescence intensity measurements of the cell culture media (with 530-560nm excitation and 590nm emission) were taken and the percentage of reduction was calculated. The percentage of viability was then calculated for each sample as the percentage of reduction from the test condition over the percentage of reduction from untreated cells on TCPS multiplied by 100 (Equation 3.2).

$$\% \text{ Viability} = \frac{\% \text{ Reduction from Test Condition}}{\% \text{ Reduction from Untreated Sample}} \times 100 \quad (3.2)$$

3.2.8. Determining Polyplex Dosage Effects on Transfection Efficiency and Transfected Cell Density after Serial Transfections

To determine the effect that polyplex dosage has on transfection efficiency after three serial transfections, samples that were prepared for the alamarBlue assay, as described in section 3.2.7, were examined with fluorescence imaging to view the EGFP expression over large surface areas and by flow cytometry to measure the percentage of the cell population expressing EGFP. Doses of 0.25, 0.5, or 1 µg plasmid/cm^2 were tested. Twenty-four hours after the last transfection, samples were imaged without any staining to acquire large mosaic images representing the surface density of EGFP-expressing cells. Cells were then detached with TrypLE Express (Gibco), resuspended in media and counted. To fix the cells for flow cytometry, they were then spun down to remove media and resuspended in 500 µl of cold PBS. Then 500 µl of cold 2 % PFA was added followed by an incubation for 30 minutes at 4 °C. After fixing, cells were spun down at 4 °C to removed supernatant, washed once with cold PBS, resuspended in PBS and placed in fluorescence-activated cell sorting (FACS) tubes. Flow cytometry data was analyzed with FlowJo software. Gating was based on negative controls which were non-transfected hMSCs grown on TCPS substrates and positive controls which were hMSCs transfected three times with 0.5 µg/cm^2 plasmid with Lipofectamine.

Resulting measurements of EGFP positive percentages of cell populations from each condition were then combined with data from the alamarBlue assay (which gave us the number of live cells per area) to calculate the concentration of EGFP positive cells per area resulting from each condition. This calculation was done using the equation shown below (Equation 3.3).

$$\text{Number of Transfected Cells } \left(\frac{\text{cells}}{\text{cm}^2}\right) = \frac{\text{Fraction of EGFP}}{\text{Positive Cells}} \times \text{Number of Live Cells } \left(\frac{\text{cells}}{\text{cm}^2}\right) \quad (3.3)$$

3.2.9. Transdifferentiation on PDMS MARC Chip Substrates

To induce neuronal transdifferentiation of hMSCs, cells were first seeded at 12000 cells/cm^2 in MesenPRO RS medium (Gibco). The cells were given 36 hours in the incubator to adhere and adjust to their substrate. The hMSC growth medium was changed 24 hours after seeding. Cells were transfected three times with 0.25 µg/cm^2 of plasmid DNA delivered by polyplex according to the procedure described in section 3.2.4. Each transfection was separated by 48 hours as shown in the timeline below (Figure 22). Forty-eight hours after the last transfection, the complete volume of media in each sample was switched to N3 neuronal induction media composed of DMEM/F-12 (Gibco) with 25 µg/mL bovine insulin (Gemini Bio-Products), 50 µg/mL human apo-transferrin (Gemini Bio-Products), 30 nmol/L sodium selenite (Millipore Sigma), 20 nmol/L progesterone (Millipore Sigma), 100 µmol/L putrescine (Millipore Sigma), 10 ng/mL human basic fibroblast growth factor (Gibco), and 25 µg/mL gentamicin (Gibco). Cells were maintained in neuronal induction medium for 10 days and eighty percent of the medium was changed every 48 hours until cells were fixed and stained as described in section 3.2.5. Immunofluorescence imaging was then used to observe neuronal marker MAP2 and cell morphology.

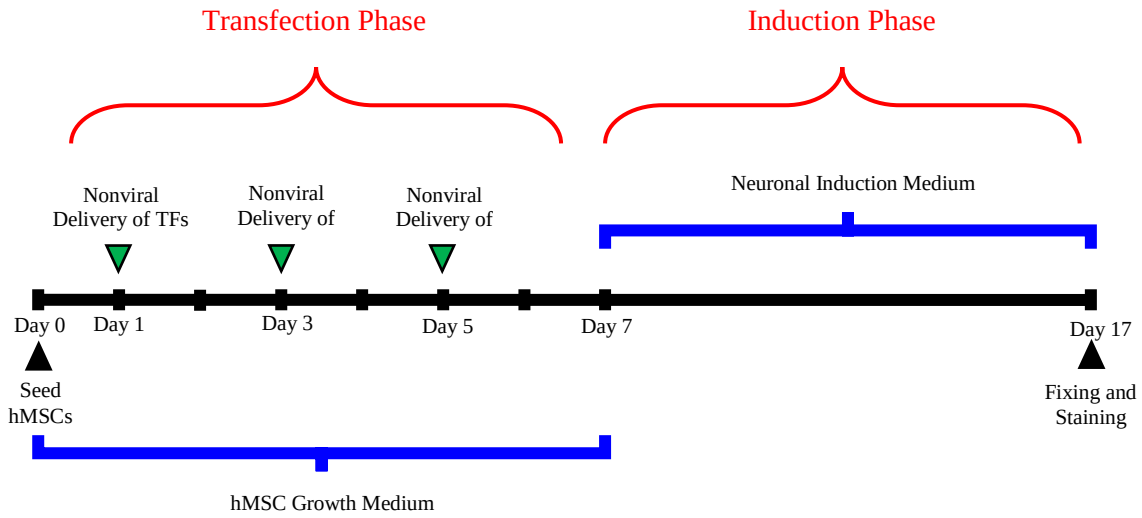

Figure 22 Timeline for inducing neuronal transdifferentiation of hMSCs. The process of neuronal induction involves a transfection phase and an induction phase (red). First hMSCs were seeded at 12000 cells/cm^2 on MARC chip substrates (PDMS) and unpatterned control substrates (PDMS and glass) in MesenPRO RS medium. The first transfection occurred 36 hours after seeding and the next two transfections followed every 48 hours. On day 7, media was switched to neuronal induction media. On day 17, samples were fixed and stained for immunofluorescent imaging.

3.2.10. Statistical Analysis

Statistical analyses were performed using a one-way ANOVA test with Tukey's multiple comparisons test or using an unpaired t-test using Prism (GraphPad). All values are presented with mean values ± standard deviation. Statistical tests were considered significant when $P \leq 0.05$ (noted by *), $P \leq 0.01$ (noted by **), $P \leq 0.001$ (noted by ***), and $P \leq 0.0001$ (noted by ****).

3.3. Results

3.3.1. Selecting Appropriate Seeding Density for Transdifferentiation

Fluorescence images taken after serial EGFP transfections of hMSCs seeded at 5000 and 12000 cells/cm^2 (Figure 23) allowed us to see the effect that this difference in seeding density had on final cell density (Figure 24) and percentage of transfected cells in the final cell population (Figure 25). On glass substrates, an initial seeding density of 5000 cells/cm^2 was sufficient for a final cell density of at least 3000 cells/cm^2. However, at this seeding density on PDMS substrates the final cell density was extremely low, around 1000 cells/cm^2. The higher seeding density of 12000 cells/cm^2 ended in final cell density of over 10000 cells/cm^2 on glass samples, and a good density of over 5000 cells/cm^2 on PDMS substrates. From this experiment, we observed that the final cell density was dependent on the initial seeding density and substrate material.

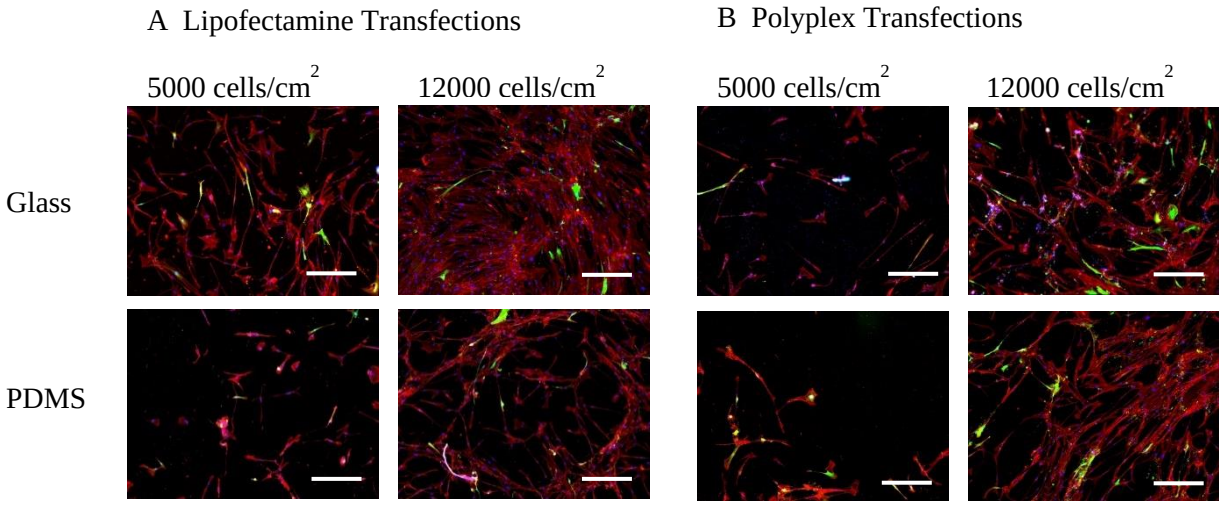

Figure 23 Fluorescence images of cells seeded at 5000 and 12000 cells/cm^2, after three serial transfections. (A) Lipofectamine-mediated transfection. (B) Polyplex-mediated transfection. Cells were initially seeded at 5000 or 12000 cells/cm^2 on glass (top row) or PDMS (bottom row) substrates. Cells were transfected with EGFP (green) and stained with Alexa Fluor 546 Phalloidin (red) and DAPI (blue). Scale Bars are 500 µm.

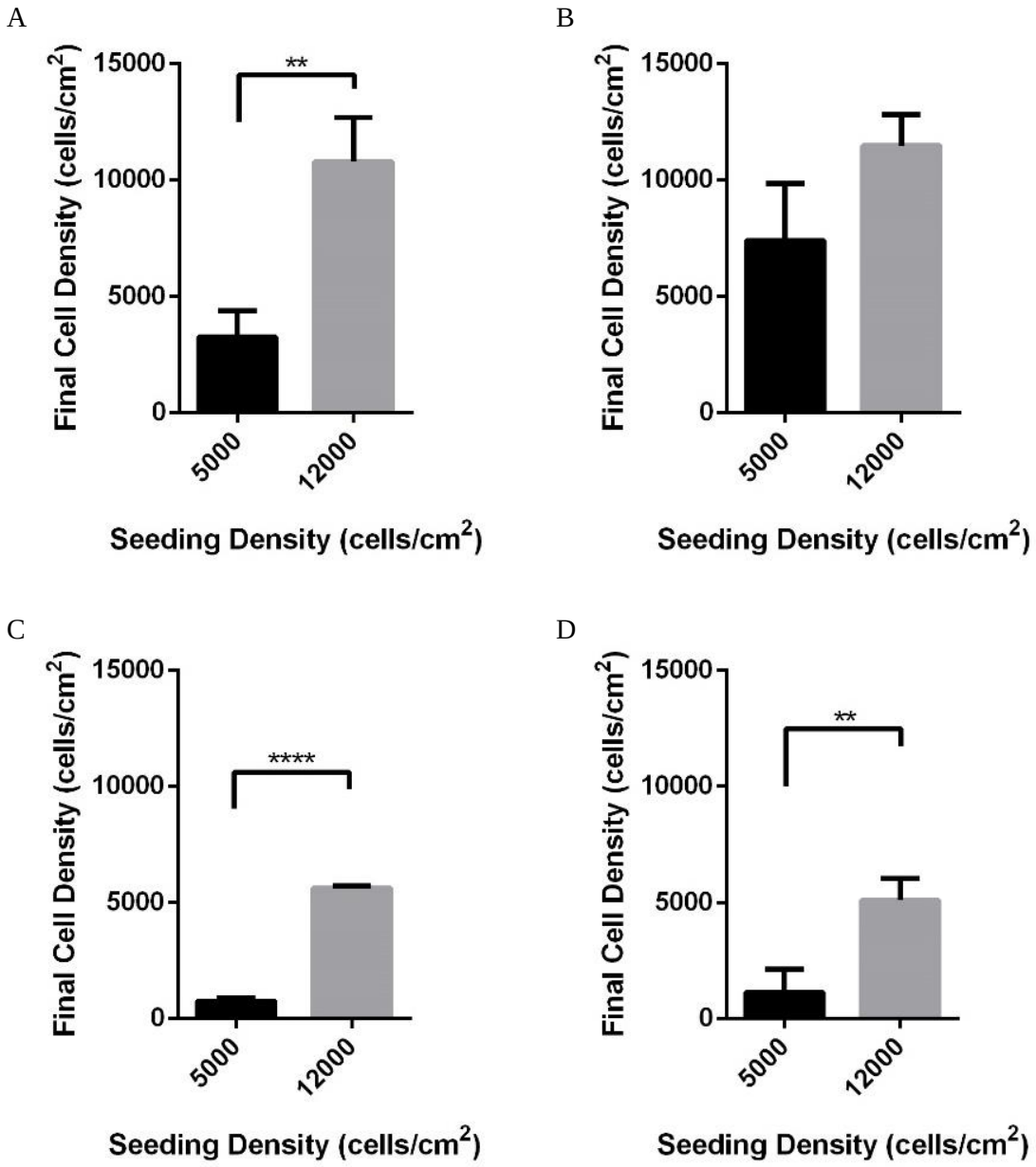

Figure 24 Quantification of final cell densities of cells seeded at 5000 or 12000 cells/cm^2, after three serial transfections. (A) Lipofectamine-mediated transfections on glass substrates. (B) Polyplex-mediated transfection on glass substrates. (C) Lipofectamine-mediated transfections on PDMS substrates. (D) Polyplex-mediated transfections on PDMS substrates. n=3. ** and **** denote statistical significance with $P \leq 0.01$ and $P \leq 0.0001$ respectively.

Although the higher seeding density was necessary for samples with PDMS substrates, the transfection efficiency on each sample was quantified to ensure that the increased seeding density would not have detrimental effects on the percentage of the final cell population that would be successfully

transfected. It was found that the percentage of transfected cells was not significantly affected by the difference in seeding density (Figure 25). The mean final percentages of cells that were transfected ranged between 2.9 % ± 1.7 % and 7.2 % ± 5.7 % on glass substrates and between 5.1 % ± 0.8 % and 9.4 % ± 5.1 % on PDMS substrates.

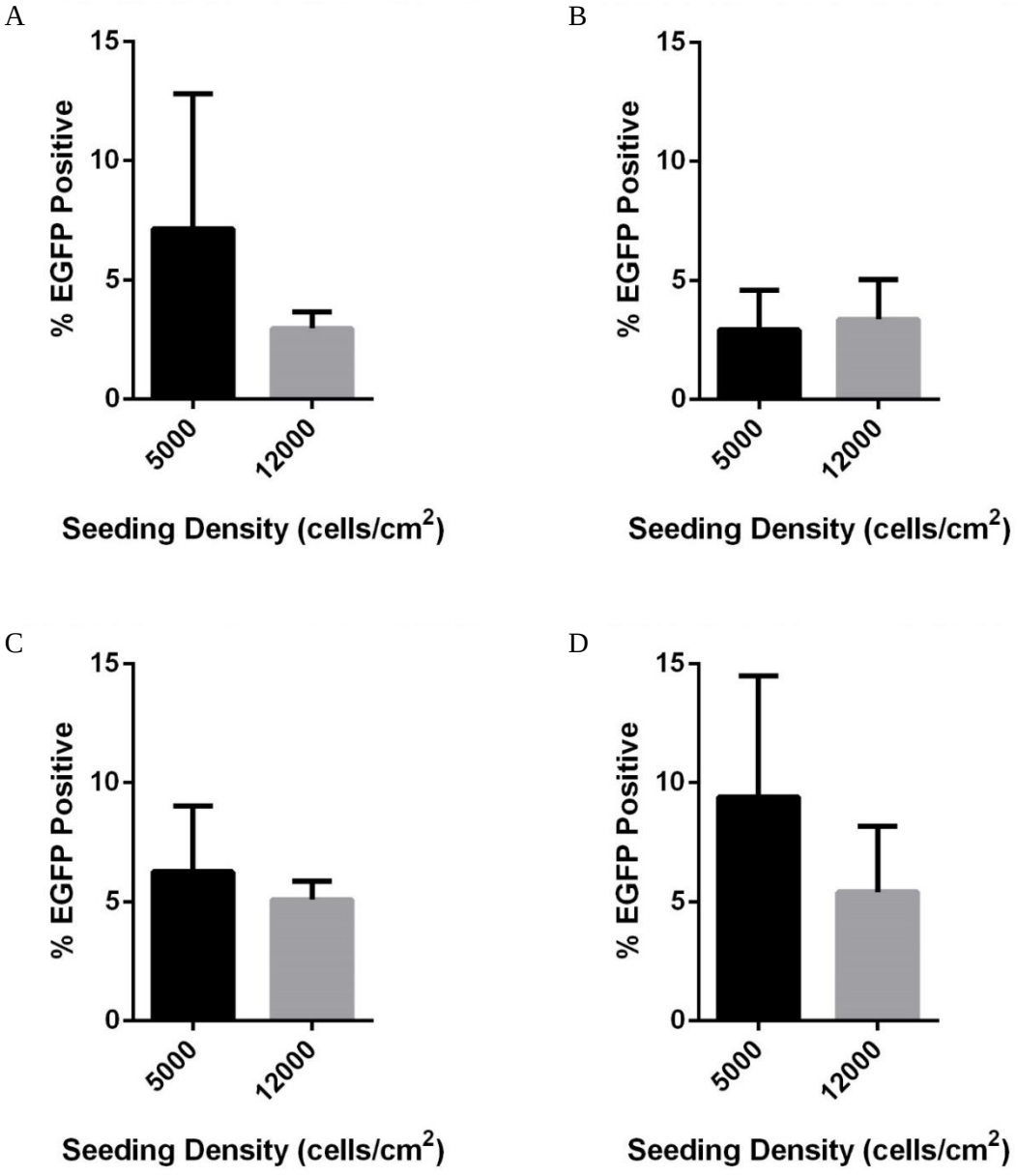

Figure 25 Quantification of percentage of transfected cells after seeding at 5000 or 12000 cells/cm^2 followed by three serial transfections. (A) Lipofectamine-mediated transfections on glass substrates. (B) Polyplex-mediated transfection on glass substrates. (C) Lipofectamine-mediated transfections on PDMS substrates. (D) Polyplex-mediated transfections on PDMS substrates. n=3. Data was not statistically significant.

A seeding density of 12000 cells/cm^2 was therefore used in our transdifferentiation studies as it resulted in a higher final density and did not affect the percentage of transfected cells on PDMS substrates after serial transfections.

3.3.2. Effect of Polyplex Dosage on Cell Viability

Before using the alamarBlue assay to measure cell viability, the appropriate incubation time for the alamarBlue assay was determined. Plotting percentage of reduction versus seeding density showed that any incubation time between 2 and 8 hours would allow us to linearly correlate the measured percentage of reduction of a sample to the density of viable cells in the sample using the alamarBlue assay (Figure 26). With a longer incubation, smaller cell densities can be detected, therefore an incubation time of 7 hours was used for our alamarBlue assays.

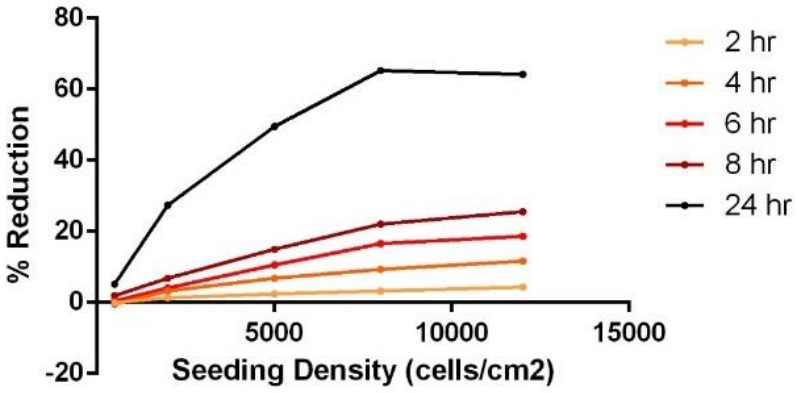

Figure 26. Plots of percent reduction versus seeding density for various alamarBlue incubation times.

The measurements of percent viability from the alamarBlue assay results showed that a 0.25 µg/cm^2 dose of DNA delivered by polyplex was less toxic to hMSCs compared to higher doses after three serial transfections; however, no significant difference was observed (Figure 27). It was also notable that samples transfected with Lipofectamine tended to have higher average percent viability, and in some

cases the difference was significant. This, however, did not deter our interest in using the polyplex since its advantage is translatability to *in vivo* clinical applications. The toxicity may be specific to hMSCs since it has been shown that fibroblasts transfected with similar doses of the same type of polyplex had between 80 and 100 % viability after one or two serial transfections[15].

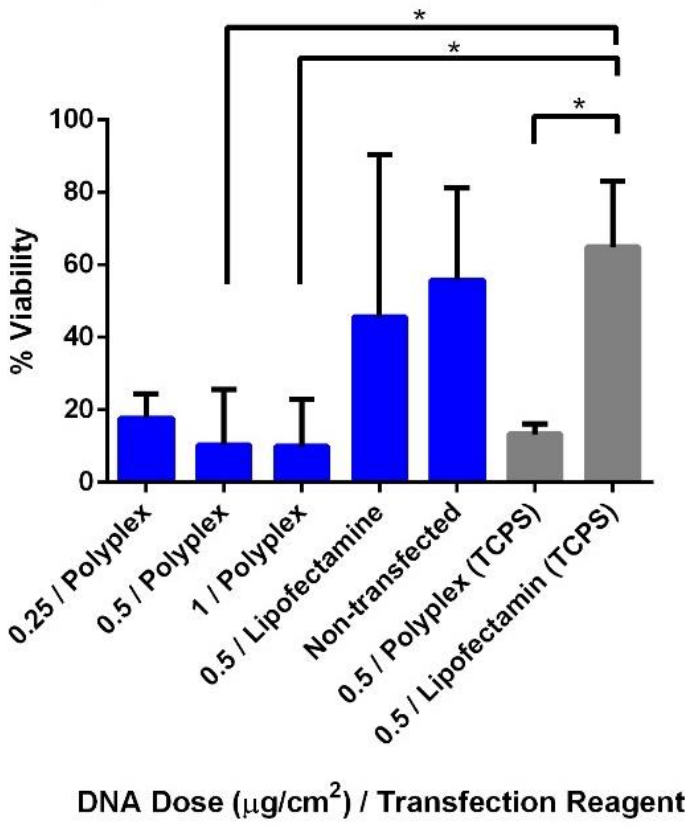

Figure 27. Percent viability measurements from alamarBlue assay after three serial transfections. Blue indicates samples on PDMS substrates and grey indicates samples on TCPS substrates. n=4. * denotes statistical significance with $P \leq 0.05$.

Cell morphology was imaged by phase contrast microscopy before and after the three serial transfections, and the cell health, judged by visible blebbing, correlated with the decrease in the mean of percentage of cell viability with increasing dose seen in results from the alamarBlue assay (Figure 28). Cells transfected with the lowest tested dose of polyplex (Figure 28 A) showed a healthier morphology compared to those transfected with higher doses (Figure 28 B and C). However, what was observed to be

blebbing might have been aggregates of polyplex, which could be verified by DAPI staining in future experiments. Samples transfected with Lipofectamine showed heathier cell morphology and higher cell density compared to samples transfected with polyplex (Figure 29), which also agreed with alamarBlue results.

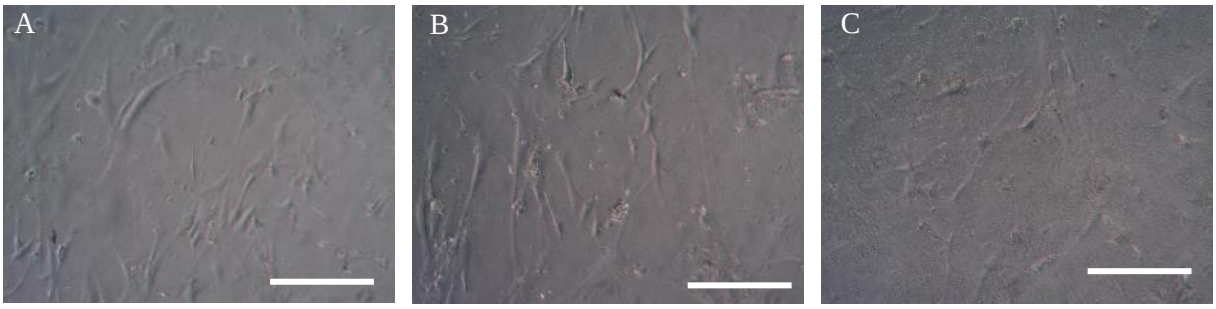

Figure 28 Phase contrast images taken after three serial transfections (on day 6) with different doses of polyplex. Human MSCs on PDMS substrates after three serial transfections with (A) 0.25 μg/cm^2, (B) 0.5 μg/cm^2, and (C) 1 μg/cm^2 of EGFP-expressing plasmid DNA. Scale ars are 250 μm.

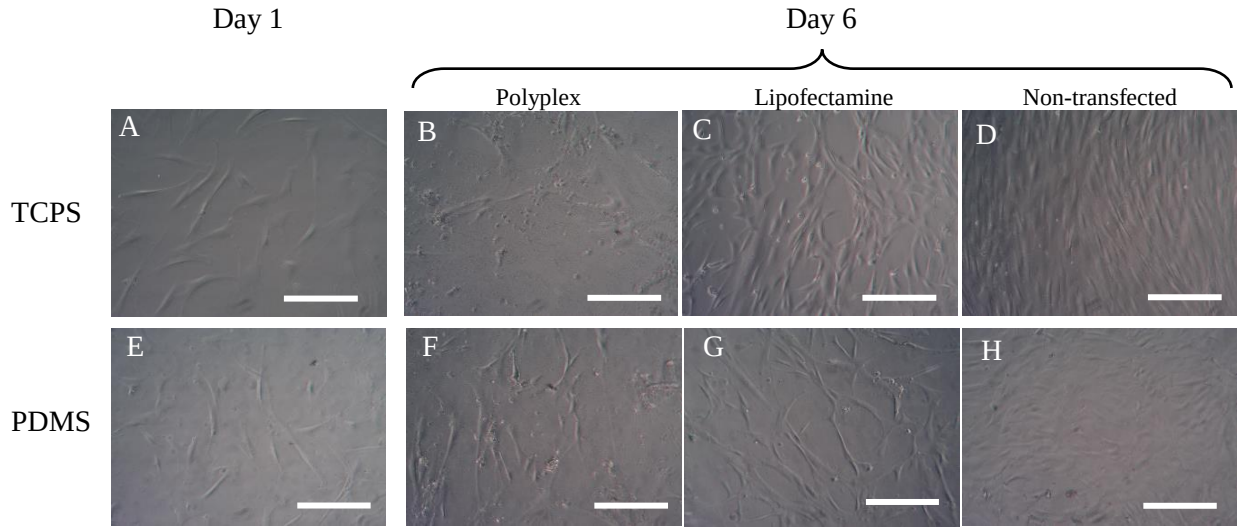

Figure 29 Phase contrast images taken before and after three serial transfections. Images are shown on both TCPS (top row, A to D) and PDMS (bottom row, F to H) substrates. (A and E) hMSCs on day 1 before the first transfection. (B and F) hMSCs on day 6 after three polyplex-mediated transfections. (C and G) hMSCs on day 6 after three Lipofectamine-mediated transfections. (D and H) Untransfected hMSCs on day 6. All transfections were with a 0.5 μg/cm^2 dose of of EGFP-expressing plasmid DNA. Scale bars are 250 μm.

3.3.3. Effect of Polyplex Dosage on Transfection Efficiency and Final Transfected Cell Density

Flow cytometry showed that there was no statistically significant difference in the percentage of cells that were successfully transfected when they were transfected three times with polyplex delivering 0.25, 0.5, or 1 μg/cm^2 doses of DNA (Figure 30). All transfections were done with a polymer:DNA mass ratio of 45:1. The mean percentage of EGFP positive cells from samples transfected with a 0.5 μg/cm^2 dose by Lipofectamine was lower than that of the samples transfected with polyplex, however, the difference was not found to be statistically significant.

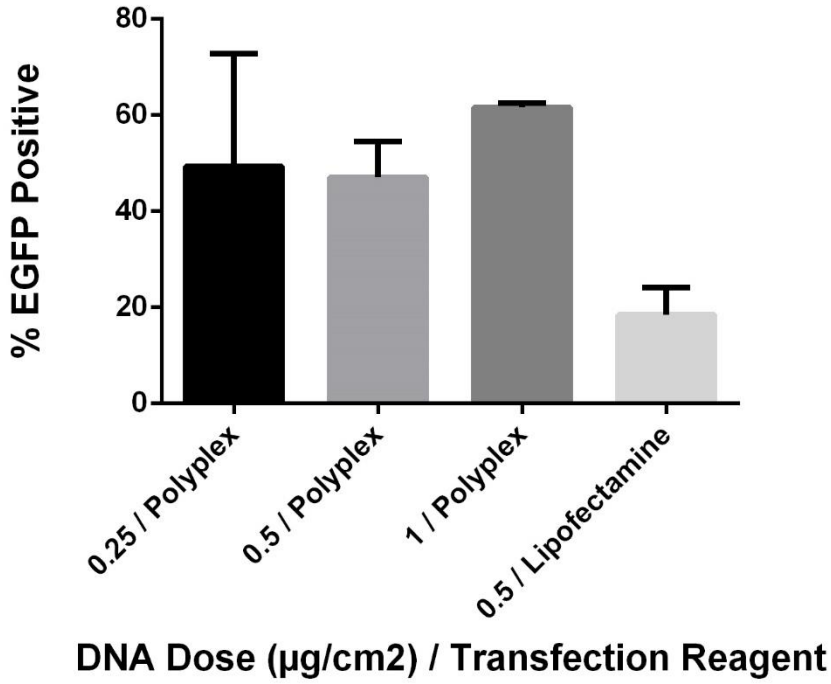

Figure 30. Percentages of hMSC population expressing EGFP after serial transfection with varying polyplex dosages. Polyplex transfections were done with a pABOL:DNA mass ratio of 45:1. For the control, Lipofectamine transfections were done with a Lipofectamine (μl):DNA (μg) ratio of 0.4:1. n=2.

Figure 31 shows the EGFP positive cell populations after three serial polyplex-mediated transfections with doses of either 0.25, 0.5, or 1 μg/cm^2 DNA (with pABOL:DNA mass ratio of 45:1) and

after serial Lipofectamine-mediated transfections with 0.5 μg/cm^2 DNA (with Lipofectamine (μl):DNA (μg) ratio of 0.4:1) as a positive control. There was comparable EGFP expression per area after polyplex transfections with 0.25 and 0.5 μg/cm^2 of DNA (Figure 32). A slightly lower EGFP expression per area after transfection with 1 μg/cm^2 of DNA was observed, which could be because of the lower cell density resulting from higher toxicity. The EGFP expression per area from Lipofectamine transfections appeared, from these images, to be comparable to that resulting from the 1 μg/cm^2 dose polyplex transfections. Although flow cytometry measurements showed that Lipofectamine produced a lower percentage of EGFP positive cells, Lipofectamine was also less toxic to the cells (Figure 27) which would have increased the number of EGFP positive cells per area.

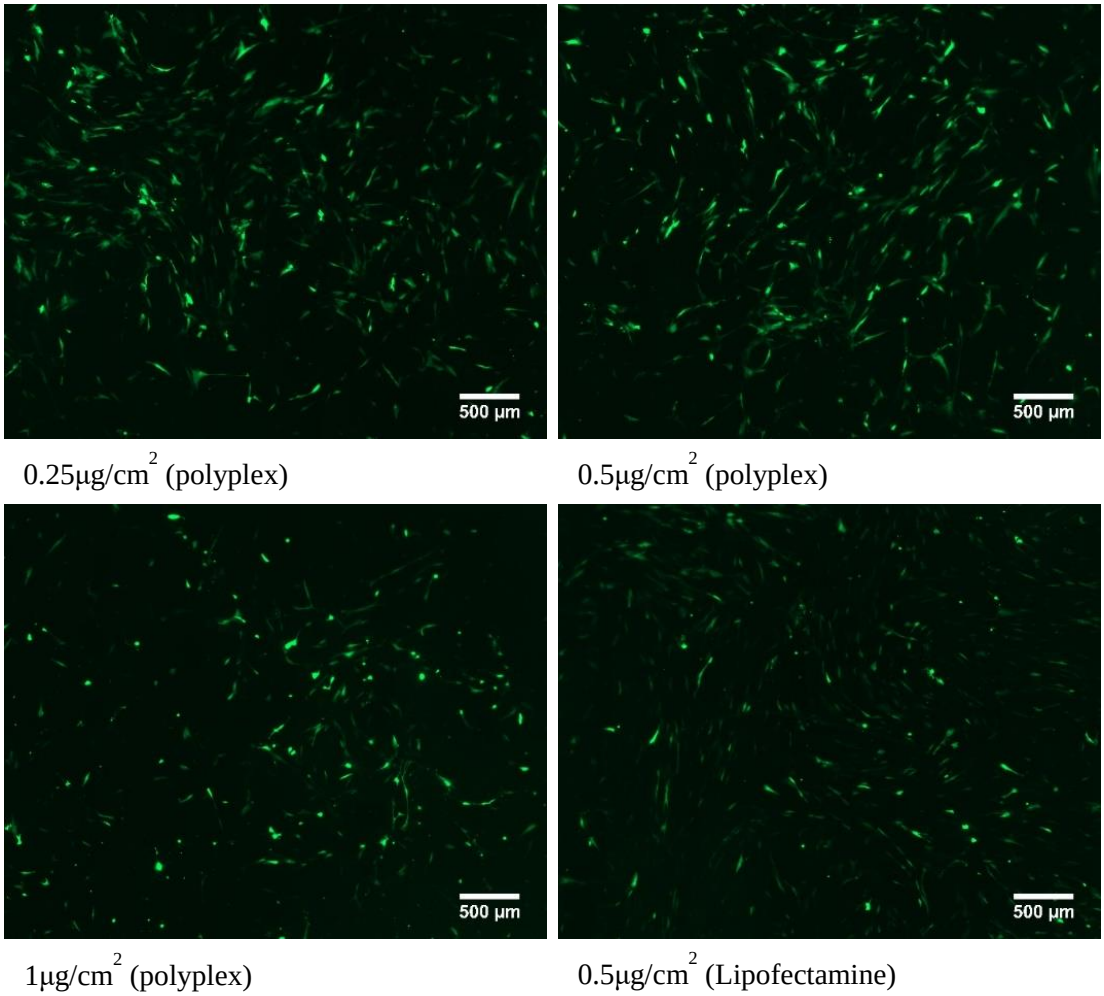

Figure 31. Fluorescence images showing the EGFP positive cell population after three serial transfections with varying polyplex dosages. Lipofectamine-mediated transfection with the middle sized dose was used as a control (bottom right). Scale bars are 500 µm.

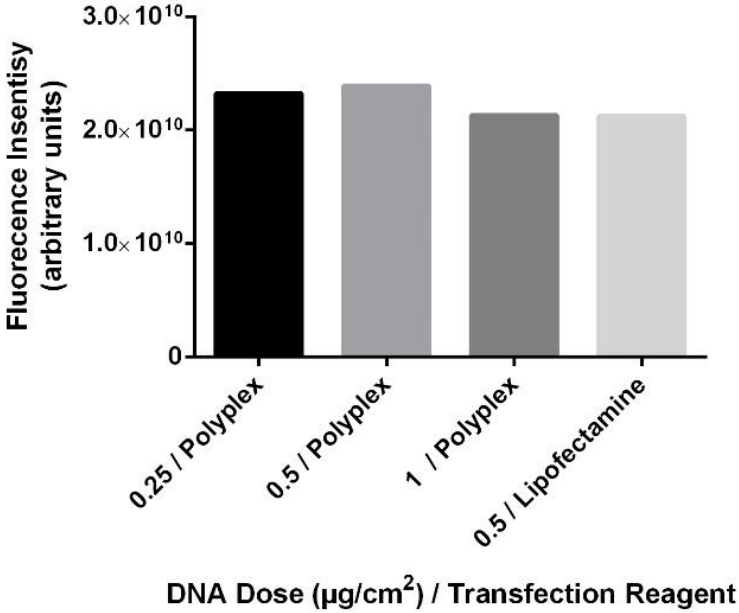

Figure 32 Fluorescence intensity measurements of images showing EGFP positive cell population after three serial transfections with varying polyplex dosages. Here fluorescence intensity was measured by taking the integrated density measurements of the images in Figure 31 with ImageJ software. n =1.

The table below summarizes the fractions of EGFP positive cells in final cell populations of samples transfected with 0.25, 0.5, or 1 µg/cm^2 doses of DNA (measured by flow cytometry, Figure 30), the number of live cells per area after transfections for each test condition, and the number of transfected cells per area calculated by equation 3.3.

Transfection Reagent	DNA Dose (µg/cm^2)	Fraction of EGFP Positive Cells	Number of Live Cells (cells/cm^2)	Number of Transfected (cells/cm^2)
Polyplex	0.25	0.494 ± 0.234	7200 ± 3730	3550
Polyplex	0.5	0.471 ± 0.075	2250 ± 3630	1060
Polyplex	1	0.617 ± 0.009	2350 ± 3230	1450
Lipofectamine	0.5	0.185 ± 0.059	16 080 ± 10 270	2980

Table 3 Number of transfected cells per area after three serial transfections with varying polyplex dosages. DNA Dose is the amount of DNA that was delivered three times to each sample with a Lipofectamine (µl):DNA (µg) ratio of 0.4:1 or a pABOL:DNA mass ratio of 45:1. Mean Fraction of EGFP Positive Cells was determined by flow cytometry (n=2, same data as shown in Figure 30). Number of Live Cells per area was determined with alamarBlue results (n=4). The Number of Transfected Cells per area was calculated with equation 3.3. All values are shown as mean ± standard deviation.

From the calculated numbers of transfected cells per area, we observed that the mean density of transfected cells resulting from serial polyplex-mediated transfections with 0.25 μg/cm^2 doses of DNA was the highest. The resulting density of transfected cells from Lipofectamine controls was higher than from serial polyplex-mediated transfections with 0.5 and 1 μg/cm^2 doses of DNA due to the high total number of living cells.

3.3.4. Transdifferentiation on PDMS MARC Chip Substrates

Immunofluorescence staining was similar in all of the unpatterned control samples (Figure 33). Slight differences between the non-transfected hMSCs on glass substrates (Figure 33 A) and the positive controls on both glass and unpatterned PDMS (Figure 33 B and D) could be observed. Non-transfected hMSCs on unpatterned PDMS (Figure 33 C) showed levels of staining visually very similar to both positive controls.

By visual observation of MAP2 immunofluorescence staining, none of the patterned PDMS substrates had an enhancing effect on the expression of MAP2 (Figure 34). Morphological changes could be seen as a result of topographical influence. Gratings designed to have height of 2 μm caused cells to consistently align along the grating axis. Attachment of cells was also a factor influenced by certain topographies. Specifically, gratings, pillars, and wells had similar confluency compared to unpatterned controls, while lens topographies resulted in more cell detachment throughout the 10 day induction period.

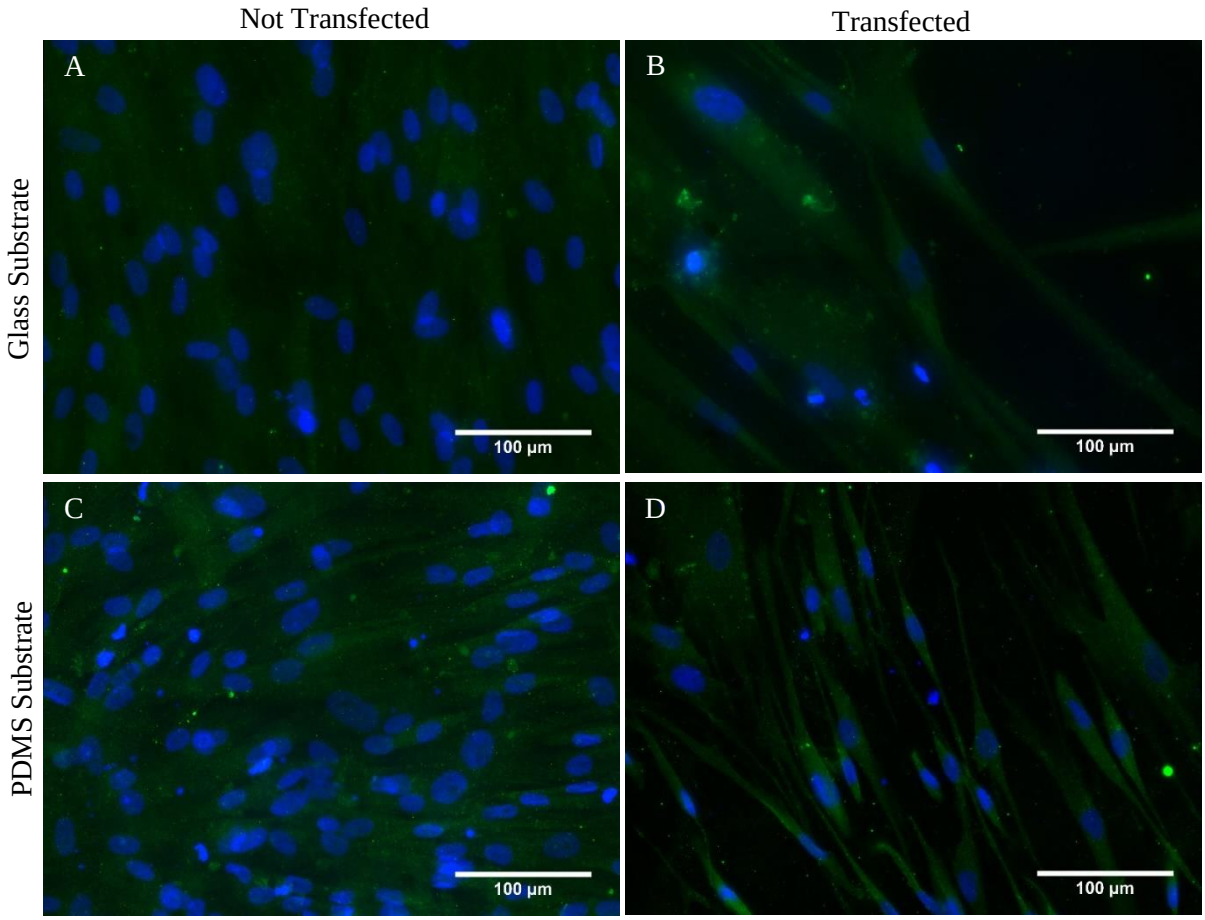

Figure 33. Immunofluorescence images of positive and negative control samples on unpatterned substrates. (A) Non-transfected cells on glass substrates. (B) Transfected cells on glass substrates. (C) Non-transfected cells on PDMS substrates. (D) Transfected cells on PDMS substrates. Scale bars are 100 µm. Cells are stained with anti-MAP2 (Green) and DAPI (blue).

Figure 34. Immunofluorescence images of hMSCs treated with transdifferentiation protocol on topographically patterned areas of the PDMS MARC chip. Scale bars are 100 µm. Cells are stained with anti-MAP2 (green) and DAPI (blue).

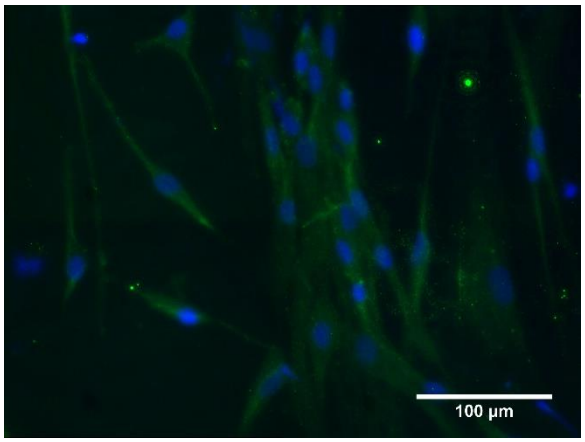

1 - 250 nm lines, 250 nm space, 250 nm height

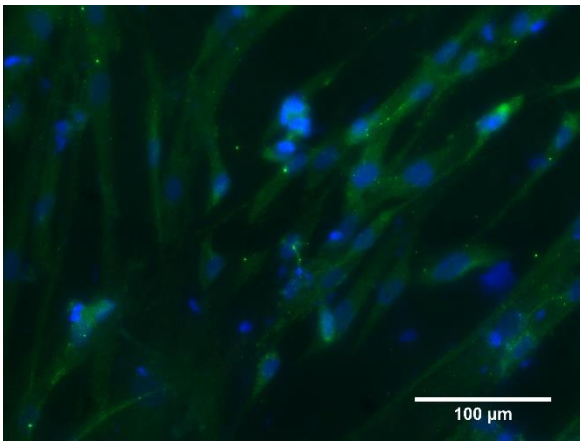

2 - 250 nm lines, 250 nm space, 110 nm height

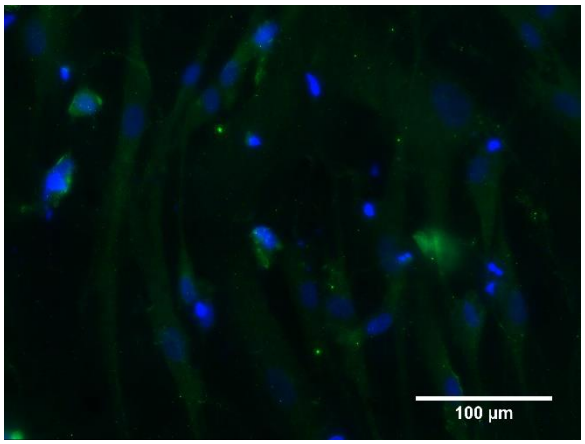

3 - 460 nm lines, 70 nm space, 40 nm height

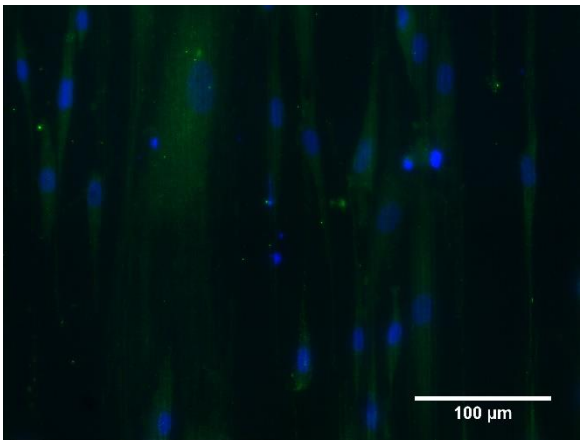

4 - 2 µm lines, 2 µm space, 2 µm height

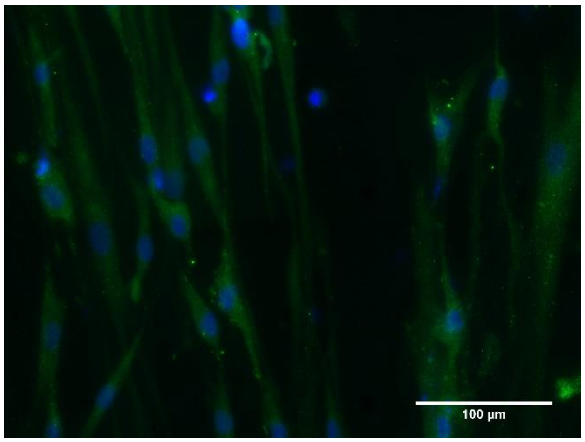

5 - 1 µm lines, 2 µm space, 120 nm height

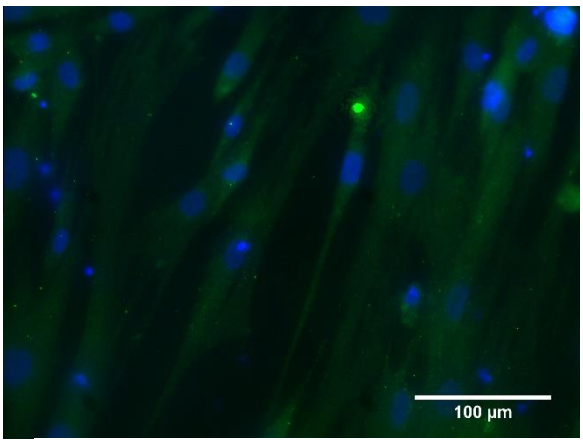

6 - 2 µm lines, 1µm space, 80 nm height

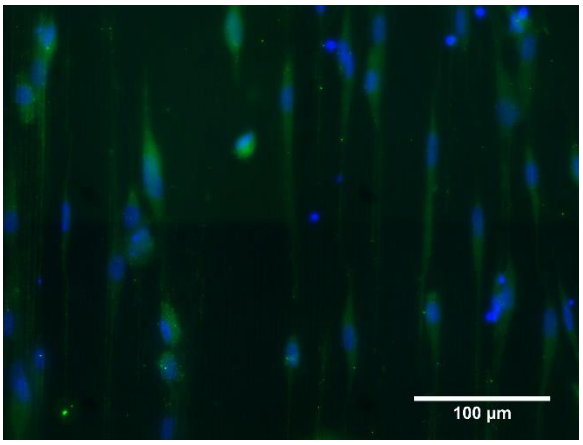

7 - 250 nm lines on 2 µm lines (perpendicular)

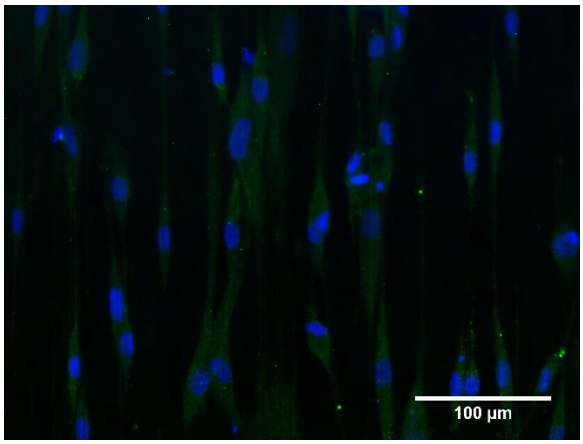

8 - 250 nm lines on 2 µm lines (parallel)

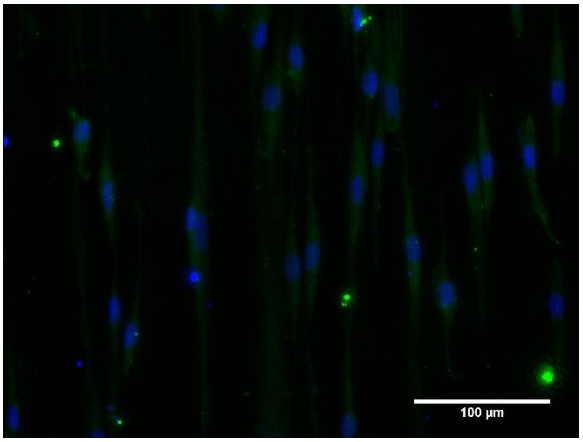

9 - 250 nm pillars on 2 µm lines

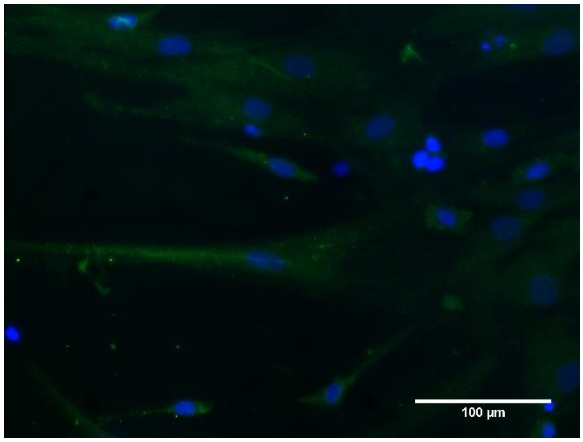

10 - 1 µm diameter & pitch, 0.3 µm sag concave lenses

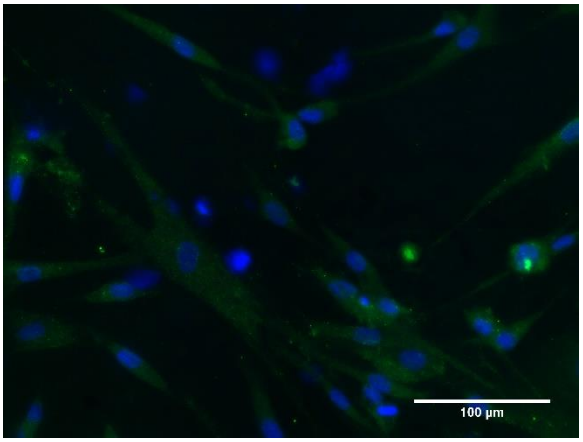

11 - 1 µm diameter & pitch, 0.3 µm sag convex lenses

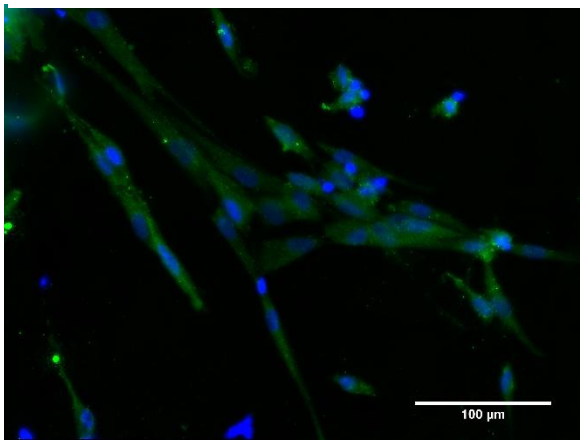

12 - 1.8 µm diameter, 2 µm pitch, 0.7 µm sag concave lenses

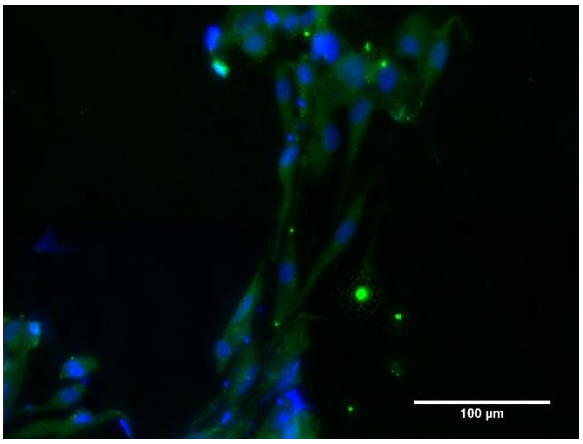

13 - 1.8 µm diameter, 2 µm pitch, 0.7 µm sag convex lenses

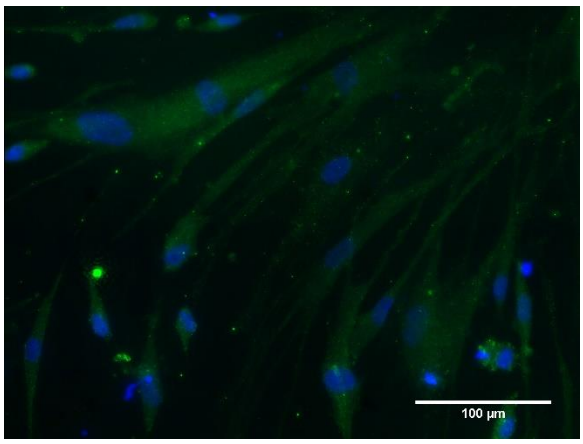

14 - 2 µm pillars, 12 µm pitch, 2 µm height

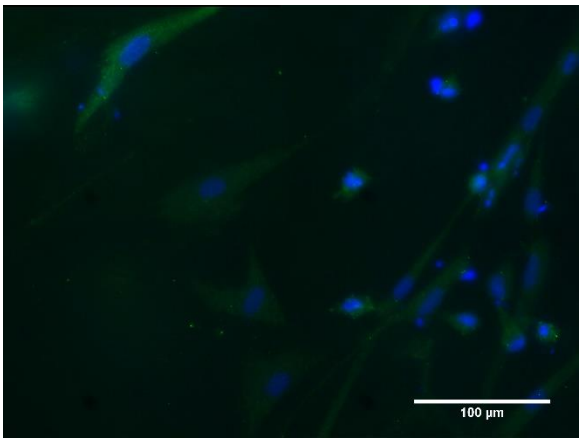

15 - 1 µm holes, 6.5 µm pitch, 1 µm depth

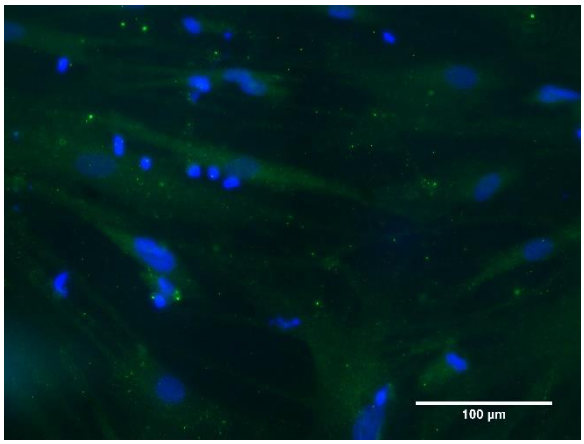

16 - 250 nm pillars, 400 nm pitch, 250 nm

3.4. Discussion

The first focus of this work was to set up the baseline conditions to use when inducing neuronal transdifferentiation of hMSCs on PDMS substrates. This involved testing parameters such as initial seeding density and polyplex dosage on unpatterned substrates before moving on to investigating the effect that topographically patterned substrates would have on the cell conversion. To decide on the values to use for these parameters we looked into the effect that initial seeding density has on cell density

and transfection efficiency of the samples after serial transfections and at the effect that polyplex dosage has on transfection efficiency, viability, and overall resulting surface density of transfected cells after serial transfections (Figure 20).

The reasons for testing different initial seeding densities was to find the density that would leave us with a sufficient number of cells to analyze after the entire cell conversion process. This is a concern because as cells convert to neurons they are expected to become post-mitotic which limits their population[35]. We found that on unpatterned PDMS substrates, an initial seeding density of 12000 cells/cm^2 would leave samples with a cell density of 5098 ± 931 cells/cm^2, which was equivalent to ~50 % confluency, after the transfection period of the cell conversion process. With this density of cells after the serial transfections, we were confident that there would be enough cells to analyze even after the expected cell death during the following induction phase. When we moved forward with our initial transdifferentiation experiments on the MARC chip (results from these experiments were not included in results section), we found cells remained above ~30% confluent by the final day of induction. However, during fixing of the samples, most of the cells would detach from our substrate due to very weak attachment. To mediate this we decided to additionally coat the PDMS substrates with fibronectin before seeding and add fibronectin to the media of samples 2 weeks after seeding. With this fibronectin coating, cells remained above ~30% confluent throughout and did not detach during fixing or staining.

Since we decided on using a seeding density of 12000 cells/cm^2, it was important to ensure that this would not have detrimental effects on the transfection efficiency. As we have discussed in the previous chapter, high cell density can reduce transfection efficiency due to contact inhibition. We found that when compared to using a standard seeding density for hMSCs of 5000 cells/cm^2, there was no significant difference in the resulting transfection efficiency after serial transfections. Hence, we were confident in deciding to use a seeding density of 12000 cells/cm^2 for our transdifferentiation experiments on PDMS substrates.

Because of the strong positive and negative correlations that dosage can have with transfection efficiency and cell viability, respectively, we sought to tune the dosage we would use in our experiments to balance these two important factors. Achieving this balance would effectively maximize the final surface density of transfected cells. From phase contrast imaging and the alamarBlue assay after three serial transfections, we found that cells showed healthier morphology and there were a higher number of living cells in samples that were transfected with a 0.25 μg/cm^2 dose of DNA delivered by polyplex (although this was not statistically significant). The transfection efficiency was not significantly different between samples transfected with the different doses of polyplex. When the mean transfection efficiencies and the cell counts were used to calculate the number of transfected cells per area, the two higher doses had very similar results while the lower dose resulted in a higher final number of transfected cells. With this information we determined that using the lowest dose (0.25 μg/cm^2) was beneficial, and chose to move forward using this dose in all subsequent experiments. It can be noted that a higher dose (1 μg/cm^2) resulted in transfection efficiencies with less variability between repeat samples compared to lower doses, which may be beneficial to consider in future studies.

In the literature, poly(amido amine)s containing repetitive disulfide linkages, like the p(ABOL) used in our study, were designed to be highly efficient intracellularly degradable gene delivery vectors. They were found to be relatively stable in the extracellular setting but were prone to fast degradation in a reductive environment analogous to that in the cytoplasm[82]. The balance between extracellular stability and intracellular unpacking was expected to support high transfection efficiency and reduce toxicity of the polymer vector. As transfection reagents, these polymers have been shown to be essentially nontoxic and have transfection efficiencies significantly higher than those of branched polyethylenimine (pEI, a gold standard polymeric gene carrier). These studies were done on COS-7 cells (fibroblast-like cells derived from monkey kidney tissue). Poly(ABOL) was used to non-virally transfect mouse embryonic fibroblasts with BAM transcription factors in order to induce neuronal transdifferentiation[15]. Due to the transfection reagent's low toxicity, they were able to use repeated dosing which they hypothesized would be a

requirement to generate induced neurons efficiently. Using a polymer:DNA mass ratio of 45:1, they found that serial delivery of 0.5 μg/cm^2 was almost entirely nontoxic compared to untransfected controls. A second dose after 48 hours did not show any compounding toxicity. Hence, they used serial transfections with this dose to induce neuronal transdifferentiation and produced up to 7.6 % Tuj1 (neuron-specific class III β-tubulin) positive cells. In contrast to their results, we found that polyplex delivered to hMSCs three times at 48 hour intervals caused higher toxicity. Even delivering doses of only 0.25 μg/cm^2 (with a polymer:DNA mass ratio of 45:1) resulted in less than 20 % viability. They were also able to achieve transfection efficiencies of ~70 % and ~80 % GFP positive cells by transfections with 0.5 μg/cm^2 doses or 1 μg/cm^2 after one or two doses. In contrast, we only achieved ~60 % GFP positive cells by transfection with 1 μg/cm^2 after three doses.

The lower transfection efficiency and viability that we saw, in comparison to this literature, could have been due to the fact that we were using hMSCs rather than fibroblasts or COS-7 cells. Another study in the literature studied the effect of the overall net charge of bioreducible PAAs composed of repeating units of cystamine bisacrylamide (CBA), 4-aminobutylguanidine (AGM), and 4-aminobutanol (ABOL) on human embryonic kidney 293 (HEK 293) cells, mesenchymal stem cells (MSC)s, and A2780 human ovarian carcinoma[120] . They controlled the net charge of their polymers by adjusting the percentage of AGM, the primary source of cationic charge, relative to ABOL within the polymer. They found that higher transfection could be achieved in MSCs and HEK 293 cells when the poly(CBA-ABOL/AGM) contained a higher AGM:ABOL ratio, whereas, the ratio of AGM:ABOL was less critical for high transfection of A278 cells. This demonstrates that different cell types can react differently to specific transfection reagents depending on their overall net charge and that a co-polymer with a high content of ABOL (lower net charge), like the one used in our study, is less effective on MSCs than on some other cell types. They also showed that higher mass ratios of polymer:DNA were more toxic to hMSCs compared to lower ratios and that the poly(amido amine) caused higher toxicity in hMSCs compared to HEK 293 cells.

Two studies that focused specifically on developing a transfection reagent to use on hMSCs, evaluated arrays of poly(β-amino esters) (PBAEs) with different end groups[121, 122]. The first paper looked at plasmid DNA transfection in different cell types and saw that different end-groups would change transfection efficiency drastically in a cell-type specific manner[121]. They found that a polymer composed of repeating units of 1,4-butanediol diacrylate and 5-amino-1-pentanol capped with a specific amine capping molecule mediated significantly higher transfection in hMSCs than Lipofetamine 2000. The other study found a synthetic end-modified PBAE optimized for small interfering RNA (siRNA) delivery to hMSCs[122]. Cyctamine-terminated PBAEs were the most effective, achieving 91% knockdown via RNA interference. These studies suggest that poly(β-amino esters) with specifically selected end groups may be a good alternative transfection reagent option for transfection of hMSCs.

The second focus of this work was to test transdifferentiation on unpatterned substrates and MARC chip substrates. The success of transdifferentiation was analyzed by checking for expression of neuronal markers by immunofluorescence staining and change in cell morphology. We could not conclude that any induced neurons were produced in any of our samples. Weak signal of immunofluorescent-staining of MAP2 appeared in treated samples as well as negative controls. Specific MAP2 immunofluorescence staining will stain the microtubule structure of neurons. In our imaging, we did not specifically see staining of cytoskeletal filaments, and hence the staining did not appear to be specific. There is a chance that the signal seen was a combination of weak MAP2 expression and non-specific staining.

One explanation for the similarity in staining across all of the samples and specifically for the staining that appeared on the negative controls is that hMSCs are capable of weakly expressing MAP2 without any specific induction, while increased levels can be seen after induction[123, 124] . This low expression could be what we are seeing across our negative controls and test samples. However, in that case we could have expected to have seen an increased expression of MAP2 in treated samples simply from effects of the induction medium. Another hypothesis for why staining was similar across all of the

samples could be that it was due to the influences on these cells caused by the high confluence that was reached by the end of the transfection phase.

As we observed from phase contrast images that were taken periodically throughout the transdifferentiation treatment, the cells became 100% confluent by the end of the transfection period (Figure 35) and then became less confluent during the induction phase (Figure 36 and Figure 37). Although cell density at the end of the transfection period was tested when deciding on initial seeding density, those tests were done without coating sample substrates with fibronectin. As was mentioned, we later realized fibronectin coating was required, to keep cells from detaching, only once we had begun transdifferentiation experiments. The addition of fibronectin coating could have been the cause of the increased confluence that was observed. One way in which high confluence could have affected the conversion process is by decreasing the rate of transfection. As was seen in Chapter 2 and has been documented in other literature, high confluence can reduce the efficiency of non-viral transfection[86] . Alternatively, we question whether the physical impact of high confluence on hMSCs could be causing differential gene expression through mechanotransduction. In previous studies, it has been shown that physical factors which cause alignment and elongation of hMSC morphology can also cause increased MAP2 expression due to spatial regulation of focal adhesions [19]. The morphology of highly confluent hMSCs is reminiscent of this alignment and elongation. Thirdly, the physical forces from high confluence may have overpowered topographical influences on the cells. The high confluence did have strong influence on the cells' spatial arrangement that lasted until the end of the induction phase, as can be seen in Figure 35 to Figure 37 and Figure 38. Cells on micro-gratings were observably influenced by the topography because their spatial arrangement was aligned with the grating axis, however, on other topographies it is unclear to what extent the forces from high confluence may have overpowered cell-topography interactions.

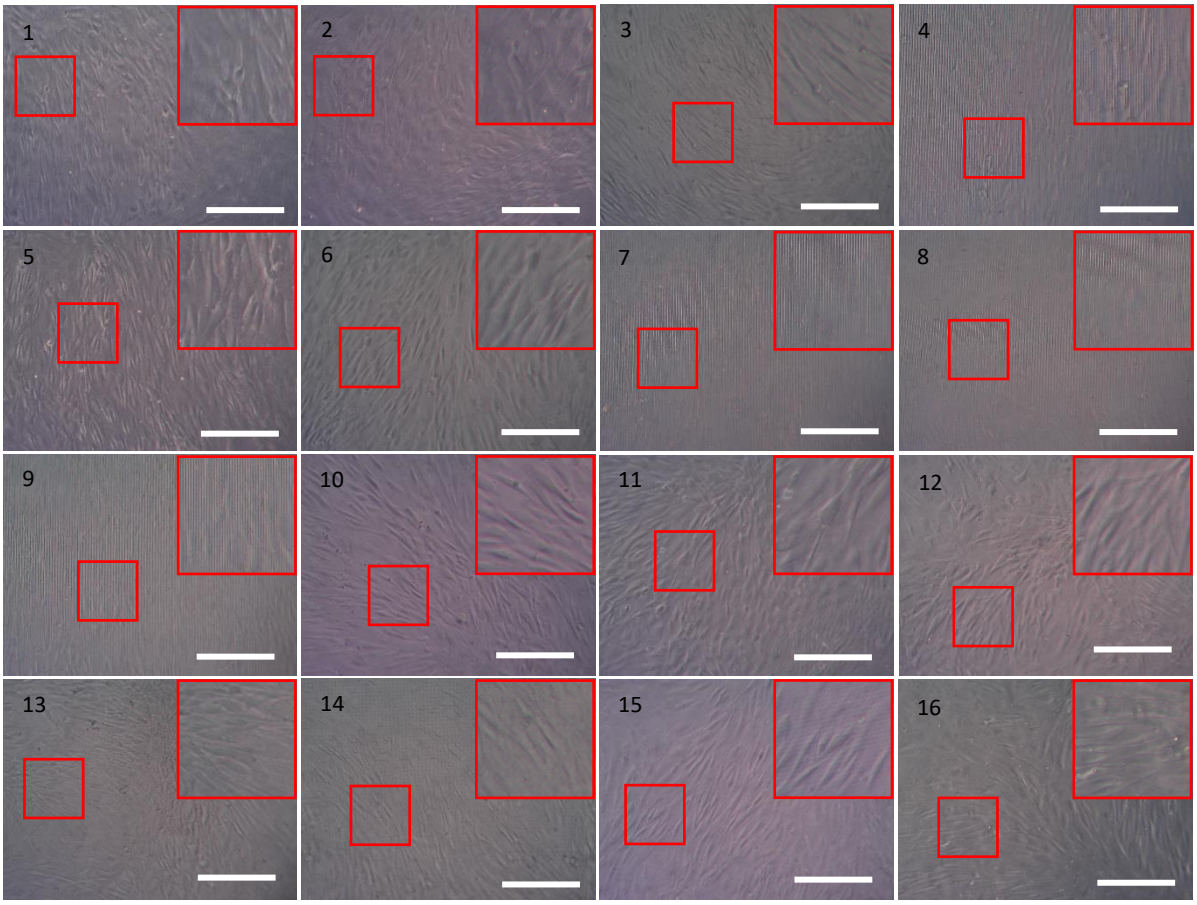

Figure 35. Phase contrast images of cell confluence taken on day 8 of transdifferentiation induction. Scale bars are 250 µm.

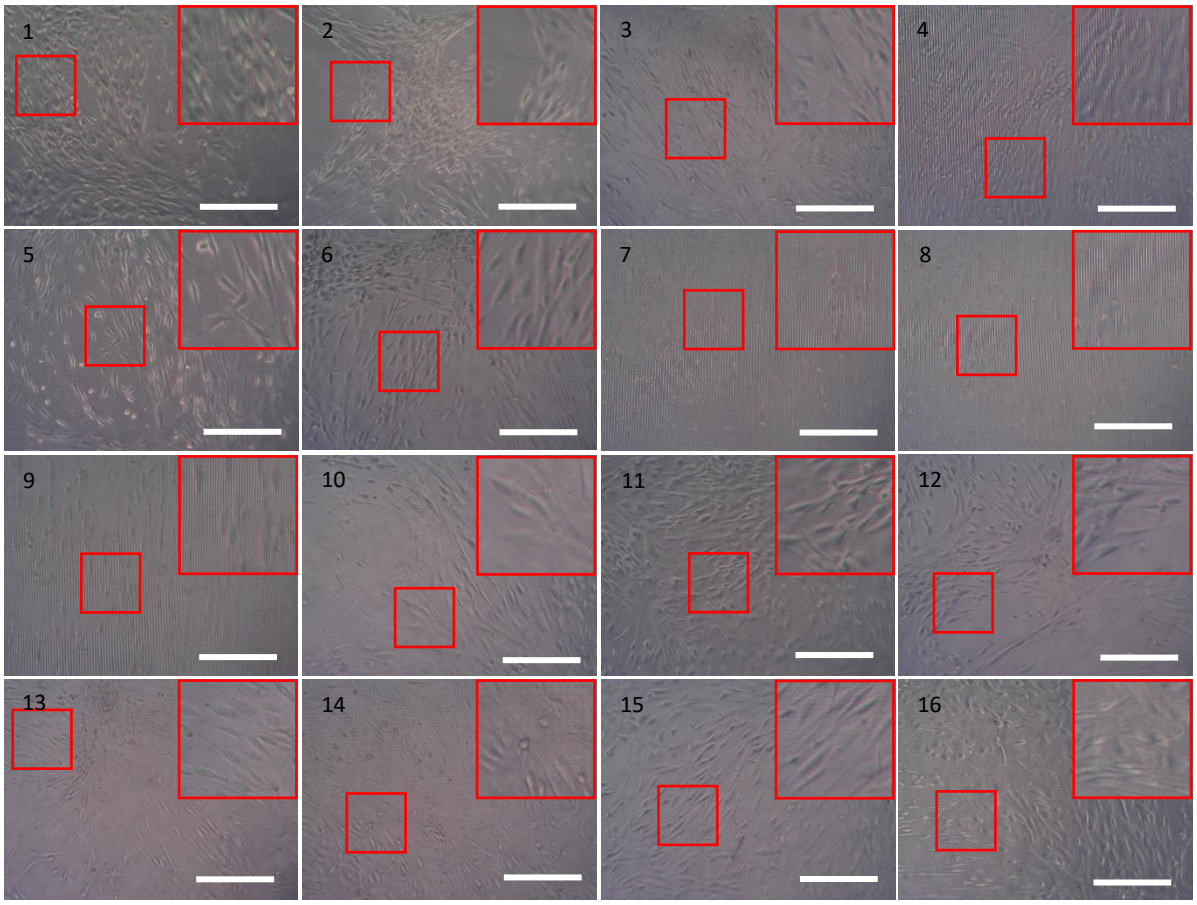

Figure 36. Phase contrast images of cell confluence taken on day 13 of transdifferentiation induction. Scale bars are 250 µm.

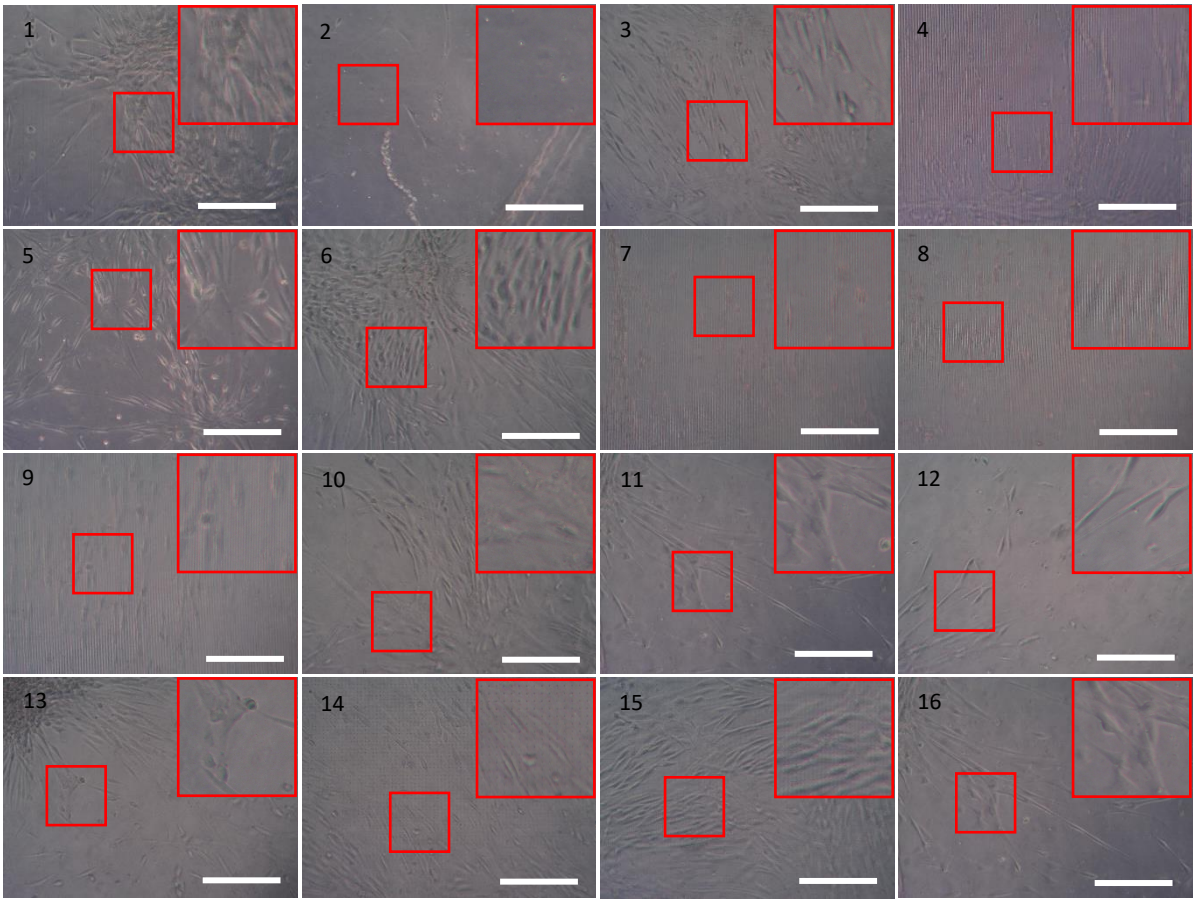

Figure 37. Phase contrast images of cell confluence taken on day 17 of transdifferentiation induction. Scale bars are 250 µm.

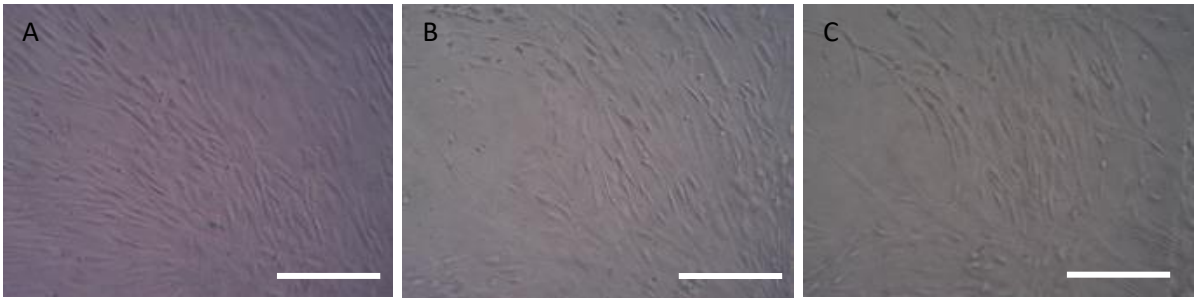

Figure 38 Influence on spatial arrangement from high confluence at day 8. These phase contrast images show hMSCs on 1 µm concave lenses (pattern 10) at (A) day 8, (B) day 13, and (C) day 17 of the neuronal induction protocol. These images show the lasting influence that high confluence had on the spatial arrangement of the cells which may have competed with influences from topography. Scale bars are 250 µm.

In addition to staining for MAP2, attempts were made to identify induced neuronal-like cells by staining for Tuj1 and Synapsin1 (this data was not shown in the results section). The first that we tried was Tuj1. The staining was bright in our negative control samples. Indeed, high expression of Tuj1 can be expected in hMSCs regardless of the number of culture passages and the culture conditions[123, 124]. Hence, we quickly moved on to test alternative neuronal markers. Synapsin1 staining only showed non-specific staining on negative controls and test samples, as staining was clearly not in the location of synaptic vesicles.

Chapter 4: Conclusions and Recommendations

4.1. Conclusions

Non-viral transfection and non-viral transdifferentiation are two processes that are likely to have significant impact on the field of regenerative medicine in the near future. Non-viral transfection will provide benefits to gene therapies, vaccines, and induction of therapeutically relevant cell types[13, 60-62]. Non-viral transdifferentiation will provide benefits to modeling of diseases and disorders, drug testing, and regenerative medicine strategies including cell therapy and tissue engineering[125-128]. A robust method to non-virally transfect cells would give promise for a safe clinically relevant strategy to induce cell conversions including transdifferentiation. Non-viral neuronal transdifferentiation specifically, would lead to the development of treatments for nerve damage and neurodegenerative diseases. The problem remaining with both non-viral transfection and non-viral transdifferentiation is their low efficiency. The transition to using non-viral transfection in applications which have routinely been studied using viral transfection brings many researched techniques a step closer to clinical applicability by improving their safety, however, it is challenging due to their decrease in efficiency. Neuronal transdifferentiation is one example of the many researched techniques that has begun to transition from being dependent on viral transfection to non-viral transfection for a better chance of becoming a clinically valid technique, but suffers more than ever from inefficiency. Therefore, in this thesis project it was our goal to investigate whether substrate nano- or micro- topography could (1) increase non-viral transfection efficiency of hMSCs and (2) enhance non-viral neuronal transdifferentiation.

From our studies screening the influence of 16 topographical patterns on non-viral transfection, we selected five topographical patterns including nano- and micro-gratings, concave micro-lenses, micro-holes, and nano-pillars, that increased the average measured transfection efficiency compared to

unpatterned substrates, for further study. Convex micro-lenses showed opposite effects on cell density, cell area, and transfection efficiency compared to concave micro-lenses. Hence, they were added as a sixth topography to our selection of patterns for further study. The results we based these selections on did not show statistical significance, but were a hint towards which topographies could be useful to study further with more rigorous methods. Quantification of topographical effects on cell density and average cell area gave some insight into possible explanations for why certain topographies increased transfection. We found some evidence that there may be a relationship between (i) topography size, (ii) average cell area, (iii) cell density, and (iv) the relationship between cell density and transfection efficiency. Previous studies investigating topography influence on non-viral transfection have looked into the effects of PMMA substrates with nano- and micro-pillars and nano-gratings and found that nano-pillars could significantly increase non-viral transfection of hMSCs compared to unpatterned substrates[17]. Another study screened 160 different micro-scale pitted geometries on PDMS substrates, and found that the efficiency of transfecting human dermal fibroblasts was improved 25 % with pits of 4µm width and 1µm spacing compared to unpatterned substrates[16]. In contrast, our study investigated a different combination of cell type and substrate material (hMSCs on PDMS), and screened an array of nano- and micro-scale patterns with a wide variety of geometries. We also observed that both micro-pits (although different in size and spacing) and nano-pillars increased non-viral transfection efficiency. This shows that topographical influence may be translatable between non-viral transfection of different cell types and different substrate materials.

Our neuronal transdifferentiation studies started with determining the polyplex dosage that should be used based on balancing effects on cytotoxicity and transfection efficiency. We found that a dosage of 0.25 µg DNA/cm^2, with a polymer:DNA mass ratio of 45:1, caused equivalent transfection efficiency and resulted in cells with heathier morphology (less blebbing) and higher cell viability compared to higher doses. In comparison to studies in literature, our cells experienced lower transfection efficiencies and higher toxic effects from transfections with pABOL[15, 82]. This could have been due to the difference in the

type of cells being transfected. Overall net charge of a polymer transfection reagent can affect the transfection efficiency of different cell types in different ways[120]. It has been shown that transfection efficiency of hMSCs benefits from polymers with a higher overall net charge than pABOL. Additionally, polyplex transfections with higher polymer:DNA ratio can be more toxic to hMSCs compared to other cell types which may explain the lower viability we saw in comparison to other studies. Screening of topographical influence on neuronal transdifferentiation showed that weak MAP2 expression was present in all samples including cells on unpatterned substrates that had not been transfected or exposed to neuronal induction media. It was observed that the cells became up to 95-100 % confluent during the transdifferentiation protocol, reaching their highest confluence close to the time when media was changed from MesenPRO RS medium (hMSC growth medium) to N3 neuronal induction medium. This high confluence could have interfered with the transfection of cells therefore hindering their conversion to neuronal cells. It is generally recommended that cells be kept below 90% confluent before transfection since allowing cells to become highly confluent may slow their growth rate and decrease transfection[86, 117]. Additionally, physical forces from high confluence may have overpowered topographical influences on the cells reducing any effect the topographies may have had in promoting transdifferentiation.

4.2. Recommendations

To continue the study of topographical influence on non-viral transfection, the six topographies that were selected due to their influence on transfection efficiency, cell density, and cell area should be studied on single-patterned substrates. A study on single-patterned substrates will give more accurate data due to the larger surface areas to analyze per sample providing an opportunity to see if there is any statistically significant changes caused by the topographies. On single patterned substrates, the cells can also be detached and the percentage of EGFP-expressing cells can be analyzed by flow cytometry. This

could be used instead of or in addition to fluorescence imaging analysis and may reduce human error in quantifying transfected cells. If statistical significance is found, the relationships between (i) topography size, (ii) average cell area, (iii) cell density, and (iv) the relationship between cell density and transfection efficiency should be investigated and evaluated with multivariate analysis.

To continue a fundamental scientific study of topography influence on non-viral neuronal transdifferentiation, it could be beneficial to continue studies with a different cell type. Fibroblasts have frequently been used for neuronal transdifferentiation studies in literature. Thus, the methods for characterizing the success of neuronal induction from fibroblasts are better established, better understood, and more consistently accepted. Since hMSCs have been shown to express neuronal markers without any intentionally applied neuronal induction, it is more difficult to determine whether neuronal marker expression has been induced by the transdifferentiation treatment or was innately present in the hMSCs [123, 129 124]. On the other hand, the innate neuronal marker expression seen in hMSCs may also be seen as a predisposition for hMSCs to differentiate into neurons[130]. Therefore, study of conversion of hMSCs to neurons could be useful to develop potential clinical treatment options, and should be further studied prior to investigating effects of topography. Since the high confluence reached during our transdifferentiation studies could have been a barrier to their success, the initial seeding density could be retuned and tested to see if it makes a difference. Other factors that should still be optimized for neuronal transdifferentiation of hMSCs are the number of serial transfections used and length of the induction phase. Additionally, polymers with a higher overall net charge and polyplexes with lower ratios of polymer:DNA should be tested to see if they are a benefit to hMSC transfection and neuronal transdifferentiation. Adjusting these parameters may help to achieve successful results.

References

1. Berthiaume, F.; Maguire, T. J.; Yarmush, M. L., Tissue engineering and regenerative medicine: history, progress, and challenges. *Annu Rev Chem Biomol Eng* **2011,** *2*, 403-30.
2. Gitler, A. D.; Dhillon, P.; Shorter, J., Neurodegenerative disease: models, mechanisms, and a new hope. *Disease models & mechanisms* **2017,** *10* (5), 499-502.
3. Monaghan, M. G.; Holeiter, M.; Layland, S. L.; Schenke-Layland, K., Cardiomyocyte generation from somatic sources - current status and future directions. *Curr Opin Biotechnol* **2016,** *40*, 49-55.
4. Hou, S.; Lu, P., Direct reprogramming of somatic cells into neural stem cells or neurons for neurological disorders. *Neural Regen Res* **2016,** *11* (1), 28-31.
5. Yang, N.; Ng, Y. H.; Pang, Z. P.; Südhof, T. C.; Wernig, M., Induced neuronal cells: how to make and define a neuron. *Cell Stem Cell* **2011,** *9* (6), 517-25.
6. World Health Organization, Neurological disorders affect millions globally: WHO Report. http://www.who.int/mediacentre/news/releases/2007/pr04/en/ (accessed 1 November 2016).
7. Omole, A. E.; Fakoya, A. O. J., Ten years of progress and promise of induced pluripotent stem cells: historical origins, characteristics, mechanisms, limitations, and potential applications. *PeerJ* **2018,** *6*, e4370.
8. Mollinari, C.; Zhao, J.; Lupacchini, L.; Garaci, E.; Merlo, D.; Pei, G., Transdifferentiation: a new promise for neurodegenerative diseases. *Cell Death Dis* **2018,** *9* (8), 830.
9. Lo, B.; Parham, L., Ethical issues in stem cell research. *Endocr Rev* **2009,** *30* (3), 204-13.
10. Lewandowski, J.; Kurpisz, M., Techniques of human embryonic stem cell and induced pluripotent stem cell derivation. *Arch Immunol Ther Exp (Warsz)* **2016,** *64* (5), 349-70.
11. Caiazzo, M.; Dell'Anno, M. T.; Dvoretskova, E.; Lazarevic, D.; Taverna, S.; Leo, D.; Sotnikova, T. D.; Menegon, A.; Roncaglia, P.; Colciago, G.; Russo, G.; Carninci, P.; Pezzoli, G.; Gainetdinov, R. R.; Gustincich, S.; Dityatev, A.; Broccoli, V., Direct generation of functional dopaminergic neurons from mouse and human fibroblasts. *Nature* **2011,** *476* (7359), 224-7.
12. Pang, Z. P.; Yang, N.; Vierbuchen, T.; Ostermeier, A.; Fuentes, D. R.; Yang, T. Q.; Citri, A.; Sebastiano, V.; Marro, S.; Südhof, T. C.; Wernig, M., Induction of human neuronal cells by defined transcription factors. *Nature* **2011,** *476* (7359), 220-3.
13. Jayant, R. D.; Sosa, D.; Kaushik, A.; Atluri, V.; Vashist, A.; Tomitaka, A.; Nair, M., Current status of non-viral gene therapy for CNS disorders. *Expert Opin Drug Deliv* **2016,** *13* (10), 1433-45.
14. Biasco, L.; Baricordi, C.; Aiuti, A., Retroviral integrations in gene therapy trials. *Mol Ther* **2012,** *20* (4), 709-16.
15. Adler, A. F.; Grigsby, C. L.; Kulangara, K.; Wang, H.; Yasuda, R.; Leong, K. W., Nonviral direct conversion of primary mouse embryonic fibroblasts to neuronal cells. *Mol Ther Nucleic Acids* **2012,** *1*, e32.
16. Adler, A. F.; Speidel, A. T.; Christoforou, N.; Kolind, K.; Foss, M.; Leong, K. W., High-throughput screening of microscale pitted substrate topographies for enhanced nonviral transfection efficiency in primary human fibroblasts. *Biomaterials* **2011,** *32* (14), 3611-9.

17. Teo, B. K.; Goh, S. H.; Kustandi, T. S.; Loh, W. W.; Low, H. Y.; Yim, E. K., The effect of micro and nanotopography on endocytosis in drug and gene delivery systems. *Biomaterials* **2011,** *32* (36), 9866-75.
18. Yim, E. K.; Pang, S. W.; Leong, K. W., Synthetic nanostructures inducing differentiation of human mesenchymal stem cells into neuronal lineage. *Exp Cell Res* **2007,** *313* (9), 1820-9.
19. Teo, B. K.; Wong, S. T.; Lim, C. K.; Kung, T. Y.; Yap, C. H.; Ramagopal, Y.; Romer, L. H.; Yim, E. K., Nanotopography modulates mechanotransduction of stem cells and induces differentiation through focal adhesion kinase. *ACS Nano* **2013,** *7* (6), 4785-98.
20. Grigsby, C.; Lawrence. Improving nonviral gene transfer and cellular reprogramming with microfluidic nanomanufacturing. Duke University, Durham, North Carolina, USA, 2014.
21. NationalCancerInstitute (NIH), Dictionary of cancer terms, Cell differentiation. https://www.cancer.gov/publications/dictionaries/cancer-terms/def/cell-differentiation (accessed 7 September 2018).
22. Evans, M. J.; Kaufman, M. H., Establishment in culture of pluripotential cells from mouse embryos. *Nature* **1981,** *292* (5819), 154-6.
23. Martin, G. R., Isolation of a pluripotent cell line from early mouse embryos cultured in medium conditioned by teratocarcinoma stem cells. *Proc Natl Acad Sci U S A* **1981,** *78* (12), 7634-8.
24. Thomson, J. A.; Itskovitz-Eldor, J.; Shapiro, S. S.; Waknitz, M. A.; Swiergiel, J. J.; Marshall, V. S.; Jones, J. M., Embryonic stem cell lines derived from human blastocysts. *Science* **1998,** *282* (5391), 1145-7.
25. Swijnenburg, R. J.; van der Bogt, K. E.; Sheikh, A. Y.; Cao, F.; Wu, J. C., Clinical hurdles for the transplantation of cardiomyocytes derived from human embryonic stem cells: role of molecular imaging. *Curr Opin Biotechnol* **2007,** *18* (1), 38-45.
26. Bradley, J. A.; Bolton, E. M.; Pedersen, R. A., Stem cell medicine encounters the immune system. *Nat Rev Immunol* **2002,** *2* (11), 859-71.
27. Takahashi, K.; Yamanaka, S., Induction of pluripotent stem cells from mouse embryonic and adult fibroblast cultures by defined factors. *Cell* **2006,** *126* (4), 663-76.
28. Takahashi, K.; Tanabe, K.; Ohnuki, M.; Narita, M.; Ichisaka, T.; Tomoda, K.; Yamanaka, S., Induction of pluripotent stem cells from adult human fibroblasts by defined factors. *Cell* **2007,** *131* (5), 861-72.
29. Medvedev, S. P.; Shevchenko, A. I.; Zakian, S. M., Induced pluripotent stem cells: Problems and advantages when applying them in regenerative medicine. *Acta Naturae* **2010,** *2* (2), 18-28.
30. Shen, C. N.; Burke, Z. D.; Tosh, D., Transdifferentiation, metaplasia and tissue regeneration. *Organogenesis* **2004,** *1* (2), 36-44.
31. Davis, R. L.; Weintraub, H.; Lassar, A. B., Expression of a single transfected cDNA converts fibroblasts to myoblasts. *Cell* **1987,** *51* (6), 987-1000.
32. Takeuchi, J. K.; Bruneau, B. G., Directed transdifferentiation of mouse mesoderm to heart tissue by defined factors. *Nature* **2009,** *459* (7247), 708-11.
33. Ieda, M.; Fu, J. D.; Delgado-Olguin, P.; Vedantham, V.; Hayashi, Y.; Bruneau, B. G.; Srivastava, D., Direct reprogramming of fibroblasts into functional cardiomyocytes by defined factors. *Cell* **2010,** *142* (3), 375-86.
34. Hack, M. A.; Saghatelyan, A.; de Chevigny, A.; Pfeifer, A.; Ashery-Padan, R.; Lledo, P. M.; Götz, M., Neuronal fate determinants of adult olfactory bulb neurogenesis. *Nat Neurosci* **2005,** *8* (7), 865-72.

35. Vierbuchen, T.; Ostermeier, A.; Pang, Z. P.; Kokubu, Y.; Südhof, T. C.; Wernig, M., Direct conversion of fibroblasts to functional neurons by defined factors. *Nature* **2010,** *463* (7284), 1035-41.
36. Pfisterer, U.; Kirkeby, A.; Torper, O.; Wood, J.; Nelander, J.; Dufour, A.; Björklund, A.; Lindvall, O.; Jakobsson, J.; Parmar, M., Direct conversion of human fibroblasts to dopaminergic neurons. *Proc Natl Acad Sci U S A* **2011,** *108* (25), 10343-8.
37. Ring, K. L.; Tong, L. M.; Balestra, M. E.; Javier, R.; Andrews-Zwilling, Y.; Li, G.; Walker, D.; Zhang, W. R.; Kreitzer, A. C.; Huang, Y., Direct reprogramming of mouse and human fibroblasts into multipotent neural stem cells with a single factor. *Cell Stem Cell* **2012,** *11* (1), 100-9.
38. Prasad, A.; Manivannan, J.; Loong, D. T.; Chua, S. M.; Gharibani, P. M.; All, A. H., A review of induced pluripotent stem cell, direct conversion by trans-differentiation, direct reprogramming and oligodendrocyte differentiation. *Regen Med* **2016,** *11* (2), 181-91.
39. Efe, J. A.; Hilcove, S.; Kim, J.; Zhou, H.; Ouyang, K.; Wang, G.; Chen, J.; Ding, S., Conversion of mouse fibroblasts into cardiomyocytes using a direct reprogramming strategy. *Nat Cell Biol* **2011,** *13* (3), 215-22.
40. Kim, J.; Efe, J. A.; Zhu, S.; Talantova, M.; Yuan, X.; Wang, S.; Lipton, S. A.; Zhang, K.; Ding, S., Direct reprogramming of mouse fibroblasts to neural progenitors. *Proc Natl Acad Sci U S A* **2011,** *108* (19), 7838-43.
41. Wang, L.; Huang, W.; Su, H.; Xue, Y.; Su, Z.; Liao, B.; Wang, H.; Bao, X.; Qin, D.; He, J.; Wu, W.; So, K. F.; Pan, G.; Pei, D., Generation of integration-free neural progenitor cells from cells in human urine. *Nat Methods* **2013,** *10* (1), 84-9.
42. Cieślar-Pobuda, A.; Knoflach, V.; Ringh, M. V.; Stark, J.; Likus, W.; Siemianowicz, K.; Ghavami, S.; Hudecki, A.; Green, J. L.; Łos, M. J., Transdifferentiation and reprogramming: Overview of the processes, their similarities and differences. *Biochim Biophys Acta* **2017,** *1864* (7), 1359-1369.
43. Wang, H.; Li, X.; Gao, S.; Sun, X.; Fang, H., Transdifferentiation via transcription factors or microRNAs: Current status and perspective. *Differentiation* **2015,** *90* (4-5), 69-76.
44. Latchman, D. S., Transcription factors: an overview. *Int J Biochem Cell Biol* **1997,** *29* (12), 1305-12.
45. Qin, H.; Zhao, A.; Fu, X., Small molecules for reprogramming and transdifferentiation. *Cell Mol Life Sci* **2017,** *74* (19), 3553-3575.
46. Chanda, S.; Marro, S.; Wernig, M.; Südhof, T. C., Neurons generated by direct conversion of fibroblasts reproduce synaptic phenotype caused by autism-associated neuroligin-3 mutation. *Proc Natl Acad Sci U S A* **2013,** *110* (41), 16622-7.
47. Zou, Q.; Yan, Q.; Zhong, J.; Wang, K.; Sun, H.; Yi, X.; Lai, L., Direct conversion of human fibroblasts into neuronal restricted progenitors. *J Biol Chem* **2014,** *289* (8), 5250-60.
48. Son, E. Y.; Ichida, J. K.; Wainger, B. J.; Toma, J. S.; Rafuse, V. F.; Woolf, C. J.; Eggan, K., Conversion of mouse and human fibroblasts into functional spinal motor neurons. *Cell Stem Cell* **2011,** *9* (3), 205-18.
49. Najm, F. J.; Lager, A. M.; Zaremba, A.; Wyatt, K.; Caprariello, A. V.; Factor, D. C.; Karl, R. T.; Maeda, T.; Miller, R. H.; Tesar, P. J., Transcription factor-mediated reprogramming of fibroblasts to expandable, myelinogenic oligodendrocyte progenitor cells. *Nat Biotechnol* **2013,** *31* (5), 426-33.
50. Jin, Y.; Seo, J.; Lee, J. S.; Shin, S.; Park, H. J.; Min, S.; Cheong, E.; Lee, T.; Cho, S. W., Triboelectric nanogenerator vccelerates highly efficient nonviral direct conversion and in

vivo reprogramming of fibroblasts to functional neuronal cells. *Adv Mater* **2016,** *28* (34), 7365-74.
51. Ambasudhan, R.; Talantova, M.; Coleman, R.; Yuan, X.; Zhu, S.; Lipton, S. A.; Ding, S., Direct reprogramming of adult human fibroblasts to functional neurons under defined conditions. *Cell Stem Cell* **2011,** *9* (2), 113-8.
52. Yoo, A. S.; Sun, A. X.; Li, L.; Shcheglovitov, A.; Portmann, T.; Li, Y.; Lee-Messer, C.; Dolmetsch, R. E.; Tsien, R. W.; Crabtree, G. R., MicroRNA-mediated conversion of human fibroblasts to neurons. *Nature* **2011,** *476* (7359), 228-31.
53. Victor, M. B.; Richner, M.; Hermanstyne, T. O.; Ransdell, J. L.; Sobieski, C.; Deng, P. Y.; Klyachko, V. A.; Nerbonne, J. M.; Yoo, A. S., Generation of human striatal neurons by microRNA-dependent direct conversion of fibroblasts. *Neuron* **2014,** *84* (2), 311-23.
54. Xu, A.; Cheng, L., Chemical transdifferentiation: closer to regenerative medicine. *Front Med* **2016,** *10* (2), 152-65.
55. Dai, P.; Harada, Y.; Takamatsu, T., Highly efficient direct conversion of human fibroblasts to neuronal cells by chemical compounds. *J Clin Biochem Nutr* **2015,** *56* (3), 166-70.
56. Li, X.; Zuo, X.; Jing, J.; Ma, Y.; Wang, J.; Liu, D.; Zhu, J.; Du, X.; Xiong, L.; Du, Y.; Xu, J.; Xiao, X.; Chai, Z.; Zhao, Y.; Deng, H., Small-molecule-driven direct reprogramming of mouse fibroblasts into functional neurons. *Cell Stem Cell* **2015,** *17* (2), 195-203.
57. Hu, W.; Qiu, B.; Guan, W.; Wang, Q.; Wang, M.; Li, W.; Gao, L.; Shen, L.; Huang, Y.; Xie, G.; Zhao, H.; Jin, Y.; Tang, B.; Yu, Y.; Zhao, J.; Pei, G., Direct conversion of normal and Alzheimer's Disease human fibroblasts into neuronal cells by small molecules. *Cell Stem Cell* **2015,** *17* (2), 204-12.
58. Ladewig, J.; Mertens, J.; Kesavan, J.; Doerr, J.; Poppe, D.; Glaue, F.; Herms, S.; Wernet, P.; Kögler, G.; Müller, F. J.; Koch, P.; Brüstle, O., Small molecules enable highly efficient neuronal conversion of human fibroblasts. *Nat Methods* **2012,** *9* (6), 575-8.
59. Pfisterer, U.; Ek, F.; Lang, S.; Soneji, S.; Olsson, R.; Parmar, M., Small molecules increase direct neural conversion of human fibroblasts. *Sci Rep* **2016,** *6*, 38290.
60. Ibraheem, D.; Elaissari, A.; Fessi, H., Gene therapy and DNA delivery systems. *Int J Pharm* **2014,** *459* (1-2), 70-83.
61. Saroja, C.; Lakshmi, P.; Bhaskaran, S., Recent trends in vaccine delivery systems: A review. *Int J Pharm Investig* **2011,** *1* (2), 64-74.
62. Long, J.; Kim, H.; Kim, D.; Lee, J. B.; Kim, D.-H., A biomaterial approach to cell reprogramming and differentiation. *Journal of Materials Chemistry B* **2017,** *5* (13), 2375-2389.
63. Nayerossadat, N.; Maedeh, T.; Ali, P. A., Viral and nonviral delivery systems for gene delivery. *Adv Biomed Res* **2012,** *1*, 27.
64. Gao, H.; Shi, W.; Freund, L. B., Mechanics of receptor-mediated endocytosis. *Proc Natl Acad Sci U S A* **2005,** *102* (27), 9469-74.
65. Zhang, S.; Li, J.; Lykotrafitis, G.; Bao, G.; Suresh, S., Size-Dependent Endocytosis of Nanoparticles. *Adv Mater* **2009,** *21*, 419-424.
66. Mamaeva, V.; Sahlgren, C.; Lindén, M., Mesoporous silica nanoparticles in medicine--recent advances. *Adv Drug Deliv Rev* **2013,** *65* (5), 689-702.
67. Chen, W.; Tsai, P. H.; Hung, Y.; Chiou, S. H.; Mou, C. Y., Nonviral cell labeling and differentiation agent for induced pluripotent stem cells based on mesoporous silica nanoparticles. *ACS Nano* **2013,** *7* (10), 8423-40.

68. Walters, R.; Welsh, M., Mechanism by which calcium phosphate coprecipitation enhances adenovirus-mediated gene transfer. *Gene Ther* **1999,** *6* (11), 1845-50.
69. Lee, C. H.; Kim, J. H.; Lee, H. J.; Jeon, K.; Lim, H.; Choi, H.; Lee, E. R.; Park, S. H.; Park, J. Y.; Hong, S.; Kim, S.; Cho, S. G., The generation of iPS cells using non-viral magnetic nanoparticle based transfection. *Biomaterials* **2011,** *32* (28), 6683-91.
70. Scherer, F.; Anton, M.; Schillinger, U.; Henke, J.; Bergemann, C.; Krüger, A.; Gänsbacher, B.; Plank, C., Magnetofection: enhancing and targeting gene delivery by magnetic force in vitro and in vivo. *Gene Ther* **2002,** *9* (2), 102-9.
71. Kong, L.; Alves, C. S.; Hou, W.; Qiu, J.; Möhwald, H.; Tomás, H.; Shi, X., RGD peptide-modified dendrimer-entrapped gold nanoparticles enable highly efficient and specific gene delivery to stem cells. *ACS Appl Mater Interfaces* **2015,** *7* (8), 4833-43.
72. Khan, M.; Narayanan, K.; Lu, H.; Choo, Y.; Du, C.; Wiradharma, N.; Yang, Y. Y.; Wan, A. C., Delivery of reprogramming factors into fibroblasts for generation of non-genetic induced pluripotent stem cells using a cationic bolaamphiphile as a non-viral vector. *Biomaterials* **2013,** *34* (21), 5336-43.
73. Tammam, S.; Malak, P.; Correa, D.; Rothfuss, O.; Azzazy, H. M.; Lamprecht, A.; Schulze-Osthoff, K., Nuclear delivery of recombinant OCT4 by chitosan nanoparticles for transgene-free generation of protein-induced pluripotent stem cells. *Oncotarget* **2016,** *7* (25), 37728-37739.
74. Li, J. J.; Kawazoe, N.; Chen, G., Gold nanoparticles with different charge and moiety induce differential cell response on mesenchymal stem cell osteogenesis. *Biomaterials* **2015,** *54*, 226-36.
75. Patel, S.; Chueng, S. T.; Yin, P. T.; Dardir, K.; Song, Z.; Pasquale, N.; Kwan, K.; Sugiyama, H.; Lee, K. B., Induction of stem-cell-derived functional neurons by NanoScript-based gene repression. *Angew Chem Int Ed Engl* **2015,** *54* (41), 11983-8.
76. Pack, D. W.; Hoffman, A. S.; Pun, S.; Stayton, P. S., Design and development of polymers for gene delivery. *Nat Rev Drug Discov* **2005,** *4* (7), 581-93.
77. Sun, X.; Zhang, N., Cationic polymer optimization for efficient gene delivery. *Mini Rev Med Chem* **2010,** *10* (2), 108-25.
78. Felgner, P. L.; Gadek, T. R.; Holm, M.; Roman, R.; Chan, H. W.; Wenz, M.; Northrop, J. P.; Ringold, G. M.; Danielsen, M., Lipofection: a highly efficient, lipid-mediated DNA-transfection procedure. *Proc Natl Acad Sci U S A* **1987,** *84* (21), 7413-7.
79. Zabner, J., Cationic lipids used in gene transfer. *Adv Drug Deliv Rev* **1997,** *27* (1), 17-28.
80. Thapa, B.; Narain, R., Mechanism, current challenges and new approaches for non viral gene delivery. In *Polymers and Nanomaterials for Gene Therapy*, Narain, R., Ed. Elsevier Science & Technology: Waltham, MA, 2016; pp 1-27.
81. Lv, H.; Zhang, S.; Wang, B.; Cui, S.; Yan, J., Toxicity of cationic lipids and cationic polymers in gene delivery. *J Control Release* **2006,** *114* (1), 100-9.
82. Lin, C.; Zhong, Z.; Lok, M. C.; Jiang, X.; Hennink, W. E.; Feijen, J.; Engbersen, J. F., Novel bioreducible poly(amido amine)s for highly efficient gene delivery. *Bioconjug Chem* **2007,** *18* (1), 138-45.
83. Boussif, O.; Lezoualc'h, F.; Zanta, M. A.; Mergny, M. D.; Scherman, D.; Demeneix, B.; Behr, J. P., A versatile vector for gene and oligonucleotide transfer into cells in culture and in vivo: polyethylenimine. *Proc Natl Acad Sci U S A* **1995,** *92* (16), 7297-301.
84. Jin, L.; Zeng, X.; Liu, M.; Deng, Y.; He, N., Current progress in gene delivery technology based on chemical methods and nano-carriers. *Theranostics* **2014,** *4* (3), 240-55.

85. Saranya, N.; Moorthi, A.; Saravanan, S.; Devi, M. P.; Selvamurugan, N., Chitosan and its derivatives for gene delivery. *Int J Biol Macromol* **2011,** *48* (2), 234-8.
86. Adler, A. F.; Leong, K. W., Emerging links between surface nanotechnology and endocytosis: impact on nonviral gene delivery. *Nano Today* **2010,** *5* (6), 553-569.
87. Wójciak-Stothard, B.; Curtis, A.; Monaghan, W.; MacDonald, K.; Wilkinson, C., Guidance and activation of murine macrophages by nanometric scale topography. *Exp Cell Res* **1996,** *223* (2), 426-35.
88. Dalby, M. J.; Berry, C. C.; Riehle, M. O.; Sutherland, D. S.; Agheli, H.; Curtis, A. S., Attempted endocytosis of nano-environment produced by colloidal lithography by human fibroblasts. *Exp Cell Res* **2004,** *295* (2), 387-94.
89. Moerke, C.; Mueller, P.; Nebe, B., Attempted caveolae-mediated phagocytosis of surface-fixed micro-pillars by human osteoblasts. *Biomaterials* **2016,** *76*, 102-14.
90. Huang, C.; Ozdemir, T.; Xu, L. C.; Butler, P. J.; Siedlecki, C. A.; Brown, J. L.; Zhang, S., The role of substrate topography on the cellular uptake of nanoparticles. *J Biomed Mater Res B Appl Biomater* **2016,** *104* (3), 488-95.
91. Long, J.; Kim, H.; Kim, D.; Lee, J. B.; Kim, D.-H., A biomaterial approach to cell reprogramming and differentiation. *Journal of Materials Chemistry B* **2017,** *5* (13), 2375-2389.
92. Moe, A. A.; Suryana, M.; Marcy, G.; Lim, S. K.; Ankam, S.; Goh, J. Z.; Jin, J.; Teo, B. K.; Law, J. B.; Low, H. Y.; Goh, E. L.; Sheetz, M. P.; Yim, E. K., Microarray with micro- and nano-topographies enables identification of the optimal topography for directing the differentiation of primary murine neural progenitor cells. *Small* **2012,** *8* (19), 3050-61.
93. Chua, J. S.; Chng, C. P.; Moe, A. A.; Tann, J. Y.; Goh, E. L.; Chiam, K. H.; Yim, E. K., Extending neurites sense the depth of the underlying topography during neuronal differentiation and contact guidance. *Biomaterials* **2014,** *35* (27), 7750-61.
94. Hajiali, H.; Contestabile, A.; Mele, E.; Athanassiou, A., Influence of topography of nanofibrous scaffolds on functionality of engineered neural tissue. *Journal of Materials Chemistry B* **2018,** *6* (6), 930-939.
95. Ankam, S.; Suryana, M.; Chan, L. Y.; Moe, A. A.; Teo, B. K.; Law, J. B.; Sheetz, M. P.; Low, H. Y.; Yim, E. K., Substrate topography and size determine the fate of human embryonic stem cells to neuronal or glial lineage. *Acta Biomater* **2013,** *9* (1), 4535-45.
96. Carlson, A. L.; Bennett, N. K.; Francis, N. L.; Halikere, A.; Clarke, S.; Moore, J. C.; Hart, R. P.; Paradiso, K.; Wernig, M.; Kohn, J.; Pang, Z. P.; Moghe, P. V., Generation and transplantation of reprogrammed human neurons in the brain using 3D microtopographic scaffolds. *Nat Commun* **2016,** *7*, 10862.
97. Kulangara, K.; Adler, A. F.; Wang, H.; Chellappan, M.; Hammett, E.; Yasuda, R.; Leong, K. W., The effect of substrate topography on direct reprogramming of fibroblasts to induced neurons. *Biomaterials* **2014,** *35* (20), 5327-36.
98. Yoo, J.; Noh, M.; Kim, H.; Jeon, N. L.; Kim, B. S.; Kim, J., Nanogrooved substrate promotes direct lineage reprogramming of fibroblasts to functional induced dopaminergic neurons. *Biomaterials* **2015,** *45*, 36-45.
99. Hajiali, H.; Contestabile, A.; Mele, E.; Athanassiou, A., Influence of topography of nanofibrous scaffolds on functionality of engineered neural tissue. *Journal of Materials Chemistry B* **2018,** *6* (6), 930-939.
100. Subramaniam, A.; Sethuraman, S., Biomedical applications of nondegradable polymers. In *Natural and Synthetic Biomedical Polymers*, Kumbar, S. G.; Laurencin, C. T.; Deng, M., Eds. Elsevier: Burlington, MA, USA, 2014; pp 301-308.

101. Leclerc, E.; Sakai, Y.; Fujii, T., Cell Culture in 3-Dimensional Microfluidic Structure of PDMS (polydimethylsiloxane). *Biomedical Microdevices* **2003,** *5* (2), 109-114.
102. Lee, J. N.; Jiang, X.; Ryan, D.; Whitesides, G. M., Compatibility of mammalian cells on surfaces of poly(dimethylsiloxane). *Langmuir* **2004,** *20* (26), 11684-91.
103. Kukumberg, M.; Yao, J. Y.; Neo, D. J. H.; Yim, E. K. F., Microlens topography combined with vascular endothelial growth factor induces endothelial differentiation of human mesenchymal stem cells into vasculogenic progenitors. *Biomaterials* **2017,** *131*, 68-85.
104. Lipomi, D. J.; Martínez, R.; Cademartiri, L.; Whitesides, G. M., Soft Lithographic Approaches to Nanofabrication. In *Polymer Science: A Comprehensive Reference*, Moeller, M.; Matyjaszewski, K., Eds. Elsevier Science: Amsterdam, 2012; pp 211-231.
105. Collins, A. M., *Nanotechnology cookbook: Practical, reliable and jargon-free experimental procedures*. Elsevier Science: Amsterdam, 2012; p 324.
106. Bodas, D.; Khan-Malek, C., Hydrophilization and hydrophobic recovery of PDMS by oxygen plasma and chemical treatment—An SEM investigation. *Sensors & Actuators: B. Chemical* **2007,** *123* (1), 368-373.
107. Mcdonald, J. C.; Duffy, D. C.; Anderson, J. R.; Chiu, D. T.; Wu, H.; Schueller, O. J. A.; Whitesides, G. M., Fabrication of microfluidic systems in poly(dimethylsiloxane). *Electrophoresis* **2000,** *21* (1), 27-40.
108. Zhang, Q. Y.; Zhang, Y. Y.; Xie, J.; Li, C. X.; Chen, W. Y.; Liu, B. L.; Wu, X. A.; Li, S. N.; Huo, B.; Jiang, L. H.; Zhao, H. C., Stiff substrates enhance cultured neuronal network activity. *Sci Rep* **2014,** *4*, 6215.
109. Cui, Y.; Hameed, F. M.; Yang, B.; Lee, K.; Pan, C. Q.; Park, S.; Sheetz, M., Cyclic stretching of soft substrates induces spreading and growth. *Nature Communications* **2015,** *6* (1), 6333
110. Sia, J.; Yu, P.; Srivastava, D.; Li, S., Effect of biophysical cues on reprogramming to cardiomyocytes. *Biomaterials* **2016,** *103*, 1-11.
111. Cui, Z.; SpringerLink (Online service), Nanofabrication: Principles, capabilities and limits. 2nd ed.; Springer International Publishing : Imprint: Springer: Cham, 2017; pp. XVII, 432 p. 316 illus., 50 illus. in color. http://myaccess.library.utoronto.ca/login?url=https://link.springer.com/10.1007/978-3-319-39361-2.
112. Qin, D.; Xia, Y.; Whitesides, G. M., Soft lithography for micro- and nanoscale patterning. *Nat Protoc* **2010,** *5* (3), 491-502.
113. Delamarche, E.; Schmid, H.; Michel, B.; Biebuyck, H., Stability of molded polydimethylsiloxane microstructures. *Advanced Materials* **1997,** *9* (9), 741-746.
114. Ruedel, A.; Bosserhoff, A. K., Transfection methods. 2012; Vol. 112, pp 163-182.
115. Rejman, J.; Bragonzi, A.; Conese, M., Role of clathrin- and caveolae-mediated endocytosis in gene transfer mediated by lipo- and polyplexes. *Mol Ther* **2005,** *12* (3), 468-74.
116. Rejman, J.; Conese, M.; Hoekstra, D., Gene transfer by means of lipo- and polyplexes: role of clathrin and caveolae-mediated endocytosis. *J Liposome Res* **2006,** *16* (3), 237-47.
117. Abo-Aziza, F. A. M.; A A, Z., The Impact of Confluence on Bone Marrow Mesenchymal Stem (BMMSC) Proliferation and Osteogenic Differentiation. *Int J Hematol Oncol Stem Cell Res* **2017,** *11* (2), 121-132.
118. Thermo Fisher, alamarBlue – Reliable and accurate cell health indicator. https://www.thermofisher.com/ca/en/home/brands/molecular-probes/key-molecular-probes-products/alamarblue-rapid-and-accurate-cell-health-indicator.html.

119. Invitrogen Corporation, alamarBlue Assay TDS. 2018.
120. Won, Y. W.; Ankoné, M.; Engbersen, J. F.; Feijen, J.; Kim, S. W., Poly(amido amine)s containing agmatine and butanol side chains as efficient gene carriers. *Macromol Biosci* **2016,** *16* (4), 619-26.
121. Sunshine, J.; Green, J. J.; Mahon, K. P.; Yang, F.; Eltoukhy, A. A.; Nguyen, D. N.; Langer, R.; Anderson, D. G., Small-Molecule End-Groups of Linear Polymer Determine Cell-type Gene-Delivery Efficacy. *Adv Mater* **2009,** *21* (48), 4947-4951.
122. Tzeng, S. Y.; Hung, B. P.; Grayson, W. L.; Green, J. J., Cystamine-terminated poly(beta-amino ester)s for siRNA delivery to human mesenchymal stem cells and enhancement of osteogenic differentiation. *Biomaterials* **2012,** *33* (32), 8142-51.
123. Tondreau, T.; Lagneaux, L.; Dejeneffe, M.; Massy, M.; Mortier, C.; Delforge, A.; Bron, D., Bone marrow-derived mesenchymal stem cells already express specific neural proteins before any differentiation. *Differentiation* **2004,** *72* (7), 319-26.
124. Foudah, D.; Redondo, J.; Caldara, C.; Carini, F.; Tredici, G.; Miloso, M., Human mesenchymal stem cells express neuronal markers after osteogenic and adipogenic differentiation. *Cell Mol Biol Lett* **2013,** *18* (2), 163-86.
125. Tang, Y.; Yu, P.; Cheng, L., Current progress in the derivation and therapeutic application of neural stem cells. *Cell Death Dis* **2017,** *8* (10), e3108.
126. Wu, P.; Chen, H.; Jin, R.; Weng, T.; Ho, J. K.; You, C.; Zhang, L.; Wang, X.; Han, C., Non-viral gene delivery systems for tissue repair and regeneration. *J Transl Med* **2018,** *16* (1), 29.
127. Argyros, O.; Wong, S. P.; Gowers, K.; Harbottle, R. P., Genetic modification of cancer cells using non-viral, episomal S/MAR vectors for in vivo tumour modelling. *PLoS One* **2012,** *7* (10), e47920.
128. Ebert, A. D.; Liang, P.; Wu, J. C., Induced pluripotent stem cells as a disease modeling and drug screening platform. *J Cardiovasc Pharmacol* **2012,** *60* (4), 408-16.
129. Bertani, N.; Malatesta, P.; Volpi, G.; Sonego, P.; Perris, R., Neurogenic potential of human mesenchymal stem cells revisited: analysis by immunostaining, time-lapse video and microarray. *J Cell Sci* **2005,** *118* (Pt 17), 3925-36.
130. Scuteri, A.; Miloso, M.; Foudah, D.; Orciani, M.; Cavaletti, G.; Tredici, G., Mesenchymal stem cells neuronal differentiation ability: a real perspective for nervous system repair? *Curr Stem Cell Res Ther* **2011,** *6* (2), 82-92.
131. Johnson, R. A.; Wichern, D.W., Applied multivariate analysis. 5th ed.; Prentice Hall, Upper Saddle River, N. J., 2002.

Appendix A: Principal Component Analysis for Studies of Transfection on PDMS MARC Chips

A.1. Introduction

Principal component analysis (PCA) allows us to extract important information from multivariate data and represent this information with a set of fewer new variables, called principal components, which are linear combinations of the original variables[131]. If each original variable is thought of as a dimension, the goal of PCA is to identify principal components which describe new dimensions that contain the largest amount of variation (which can be thought of as information) in the original variables. Here we present PCA analysis on data obtained during the study of transfection on PDMS MARC chips (sections 2.2.8, 2.2.9, 2.3.4, and 2.3.5).

A.2 Methods

PCA was performed, with help from Dr. Marc Aucoin, using the FactoMineR R package. The variables considered in this PCA included measurements of normalized transfection efficiency, normalized average cell area, and normalized cell density, from five different MARC chips after Lipofectamine-mediate transfection which was performed as described in section 2.2.8, as well as independent variables describing the features of each topography (height/width aspect ratio, feature spacing, feature height, and feature width).

A.3 Results

The first two principal components explained 58.44% of the variances in our original data. The variables factor map, in ,shows the degree of involvement of each of our original variables in principal component 1 (Dim 1) and principal component 2 (Dim 2). We see that normalized transfection efficiency and normalized average cell area are positively correlated with each other and negatively correlated with normalized cell density in these principal component dimensions. Three variables describing the features of each topography (height/width aspect ratio, feature spacing, and feature height) are correlated in these dimensions, which is not surprising, since our data was made up of multiple observations involving the same 16 topographies. Feature width was positively correlated with cell density and negatively correlated with normalized transfection efficiency and normalized average cell area in these principal components.

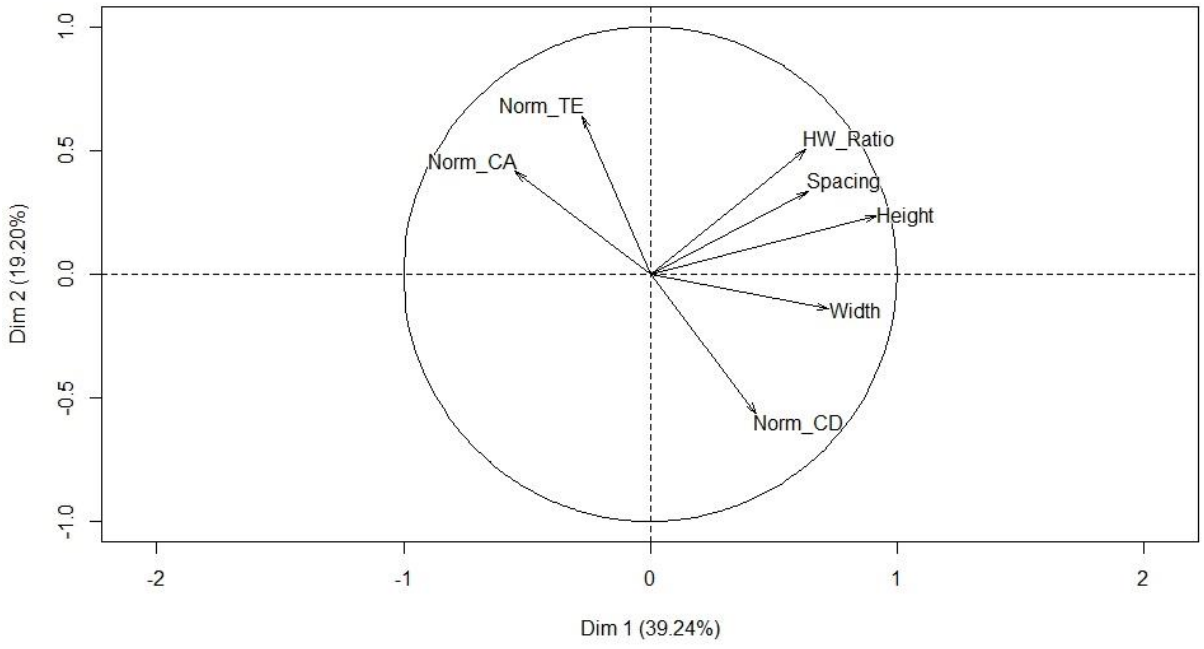

Figure 39 Variables factor map. The variables included in this PCA analysis were normalized transfection efficiency (Norm_TE), normalized average cell area (Norm_CA), normalized cell density (Norm_CD), feature height/width aspect ratio (HW_Ratio), feature spacing (Spacing), feature height (Height), and feature width (Width).